THESIS

HYDROLOGIC ALTERATION UNDER HYDROPOWER DAM OPERATIONS AND CLIMATE CHANGE: A CASE STUDY IN THE SESAN RIVER BASIN, LOWER MEKONG REGION

Submitted by

Wangmo Ghalley

Department of Civil and Environmental Engineering

In partial fulfillment of the requirements

For the Degree of Master of Science

Colorado State University

Fort Collins, Colorado

Fall 2023

Master's Committee:

Advisor: Jeffrey D. Niemann
Co-Advisor: Sangam Shrestha

Robert Ettema
N. LeRoy Poff

ABSTRACT

HYDROLOGIC ALTERATION UNDER HYDROPOWER DAM OPERATIONS AND CLIMATE CHANGE: A CASE STUDY IN THE SESAN RIVER BASIN, LOWER MEKONG REGION

Hydropower dam developments exacerbated by climate change can significantly disrupt the natural flow regimes, leading to adverse effects on river ecosystems. The Sesan River, a major tributary of the Lower Mekong Basin, is renowned for its diverse biomes and is an important resource for nearby inhabitants. Rapid expansion of hydropower dams has occurred in recent years, but the hydrologic impacts remain poorly understood, particularly when combined with the effects of climate change. This study assessed the hydrologic alterations in Sesan River streamflow due to hydropower dams and potential climate change.

Daily streamflow in the Sesan River was simulated using the Hydrologic Engineering Center-Hydrologic Modeling System (HEC-HMS), which was calibrated and evaluated based on streamflow observations. Climate change projections were based on daily precipitation and temperature, which were estimated using an ensemble of three Earth system models from the Coupled Model Intercomparison Project Phase-6 under two Socioeconomic Pathways: SSP2-4.5 (Middle of the road) and SSP5-8.5 (Fossil-fueled development). Future projections spanned 2025 to 2100, which was divided into three 25-year periods called the Near Future (NF), Mid-Future (MF), and Far Future (FF). The projections were compared to a 30-year baseline (BL) period from 1984 to 2014. Results show a consistent rise in both precipitation and temperature for the Sesan basin across all future periods and SSP scenarios. Precipitation is projected to increase by 4% to 13% for SSP2-4.5 and 7% to 29% for SSP5-8.5. Minimum temperature is projected to increase by

8% to 16% for SSP2-4.5 and 10% to 26% for SSP5-8.5, and maximum temperature is projected to increase by 3% to 7% for SSP2-4.5 and 3% to 12% for SSP5-8.5.

Hydrologic alterations were assessed using the Range of Variability Approach (RVA) within the Indicators of Hydrologic Alteration (IHA). The impact of dams was assessed by comparing streamflows with dams and without dams during the BL period. The dams significantly altered the hydrograph characteristics by decreasing the high flows and increasing the low flows. The overall alteration due to dams fell within the "moderate" category. The impact of climate change was assessed by comparing streamflows without dams between the BL and the future periods. Climate change increased the high flow rates, with the impact limited to September in the NF but impacting much of the year in the MF and FF periods. Another notable change was the shift in the timing of peak flow from August in the BL to September in the future periods. The hydrologic alteration due to climate change fell within the "low" category. Finally, the combined impact of dams and climate change was assessed by comparing the BL streamflow without dams to future streamflow with dams. Dams were found to mitigate some impacts of climate change by smoothing extreme high flows, especially in the FF period. Overall, the combined impact showed greater alteration than the individual scenarios but fell within the "moderate" category.

ACKNOWLEDGEMENTS

I am profoundly grateful to the dual degree program offered in collaboration between Colorado State University, USA and the Asian Institute of Technology, Thailand, for the opportunity to pursue this challenging and rewarding endeavor. This program has been a truly gratifying and transformative academic journey.

I would like to express my sincere gratitude to my advisor at CSU, Dr. Jeffrey D. Niemann, for his unwavering guidance, mentorship, and constant support throughout this research. His knowledge, expertise, and patience have been instrumental in shaping the direction of my work. I am equally grateful to my co-advisors, Dr. Sangam Shrestha from AIT and Dr. Robert Ettema from CSU, for their encouragement and support since the very beginning. Their insights and feedback have helped me to improve my research significantly. I would also like to extend my gratitude to the esteemed members of my thesis committee, Dr. Mohana Sundaram Shanmugam and Dr. Ho Huu Loc from AIT, and Dr. N LeRoy Poff from CSU, for their insightful feedback and constructive criticism. I am also grateful to Mr. Suwas Ghimire from AIT for his invaluable assistance and guidance, particularly during the initial stages of my research.

Finally, I would like to express my deepest appreciation to my parents, family, and friends for their unwavering support, encouragement, and understanding. A special thanks to my little niece, Reva, who helped me stay motivated.

TABLE OF CONTENTS

LIST OF TABLES

LIST OF FIGURES

Chapter 1

Introduction

1.1. Background

More than half of the world's major rivers have been dammed (Nilsson et al., 2005), and the construction of new dams continues to be driven by increasing energy demands and efforts to provide water to alleviate poverty, enhance public health, and strengthen regional economies (Zarfl et al., 2015; Zhang et al., 2017; Winemiller et al., 2016; Hecht et al., 2019). While dams provide significant benefits to human societies and economies, their construction has incurred significant ecological costs and negatively impacted ecosystem services (Postel & Richter, 2003; Richter & Thomas, 2007). One of the most pervasive and detrimental impacts of dams is the hydrologic alteration of streamflow (Poff et al., 1997, Postel & Richter, 2003). Hydrologic alteration refers to substantial changes in magnitude, duration, timing, frequency, and disruption of natural flow regimes (Poff et al., 1997). The natural ebb and flow of discharge intricately shape and sustain aquatic and riparian habitats. Anthropogenic interventions, such as construction of dams and other river structures, disturb this balance and disrupt downstream aquatic ecosystems and human livelihoods reliant on these ecosystems (Poff & Zimmerman, 2010; Gunawardana et al., 2021).

Another widely recognized key driver of hydrologic alteration is climate change. The Intergovernmental Panel on Climate Change (IPCC) defines climate change as any lasting alteration in climate, whether due to natural variability or because of human activity. Human activities have caused the Earth's climate to warm significantly since 1850, with the global temperature during 2001-2020 being 1.0°C higher than during 1850-1900 (IPCC Sixth Assessment Report-AR6, 2023). This warming has led to significant changes in the hydrological cycle,

including changes in precipitation patterns, accelerated snowmelt, increased evaporation, and intensified extreme weather events (Trang et al., 2017).

The Mekong River is one of the most prominent transboundary rivers in Southeast Asia, extending across a length of approximately 4,909 km from its source on the Tibetan Plateau to the South China Sea (Soukhaphon et al., 2021). It flows through six countries: China, Myanmar, Lao PDR, Thailand, Cambodia, and Vietnam, with a mean annual streamflow of 14,500 m^3/s (Mekong River Commission-MRC, 2010; Wang et al., 2017). The basin is home to one of the most diverse biomes globally, with over 20,000 plant species and 850 fish species identified to date (MRC, 2023). About 80% of the nearly 65 million inhabitants of the Lower Mekong River Basin (LMB) rely on the river and its resources for their livelihoods, including 47-80% of their necessary protein intake (Hortle, 2007; MRC, 2023). Within LMB lie the three primary tributaries and major contributors of flow: Sekong, Sesan, and Srepok, collectively known as the 3S rivers. With an average annual flow of 2,890 m^3/s, the 3S rivers contribute approximately 17-20% of the Mekong's total flow and 5-15% of its suspended sediment discharge (Wild et al., 2014). They are also important for aquatic biodiversity, ecosystem services, and fish production in the LMB (Piman et al., 2016).

The LMB is undergoing two significant changes, which are the expansion of hydropower dam construction and climate change. The rapid economic growth in the riparian nations has led to extensive plans for hydropower construction. As of 2019, there are 89 hydropower projects in the LMB with a total installed capacity of 12,285 MW (MRC, 2023). This expansion has raised concerns about increased water resource usage (Piman et al., 2013), and its potential impacts on livelihoods, and ecosystems (Baran & Myschowoda, 2009; Ziv et al., 2012; Intralawan et al., 2018). Furthermore, Yusuf and Francisco (2009) identified the LMB as one of the world's most

susceptible areas to climate change. Climate change is predicted to alter monsoon and precipitation patterns and to elevate temperatures within the basin (Lauri et al., 2012; MRC, 2023).

Studies in the Mekong Basin reveal that existing dams have caused significant hydrological changes. Phung et al. (2021) observed post-1995 reductions in the river's average water level, despite no change in cumulative rainfall in the Mekong Basin after the first hydropower dam's operation. Hecht et al. (2019) found that dams modify downstream seasonal flow variability, which could be mitigated or exacerbated by climate change. Research by Räsänen et al. (2016) found that the Lancang-Jiang cascade, the largest hydropower dam cascade in the Upper Mekong, increased dry season streamflow by 34-155% and decreased wet season streamflow by 29-36%, narrowing hydrological variability within dry and wet season months. Hong et al. (2013) observed that the Yali Falls dam on the Sesan River caused unprecedented and erratic flow fluctuations, damaging crops, fisheries, and livelihoods. Lauri (2012) emphasized the importance of cumulative impact assessments, noting that reservoir operations are more influential than climate change on the Mekong's hydrograph, especially during the dry season and in terms of flood pulse parameters. While dams can significantly alter hydrological regimes, there are recognized ways to mitigate these impacts through modifications to dam operation rule curves and river basin restorations (Richter & Thomas, 2007; Postel & Richter 2003).

1.2. Problem Statement

Hydropower dam construction in the LMB exacerbated by climate change has introduced complex trade-offs between energy production and ecosystem disruption (Richter & Thomas, 2007; Intralawan et al., 2018). The Sesan River, a major tributary of the LMB has been profoundly transformed by hydropower dams (MRC, 2023), but its hydrology remains poorly understood (Pokhrel et al., 2018; Hecht et al., 2019; Gunawardana et al., 2021). This study assesses the

hydrological changes in the Sesan River Basin, considering the interactions between hydropower dams and potential climate change.

1.3. Objectives of the Study

The primary objective of this study is to assess the streamflow alterations in the Sesan River resulting from the operation of hydropower dams and from potential climate changes. The specific objectives are:

1. To determine the streamflow alterations resulting from hydropower dams.
2. To determine the streamflow alterations resulting from projected climate changes.
3. To determine the streamflow alterations resulting from the combined impact of dams and climate changes.

Chapter 2

Literature Review

This chapter reviews and synthesizes literature relevant to hydrology, hydropower dams, climate change, climate models, hydrological modeling, and environmental flow assessment.

2.1. Impact of Dams on River Hydrology

Dams play a crucial role in water resource management by providing storage capacity that regulates water availability for various purposes including hydropower generation. However, the hydrologic alteration they cause has negative impacts on river ecosystems and ecosystem services. One of the most significant effects of dams is the alteration of natural flow regimes (Poff et al., 1997; Richter & Thomas, 2007). Since dams retain and release water in ways that differ from the natural variability of unregulated rivers, they disrupt the timing, magnitude, and frequency of naturally occurring flow events that have regulated river species and ecosystems (Poff et al., 1997). As a result, downstream ecosystems face modified flood pulses, which can disrupt plant and animal life that are adapted to historical flow patterns (Postel & Richter, 2003; Richter & Thomas, 2007). The alteration of natural flow patterns by these dams can also lead to changes in water temperature, which can affect aquatic ecosystems that are sensitive to temperature variations (Richter & Thomas, 2007).

In the context of the LMB, where seasonal flows sustain livelihoods and ecosystems (Baran & Myschowoda, 2009; Ziv et al., 2012), the impacts of dams on hydrology are particularly relevant. Over the last decade, there has been a rapid expansion of hydropower dams (MRC, 2023), leading to tradeoffs between energy production and adverse consequences such as disruptions to ecosystems and displacement of communities (Intralawan et al., 2018).

2.2. Impact of Climate Change on River Hydrology

The IPCC AR6 (2021) has reported that human activities since the Industrial Revolution have caused climate change, which is evident in rising temperatures, changing precipitation patterns, and weather extremes, such as heatwaves, heavy precipitation, and droughts. This impact is further reflected in the concentrations of key Greenhouse Gases (GHGs) such as carbon dioxide (CO_2), methane (CH_4), and nitrous oxide (N_2O), which have surged by 47%, 156% and 23%, respectively, since 1750 (IPCC, 2021).

Trang et al. (2017) found that climate change introduces uncertainties into hydrological processes, making them less predictable and reliable. This poses challenges in sustainable water resource management and planning (Richter & Thomas, 2007; Trang et al., 2017), and underscores the need for comprehensive understanding of climate change and its impacts (Hecht et al., 2019).

2.3. Climate Models

Climate models are numerical representations of the Earth's climate system based on its physical, chemical, and biological components, their interactions, and known attributes. They employ mathematical equations to simulate the interactions of the atmosphere, ocean, and land surface (IPCC, 2018). Climate models are used for a variety of applications, including assessing the impacts of human activities on climate, reconstructing historical climate data, and projecting future climate scenarios (Flato et al., 2013; Hartmann, 2016). There are five basic types of climate models as described below:

2.3.1. Energy Balance Models (EBM)

Energy Balance Models (EBM) are zero-dimensional (0D) climate models that represent the Earth's climate system with a single variable, the global temperature. EBMs are based on the principle of energy balance, which states that the Earth's temperature is determined by the balance

between incoming and outgoing radiation (IPCC, 2014).

2.3.2. Radiative-Convective (RC) and Single-Column Models (SCM)

Radiative-Convective (RC) and Single-Column Models (SCM) are one-dimensional (1D) climate models that represent a single vertical column of the atmosphere. RC models assume radiative-convective equilibrium and include energy transfer through radiation and convection. It can be used to study how increasing levels of CO_2 and other GHGs affect the Earth's temperature (Mackay & Khalil, 1991). SCM is a simplified numerical representation of a single grid column within a General Circulation Model (GCM) and often used to evaluate the performance of a set of model physics (Energy Exascale Earth System Model-E3SM, 2023).

2.3.3. Dimensionally Constrained Models

The dimensionally constrained models include several types of models such as the Statistical-Dynamical (SD) model, Earth System Model of Intermediate Complexity (EMIC) and Integrated Assessment Model (IAM) (IPCC, 2007). SD models focus on Earth surface processes and dynamics within a zonal average framework. EMICs combine several geographical structures such as oceans, ice features, and land types to describe the climate with moderate spatial and temporal detail. IAMs couple the climate system with economic models to assess the impact of policy choices on emissions.

2.3.4. Global Circulation Models or General Circulation Models (GCM)

Global Circulation Models (GCMs) are complex three-dimensional (3D) climate models that simulate the Earth's climate system by representing physical atmospheric and oceanic processes, based on the laws of physical and thermodynamics (IPCC, 2007; Tabari, 2021).

2.3.5. Earth System Models (ESM)

Earth System Models (ESMs) are a type of GCM that is more comprehensive and complex.

ESMs include the Earth system's chemical and biological processes in addition to the physical atmospheric and oceanic processes represented by GCMs (Hajima et al., 2014; Asch et al., 2016). This allows ESMs to capture the complex interactions driving the climate system (IPCC, 2021).

2.4. Climate Change Scenarios

Climate change scenarios are plausible future trajectories that were developed to study the potential effects of human-induced climate change (IPCC, 2007). They describe potential future developments influenced by key drivers such as demography, economics, technology, governance, and lifestyle (IPCC, 2000; Rounsevell & Metzger, 2010; O'Neill et al., 2014). Climate change scenarios can also be described by geophysical factors such as GHG emissions, emission of aerosols, and land use trends, providing a "what-if" perspective on potential consequences rather than deterministic predictions, which are subject to quantitative uncertainties (Moss et al., 2010). These scenarios are essential for developing strategies to address climate change and its associated risks. They aid in understanding the potential consequences of current choices in the face of uncertainty (Riahi et al., 2017). Climate change scenarios can be classified into three categories:

2.4.1. Synthetic Scenarios

Synthetic scenarios are the simplest kind of scenarios, where meteorological variables are directly adjusted to specific values (IPCC, 2007). These scenarios are often used in sensitivity studies as they are easy to create and produce results quickly. However, this method does not produce a realistic future climate due to its arbitrary nature (Santoso et al., 2008).

2.4.2. Analogue Scenarios

Analogue scenarios compare future climates to previously known regimes, either spatially or temporally. However, this approach can be problematic due to other factors, such as varying soil type and geography between different locations (Lough et al., 1983; Parry & Carter, 1988).

2.4.3. GCM Scenarios

GCM scenarios are physically based climate scenarios that are both spatially and temporally explicit. IPCC issued IS92 as its first set of scenarios in 1992. In 2000, the IPCC released a second set of scenarios, known as the Special Report on Emissions Scenarios (SRES). SRES scenarios A1, A2, B1, and B2 were the first to emphasize socioeconomic scenario themes, as well as other GHGs, land use change, and aerosols (IPCC, 2007; Moss et al., 2010). The Representative Concentration Pathways (RCPs) evolved from SRES in 2014, providing emissions and concentration data for various GHGs and aerosols (Taylor et al., 2012; IPCC, 2014). The Shared Socioeconomic Pathways (SSPs), introduced in 2016, enhance scenario understanding by connecting socioeconomic themes with climate modeling (Riahi et al., 2017).

SSPs depict potential socioeconomic trajectories, incorporating varying degrees of sustainable growth, regional rivalry, inequality, fossil-fuels expansion, and moderate progress. It uses a multi-model approach to project varying outcomes in energy, land use, and emission trajectories. These scenarios project global energy consumption and CO_2 emission ranges until 2100, alongside contrasting land-use change dynamics. *Table 2.1* presents a comparison of SSP and RCP scenario. The temperature anomaly is relative to the baseline period 1850-1900 (Riahi et al., 2017; IPCC AR6, 2021).

2.5. Model Data Downscaling

GCMs produce results at coarse temporal and spatial scales, with the latter varying between 100 and 300 km (Tabari et al., 2021). This limitation can pose challenges for studies that require finer-scale information, such as investigation of extreme weather events or the effects of climate change on local ecosystems (Trzaska & Schnarr, 2014). Therefore, to improve the resolution of GCM outputs and make it more realistic at a finer scale, coarse-scaled projections are downscaled.

Downscaling is a valuable tool for providing localized and fine-scale climate information. Spatial downscaling involves generating finer-resolution (<50 km) spatial climate information from coarser-resolution GCM output. Temporal downscaling focuses on deriving finer-scale temporal information, such as deriving daily rainfall data from monthly aggregated rainfall data. Two main approaches of downscaling are dynamical and statistical downscaling.

Table 2.1: *Summary of SSP scenarios and comparison with RCP scenarios*

SSP Scenario		Description	Temperature anomaly (°C)	RCP Equivalent
SSP1: Sustainability-Taking the Green Road (Low challenges to mitigation and adaptation)	SSP1-1.9	Very low end of the range of scenarios and net zero CO_2 emissions by mid-century.	Above 1.5	None
	SSP1-2.6	Low societal vulnerability and forcing, significant land use change, and net zero CO_2 emissions in the latter half of the century.	Below 2.0	RCP2.6
SSP2: Middle of the Road (Medium challenges to mitigation and adaptation)	SSP2-4.5	Intermediate societal vulnerability and forcing level combination	Between 2.7 to 3.4	RCP4.5 and, until 2050 also RCP6.0
SSP3: Regional Rivalry-A Rocky Road (High challenges to mitigation and adaptation)	SSP3-7.0	High societal vulnerability and forcing level combination, accompanied by significant land use change.	Between 3.0 to 4.9	Between RCP6.0 and RCP8.5
	SSP3-7.0-lowNTCF	Intermediate to high reference scenario SSP3-7.0, with potential CH4 and/or black carbon mitigation.	Between 2.1 to 4.7	Between RCP6.0 and RCP8.5
SSP4: Inequality-A Road Divided (Low challenges to mitigation, high challenges to adaptation)	SSP4-3.4	Fills low-end forcing gap with intermediate societal vulnerability.	Above 2.0	Between RCP 2.6 and RCP 4.5
	SSP4-6.0	Fills medium forcing range with intermediate societal vulnerability.	3.0	RCP 6.0
SSP5: Fossil-fueled Development-Taking the Highway (High challenges to mitigation, low challenges to adaptation)	SSP5-8.5	High societal vulnerability with high forcing level.	Above 4.9	RCP8.5
	SSP5-3.4-Overshoot (OS)	Simulates no mitigation until 2040, then rapid emissions reduction to zero by 2070.	Above 2.0	None, until 2040 similar to RCP8.5

2.5.1. Dynamical Downscaling

Dynamical downscaling employs Regional Climate Models (RCMs), which have higher spatial and temporal resolutions than GCMs. RCMs use GCMs as boundary conditions and physical principles to reproduce local climate features, such as temperature, precipitation, and wind patterns. However, since RCMs are nested within GCMs, the accuracy of their output relies on the GCM's large-scale forcing and reflects GCM biases. RCMs are also computationally intensive and only available for some regions (Maraun et al., 2010; Seaby et al., 2013; Trzaska & Schnarr, 2014).

2.5.2. Statistical Downscaling

Statistical downscaling uses statistical relationships to relate large-scale GCM output to local-scale climatic variables. For example, large-scale historical GCM output can be used with local-scale observations from a meteorological gage to produce high-resolution climate projections (Tabari et al., 2021). Statistical downscaling can provide site-specific climate estimates that RCMs cannot. However, this technique relies on the assumption that the relationship between large-scale circulation and local climate remains consistent in the future (Zorita & Storch, 1999), which is challenged by climate non-stationarity (Milly et al., 2008).

2.6. Bias Correction

Climate models are currently the most important source of information for projecting future climate dynamics and impacts, however, they exhibit systematic errors in their outputs due to limited spatial resolution, approximated physical and thermodynamic processes, and numerical parameterizations inside the model. These errors or biases are the relative discrepancies between simulated data and observed data. Correcting these biases is essential to improve the accuracy and

reliability of climate projections (Varis et al., 2004; Christensen et al., 2008; Teutschbein & Seibert, 2010). Different types of bias correction methods are discussed below:

2.6.1. Delta Change Method (DC)

The Delta Change (DC) method uses future changes simulated by GCMs to perturb observed data, instead of using the GCM simulations directly. Daily precipitation is corrected with a multiplying factor, which is the ratio of long-term monthly mean of model simulated future and historical data. Daily temperature is corrected with an additive factor, which is the difference between long-term monthly mean of model simulated future and historical data (Teutschbein & Seibert, 2012; Mendez et al., 2020). The DC method preserves the shape of the monthly distribution. It assumes that the local model biases are constant over time and thus, does not allow adjustments for intense weather occurrences, such as intense precipitation (Middelkoop et al., 2001; Räty et al., 2014).

2.6.2. Linear Scaling Method (LS)

The Linear Scaling (LS) method matches the monthly mean of model simulated data to the monthly mean of observed data (Teutschbein et al., 2012; Shrestha et al., 2018). Precipitation is corrected with a multiplying factor, which is the ratio of long-term monthly mean of observed and model simulated historical data. Temperature is corrected with an additive factor, which is the difference between long-term monthly mean of observed and simulated historical data.

2.6.3. Local Intensity Scaling (LOCI)

The Local Intensity Scaling (LOCI) method adjusts the intensity and frequency of model simulated precipitation data to match the observed distribution of wet-day frequencies and precipitation intensities (Schmidli et al., 2006; Luo et al., 2018).

2.6.4. Power Transformation of Precipitation (PTR)

The Power Transformation of Precipitation (PTR) method corrects the variance of model precipitation data using a power parameter estimated by matching the coefficient of variation of the corrected model precipitation data with the coefficient of variation of the observed precipitation data (Leander & Buishand, 2007; Luo et al., 2020). PTR can correct for bias in both the mean and the variance of the precipitation data (Luo et al., 2018).

2.6.5. Variance scaling of temperature (VST)

Variance scaling of temperature (VST) method corrects the temperature variance of model simulations to match observed temperature variance. VST can correct for bias in both the mean and the variance of the temperature data (Luo et al., 2018).

2.6.6. Quantile Mapping (QM)

Quantile Mapping (QM) a non-parametric method that uses a statistical relationship between the cumulative distribution functions (CDFs) of observed and model simulated data to adjust the climate model outputs (Maraun, 2013; Qian, 2021). A study by Zhao et al. (2017) found that QM is a highly effective method for correcting bias in raw GCM outputs. In another study by Satianesan et al. (2023), QM outperformed simpler bias correction methods that only corrected the mean or mean and variance of precipitation dataset.

2.7. Hydrological Modeling

Hydrological modeling is a simplified representation of a real-world hydrologic system, using mathematical equations and computer simulations to mimic its behavior. It is used to predict how a system will respond to changes in inputs, such as rainfall, and to understand the underlying physical processes (Sorooshian et al., 2008; Devi et al., 2015). Hydrological models are widely used in water and environmental resource management (Praskievicz & Chang, 2009). One

common type of hydrological model is the rainfall-runoff model. These models estimate the runoff as a function of watershed characteristics, such as rainfall, drainage area, soil properties, vegetation cover, and topography (Sitterson et al., 2017). Rainfall-runoff models can be classified based on their structure (physically based or conceptual), simulation period (event-based or continuous), treatment of spatial variation (lumped, semi-distributed or distributed), and treatment of input data (deterministic or stochastic) (Devi et al., 2015; Bartles et al., 2022). Some commonly used hydrological models are discussed below:

2.7.1. Hydrologic Engineering Centers-Hydrologic Modeling System (HEC-HMS)

The Hydrologic Engineering Centers-Hydrologic Modeling System (HEC-HMS) is a deterministic model that uses a combination of analytical model, advanced graphical interface, a data management system, and output visualization to simulate rainfall-runoff in watersheds. It is widely used for water supply planning, flood forecasting, and urban or natural watershed runoff assessment (Bajwa & Tim, 2002; Bartles et al., 2022).

2.7.2. Soil and Water Assessment Tool (SWAT)

The Soil and Water Assessment Tool (SWAT) is a spatially distributed model that simulates quality and quantity of surface to groundwater. It divides a watershed into subbasin, which are further divided into hydrologic response units (HRUs) that consist of homogeneous land use, soil characteristics and slope (Arnold et al., 2012; Kuti et al., 2021).

2.7.3. Topography-based hydrological MODEL (TOPMODEL)

The Topography-based hydrological (TOPMODEL) is a semi-distributed, physically based, variable-source area model. It simulates streamflow by computing storage deficit or water table depth, using the topographic wetness index and soil transmissivity (Nystrom et al., 2011).

2.7.4. Hydrologiska Byrans Vattenavdelning (HBV)

The Hydrologiska Byrans Vattenavdelning (HBV) is a semi-distributed conceptual model that can simulate runoff, groundwater flow recharge and actual evaporation as functions of actual water storage, and snow accumulation and melt. It divides the catchment into sub-catchments, which are further divided into elevation and vegetation zones (Bergström, 1976; Devi et al., 2015).

2.7.5. Precipitation-Runoff-Evapotranspiration Hydrologic response units (PREVAH)

The Precipitation-Runoff-Evapotranspiration Hydrologic response units (PREVAH) is a semi-distributed conceptual model that describes hydrological processes in mountainous environments. The model employs HRUs to provide insights into a variety of hydrological processes and applications (Krysanova et al., 2015; Horton et al., 2022).

2.7.6. MIKE Systeme Hydrologique Europeen (MIKE SHE)

MIKE Systeme Hydrologique Europeen (MIKE SHE) is a physically based model that can simulate a wide range of hydrological processes, including surface water flow, groundwater flow, evapotranspiration, and infiltration. (Waseem et al., 2020). It offers detailed simulations and results visualization through its pre-processing and post-processing modules (Devi et al., 2015).

2.7.7. Variable Infiltration Capacity (VIC)

The Variable Infiltration Capacity (VIC) is a semi-distributed, grid-based model that integrates energy and water balance equations. It simulates infiltration, runoff, and base flow using precipitation, temperature, and wind speed. VIC is well-suited for cold climate applications with its emphasis on soil moisture dynamics and heterogeneity (Gao, 2010; Devi et al., 2015).

2.7.8. Soil and Water Integrated Model (SWIM)

The Soil and Water Integrated Model (SWIM) is a physically based, semi-distributed, eco-hydrological model that simulates the interlinked processes of the hydrological cycle at the basin

scale. It divides the basin into smaller subbasins and hydrotopes with homogeneous land use, management, and soil units). SWIM can effectively simulate flow and extreme events in watersheds of all sizes (Krysanova et al., 2000; Devi et al., 2015).

2.8. Environmental Flow Assessment (EFA)

Environmental flows consider the quantity, frequency, timing, and quality of water and sediment that are essential for sustaining riparian ecosystems, estuaries, human livelihoods, and natural functions of rivers (The Nature Conservancy, 2009; Arthington et al., 2018). Natural seasonal fluctuations of low flows, high flow, and floods are necessary to support diversity in aquatic and riparian environments. However, human activities such as construction of dams disrupt the streamflow patterns and negatively impact the riverine organisms, ecosystems, and services (Poff & Schmidt 2016). Maintaining environmental flows is essential for the well-being of both nature and human communities. It can help to address the challenges posed by the water-energy-food nexus and climate change (King & Brown, 2018). The concept of environment flow requirements (EFR) is based on the recognition that aquatic ecosystems are adapted to natural flow conditions, and changes in flow regimes can have profound impacts on ecosystems (Dusting et al., 2017). EFA methods can be classified into four groups:

2.8.1. Hydrologic Index Methods

Hydrologic Index methods are the basis of many environmental flow assessment techniques and therefore widely used. They use historical streamflow data to determine the recommended flow regimes that sustain river ecosystems. These methods often focus on defining the minimum or fixed flows that preserve fisheries and other essential river ecology features (Cavendish & Duncan, 1986). This technique combines hydrological, biological,

geomorphological, and hydraulic criteria to determine the required flow (Tharme, 1996). Popular hydrological methods are discussed below:

2.8.2.1. Tennant Method (also known as the Montana Method) is a semi-empirical method for estimating environmental flows based on field observations and measurements of fish habitat quality. This method establishes a correlation between fish habitat quality and the percentage of average flow. However, its applicability may vary depending on the specific habitat requirements of different rivers (Tennant, 1976).

2.8.1.2. Tessman Method is a modification of the Tennant Method that adapts the latter's seasonal flow recommendations to local hydrologic and biologic conditions, including monthly variability. It is based on the percentage of the monthly median flows, and Tessman (1980) recommended that 30% and 50% of mean annual flow during two seasons (April to September and October to March) can maintain acceptable conditions for wildlife, fish, and recreation.

2.8.1.3. Flow Duration Curves (FDC) show the percentage of time a particular flow is equaled or exceeded over a period of consideration. FDCs provide information about the flow characteristics of a river and can be used to determine the time availability of any flow rate, which makes them a valuable tool for EFA (Karakoyun et al., 2018).

2.8.1.4. 7Q10 Method is a statistical method used to estimate the lowest seven-day average flow that occurs on average once every ten years. It calculates the seven-day low flow that has not been equaled in ten years, based on daily streamflow data. The 7Q10 method is commonly used to predict the minimum streamflow required to maintain water quality and to evaluate water quality protection and aquatic ecosystem preservation (Carpenter & Hayes, 1996).

2.8.1.5. Indicators of Hydrologic Alteration (IHA) evaluate hydrologic regimes in terms of their ecological significance using statistical metrics for flow magnitude, timing, and frequency.

This method establishes hydrologic restoration targets based on a natural hydrological regime, aiming to maintain aquatic ecosystems' natural composition, structure, and function. The Range of Variability Approach (RVA) within IHA can be used to compare pre- and post-impact flow records (Richter et al., 1996).

2.8.2. Hydraulic Rating Methods

Hydraulic rating methods establish correlations between in-stream resources and streamflow to quantify EFR. These methods include cross-section and transect-based techniques that correlate species-discharge relationships, leading to habitat or hydraulic rating techniques (Trihey & Stalnaker, 1985). A common technique is the wetted perimeter method, which relates changes in wetted perimeter with discharge to define the EFR (Tharme, 1996).

2.8.3. Habitat Simulation Methods

Habitat simulation methods (also known as habitat or microhabitat modeling) are used to predict the effects of changes in flow, water quality, and other environmental factors on aquatic habitats. These methods are based on the understanding that different fish species and other aquatic organisms have different habitat requirements (Tharme, 1996; Karakoyun et al., 2018).

2.8.4. Holistic Methods

Holistic methods consider all living and nonliving components of rivers in the EFA. This includes the river ecosystem, wetlands, and groundwater. It aims to preserve river morphology, sustain habitats, and protect all organisms in rivers, including social effects (Karakoyun et al., 2018).

Chapter 3

Methodology: Study Area and Data Collection

The methodology is divided into four chapters: Study Area and Data Collection, Hydrological Modeling, Climate Change Projection, and Computation of Hydrologic Alteration. These chapters detail the approaches, tools, and techniques used to achieve the study's objectives. The first chapter of the methodology provides descriptions and salient features of the study area, as well as the data collection process and analysis.

3.1. Study Area

This study focused on the transboundary Sesan River, a major tributary of the Mekong River that flows through both Vietnam and Cambodia. The Sesan River is 462 km long, with 237 km flowing through Vietnam before its confluence with the Srepok River in Cambodia. The basin is situated between latitude 21°30’ N-27°15’ N and longitude 93°30’ E-97°10’ E, covering an area of 18,890 km^2, with 11,260 km^2 in Vietnam and 7,630 km^2 in Cambodia (Meynell et al., 2014; Constable, 2015). The basin receives an annual average precipitation of 2,040 mm, with 80% of rainfall occurring during the wet season from May to November. Its streamflow pattern resembles that of the Mekong River, with a dry season flow from December to April and a wet season flow from May to November. The Sesan River's mean annual flow is 1,580 m^3/s, and it supports a population of approximately one million people (Meynell et al., 2014; MRC, 2017).

Figure 3.1 shows the Digital Elevation Model (DEM) map of the Sesan River Basin, prepared using the United States Geological Survey (USGS) DEM data at 1 arc-sec grid resolution. The basin's elevation ranges from 50 to 2,400 m above sea level, with the upper half being steep and rugged, while the lower half being relatively flat.

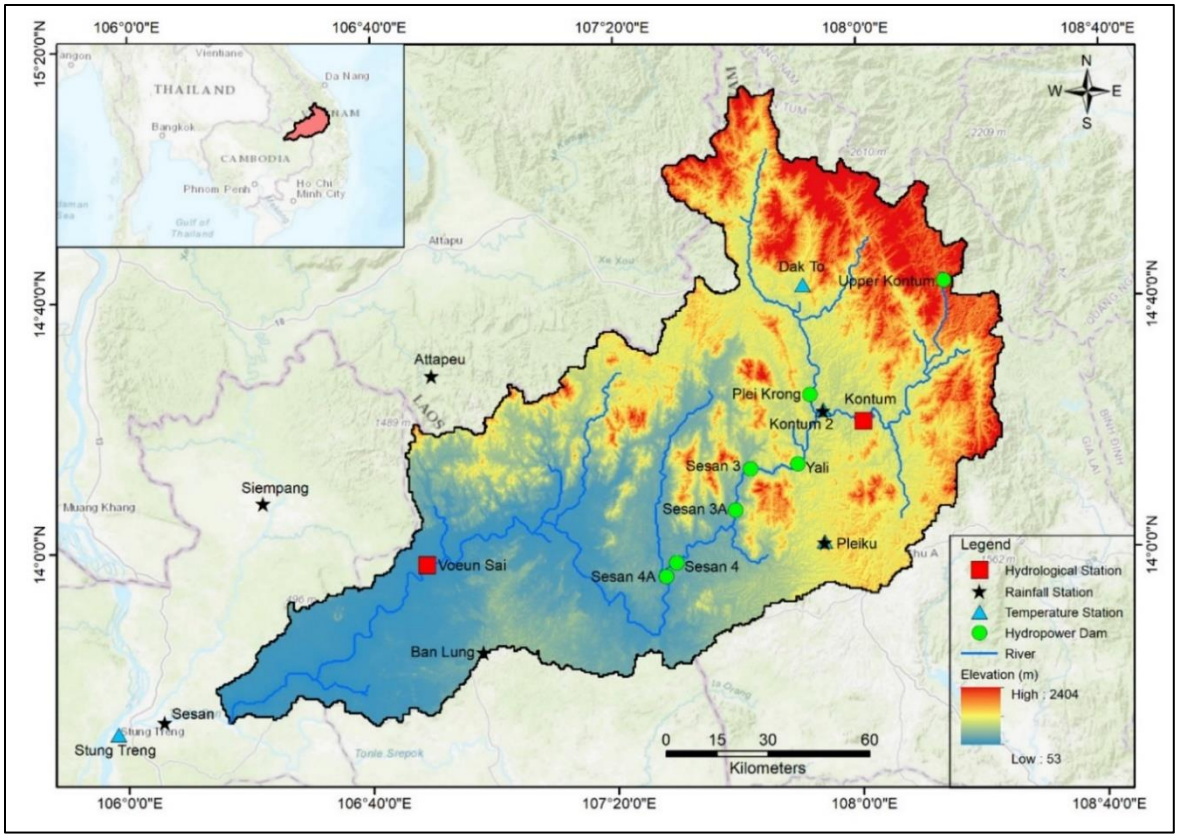

Figure 3.1: *Digital Elevation Model map of study area*

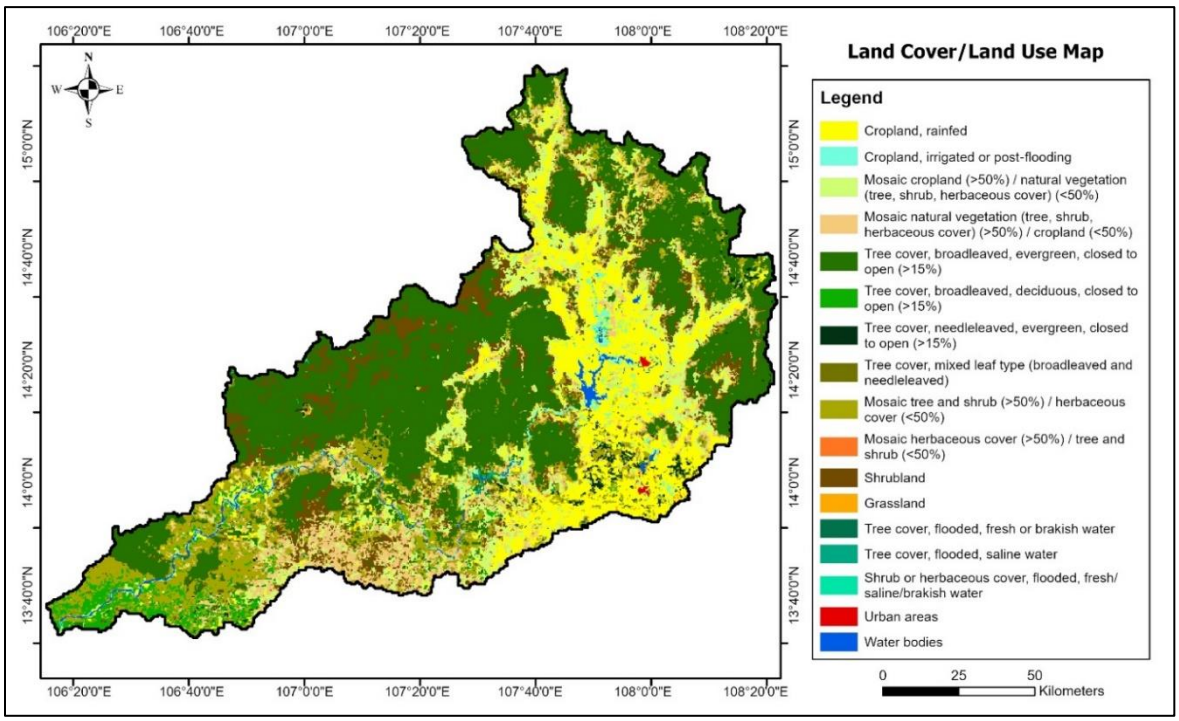

Figure 3.2: *Land Use/Land Cover map of study area*

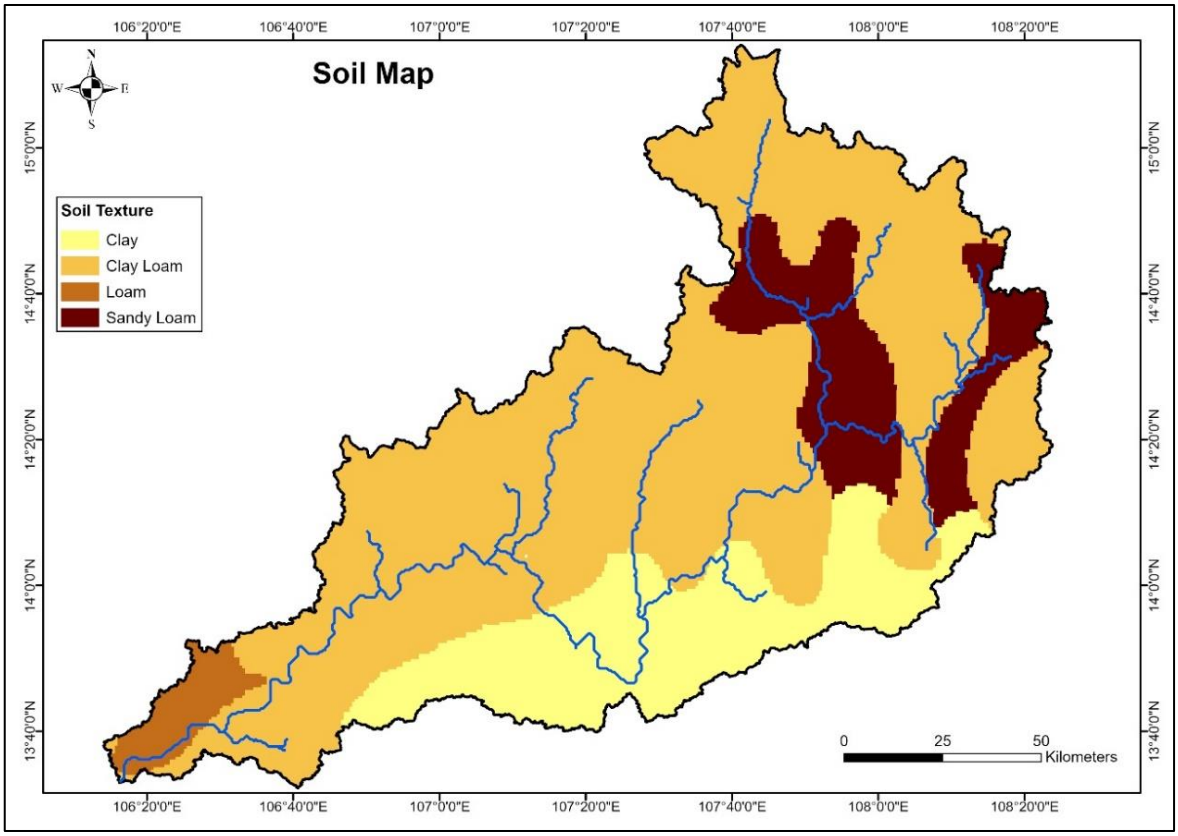

Figure 3.3: *Soil map of study area*

Figure 3.2 shows a land use/land cover map of the basin, prepared using the Food and Agriculture Organization (FAO) data at a 30 arc-second spatial resolution. The dominant land cover in the basin is forest, followed by cropland. *Figure 3.3* shows a soil map of the basin, prepared using ISRIC-World Inventory of Soil Emission Potentials (WISE) data at a 30 arc-second spatial resolution. The predominant soil type in the basin is clay loam, accounting for about 80% of the area.

3.1.1. Streamflow and Meteorological Data

There are two streamflow gages in the basin: Kontum Station located upstream and Vouen Sai Station located downstream of the cascade of dams. Daily observed streamflow data from these gages were used for calibration and evaluation of HEC-HMS. Meteorological data, including daily rainfall, minimum temperature, and maximum temperature, were obtained from seven rainfall and

four temperature gages located in and around the basin. The locations of these gages are shown in the study area DEM Map in *Figure 3.1*. The observed streamflow and metrological data were acquired from the Mekong River Commission Data Portal. *Table 3.1* presents a list of streamflow and meteorological gages along with the date range of data availability.

Table 3.1: *Streamflow and Meteorological gages*

Description	Station ID	Station	Frequency	Data availability period
Streamflow	100605	Kontum	Daily	1967-1971; 1984-2014
	440102	Voeun Sai	Daily	1965-1969; 2001-2014
Rainfall	140703	Pleiku	Daily	1965-1970; 1981-2015
	100605	Kontum-2	Daily	1966-1970; 1981-2015
	440102	Voeun Sai	Daily	1967-1968
	140705	Attapeu	Daily	1981-2015
	140603	Siempang	Daily	1981-2015
	130602	Ban Lung	Daily	1981-2015
	130605	Sesan	Daily	1981-2015
Temperature	14501	Stung Treng	Daily	1981-2015
	100605	Kontum-2	Daily	1981-2015
	140703	Pleiku	Daily	1981-2015
	140715	Dak To	Daily	1981-2012

3.1.2. Hydropower Dams

Table 3.2 provides a summary of the characteristics of the operational hydropower dams in the Sesan River Basin. These dams were commissioned between 2001 and 2011. Plei Krong has the largest active reservoir storage of 948 million m^3, followed by Yali with 779 million m^3. Yali was the first dam in the basin. Active storage capacity is the total amount of reservoir capacity available for release below the maximum storage level. It is the total reservoir capacity minus inactive storage (dead storage) capacity (NOAA, 2023). Design flow is the flow rate at which the turbine operates with maximum efficiency. It is the discharge that the dam is designed to release when the reservoir storage reaches active storage capacity (Piman et al., 2013; Meynell et al., 2014). Plei Krong, Yali, Upper Kontum and Sesan 4 provide more storage capacity during the dry season, while Sesan 3 and Sesan 3A operate as run-of-river dams. Sesan 4A is the lowest dam in

the cascade and serves as a flow regulating dam designed to balance out peak flows from the upstream dams. It operates with a drawdown of approximately 5 meters (Meynell et al., 2014). Except for Upper Kontum, all dams are situated along the main Sesan River. Upper Kontum dam is located on the Dak Nghe River, a tributary of the Sesan River.

Table 3.2: *Operational hydropower dams in Sesan River Basin (Source: MRC, 2022)*

Sl	Dam	Comission year	Catchment area (km^2)	Reservoir area (km^2)	Active storage (MCM[a])	Full supply level (masl[b])	Low supply level (masl)	Average flow (m^3/s)	Design flow (m^3/s)
1	Yali	2001	7,455	64.5	779.0	515	490	262	424
2	Sesan 3	2006	7,788	3.4	3.8	305	303	274	486
3	Sesan 3A	2007	8,084	8.8	4.0	239	239	283	500
4	Plei Krong	2009	3,216	53.3	948.0	570	537	128	368
5	Sesan 4	2010	9,326	58.4	264.2	215	210	329	719
6	Sesan 4A	2011	9,368	1.8	7.5	155	150	330	469
7	Upper Kontum	2011	350	8.6	122.7	1,170	1,146	15	31

[a] MCM is million cubic meters
[b] masl is meters above mean sea level

3.2. Methodology Conceptual Framework

The methodology used in this study is divided into four steps as illustrated in *Figure 3.4.*

1. Build a hydrological model using HEC-HMS without dams to simulate streamflows before dam constructions.
2. Build a HEC-HMS model with dams to simulate the streamflows after dam constructions.
3. Project the future climate trends using an ensemble of three ESMs from CMIP-6, under SSP2-4.5 and SSP5-8.5.
4. Assess the hydrologic alterations using RVA/IHA, under the following scenarios:
    i. Impact of existing hydropower dams only.
    ii. Impact of potential climate change only.
    iii. Combined impact of hydropower dams and potential climate change.

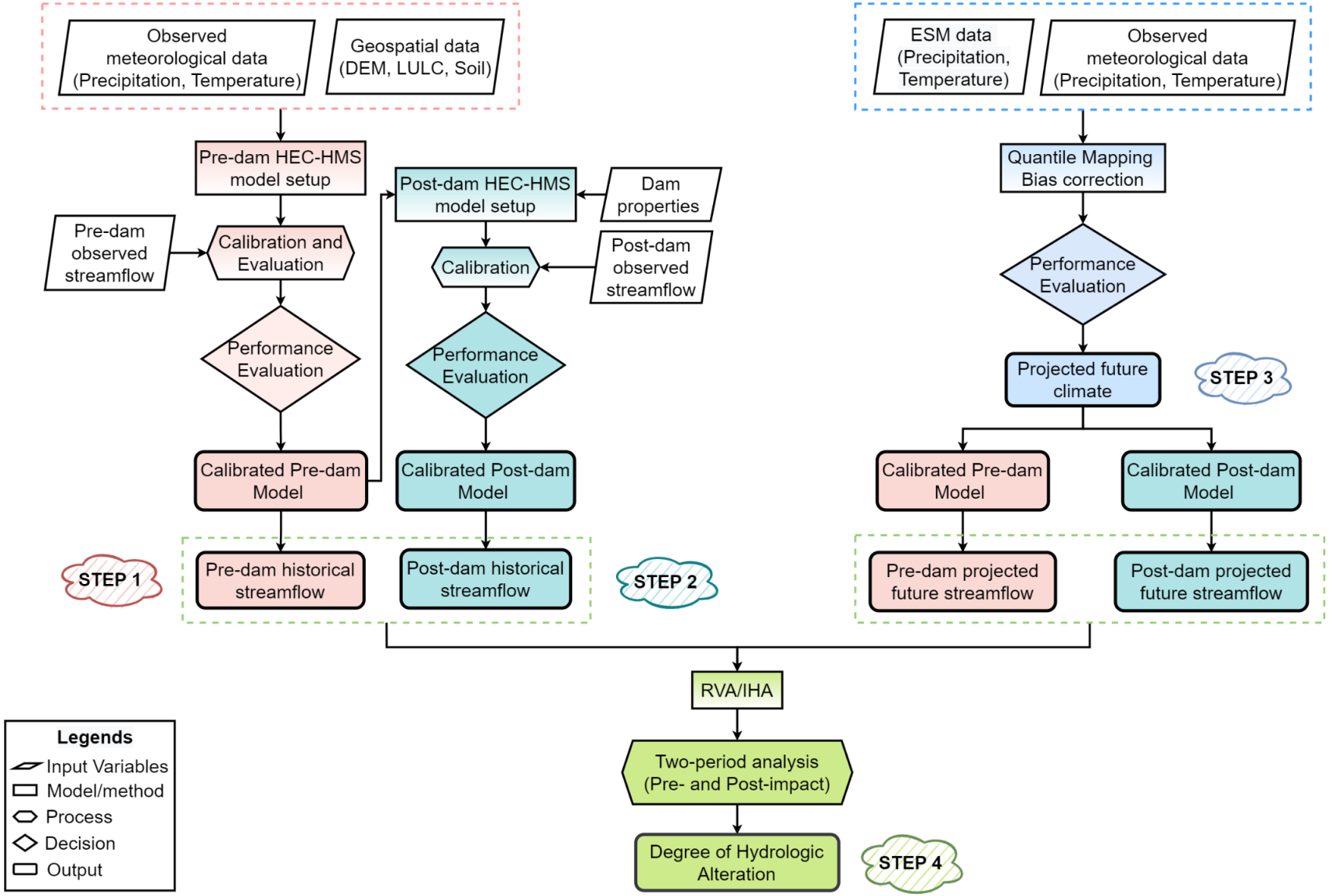

Figure 3.4: *Overall conceptual framework of methodology*

Chapter 4

Methodology: Hydrologic Modeling

The US Army Corps of Engineers' HEC-HMS was used to model the Sesan watershed and simulate streamflow. HEC-HMS represents watershed systems using elements such as sources, subbasins, reaches, junctions, reservoirs, and sinks, and simulates the precipitation-runoff-routing processes using different methods. The model structure and methods used in this study are described below:

4.1. Model Structure

A semi-distributed HEC-HMS model with smaller, homogeneous subbasins was used in this study. This allowed for a more refined representation of spatial variability within the basin, as uniform soil and vegetation characteristics were assumed within each subbasin (Sabol, 2008; Woolridge & Niemann, 2018). For the terrain data, a GIS raster file of USGS DEM at 1 arc-sec grid resolution, predefined with the Universal Transverse Mercator (UTM) Zone 48 North coordinate system was imported into HEC-HMS. This terrain data was then associated with a basin model. A shapefile with the Sesan watershed boundary was added to build walls so that the watershed delineations matched the input shapefile. Shapefiles of streamflow gages and hydropower dams were also added to precisely locate their positions in the basin model. The next steps involved preprocessing the terrain data to remove sinks, determine drainage directions, and calculate flow accumulations. The “identify streams” tool was used to define the start points of streams for subbasin determination. Due to the large watershed area, a drainage accumulation threshold of 500 km^2 was applied to facilitate the delineation of multiple subbasins and reaches. These were further adjusted through manual splitting and merging of elements to ensure

homogeneous watershed characteristics. *Figure 4.1* shows the schematic of the disaggregated model. The two streamflow gages and basin outlet were used as computation points. *Tables 4.1* and *4.2* present the geometric characteristics of reaches and subbasins, respectively.

Figure 4.1: *Disaggregation of basin in HEC-HMS*

Table 4.1: *Geometric characteristics of reaches*

Reach	Length (km)	Slope (m/m)	Relief (m)	Sinuosity
Reach-1	7.6	0.0026	20	1.18
Reach-2	18.6	0.0005	9	1.38
Reach-3	17.3	0.0012	0	1.16
Reach-4	20.3	0.0132	268	1.41
Reach-5	16.9	0.0012	21	1.31
Reach-6	33.6	0.0016	55	1.44
Reach-7	6.2	0.0036	22	1.23
Reach-8	82.6	0.0003	23	2.30
Reach-9	59.7	0.0003	19	1.50
Reach-10	106.2	0.0004	44	1.42

Table 4.2: *Geometric characteristics of subbasins*

Subbasin	Area (km^2)	Basin slope (m/m)	Longest flowpath length (km)	Centroidal flowpath length (km)	10-85 flowpath slope (m/m)
Subbasin-1	3206.9	0.31	135.0	67.5	0.004
Subbasin-2	2976.3	0.27	135.8	48.1	0.007
Subbasin-3	466.4	0.17	49.6	21.4	0.004
Subbasin-4	754.0	0.19	63.6	16.2	0.003
Subbasin-5	330.7	0.23	72.8	36.1	0.009
Subbasin-6	288.9	0.31	35.0	15.0	0.013
Subbasin-7	1253.0	0.18	93.8	49.8	0.006
Subbasin-8	1566.0	0.26	108.6	53.8	0.002
Subbasin-9	41.7	0.13	18.1	6.1	0.007
Subbasin-10	1766.9	0.13	122.2	45.4	0.003
Subbasin-11	1386.0	0.31	121.8	49.9	0.005
Subbasin-12	2344.7	0.20	122.0	42.0	0.003
Subbasin-13	2538.5	0.07	142.7	64.6	0.000

4.2. Meteorologic Model

The meteorologic model in HEC-HMS calculates the precipitation for each subbasin element. Snowmelt was not modeled because the Sesan watershed does not receive any snowfall.

4.3. Precipitation Method

The Inverse Distance Weighting (IDW) method was used to model precipitation. This method calculates subbasin average precipitation by applying an inverse distance interpolation, which assumes that closer rainfall gage data are more representative of the subbasin. The coordinates of the subbasin centroid were estimated using ArcGIS. For the period 1965-1969, rainfall data was available only from three gages: Pleiku, Kontum-2 and Vouen Sai. However, during 1984-2014, rainfall data from six gages were available. Any missing data were interpolated using the IDW method. The IDW method allows for the specification of index precipitations, which account for differences in the long-term average precipitation received at different gages. The index precipitation, presented in *Table 4.3,* was estimated as the mean of historical annual rainfall observed at respective gages.

Table 4.3: *Index precipitation (in mm)*

Period	Rainfall Gage						
	Kontum-2	Pleiku	Vouen Sai	Attapeu	Ban Lung	Siempang	Sesan
1965-1969	1447	2481	2159	-	-	-	-
1984-2000	1923	2817	-	2263	1959	1924	1845
2001-2014	1973	2121	-	2170	2034	1661	1482

4.4. Evapotranspiration Method

Potential evapotranspiration (PET) is the maximum amount of water that can be depleted from a land surface through evapotranspiration (ET), which is the sum of evaporation and transpiration, given abundant soil moisture (Amatya et al., 2014). If data for solar radiation, relative humidity, and wind speed are missing, the FAO recommends using the 1985 Hargreaves equation as a reliable alternative to accurately estimate PET. In HEC-HMS, PET is computed as (Hargreaves & Samani, 1985):

$$PET = 0.0023 \times R_a \times (TC+17.8) \times TR^{0.50} \quad (4.1)$$

where R_a is the extraterrestrial radiation, which is the amount of solar radiation that reaches the top of Earth's atmosphere. It is calculated as a function of latitude, date, and time of day.

TC is mean daily temperature in °C

TR is daily temperature range in °C ($TR = T_{max}$-T_{min})

The longitude at the center of the basin, 105°, was used as the central meridian degree. Since observed temperature data were unavailable for the pre-dam period (1965-1969), data from the National Oceanic and Atmospheric Administration (NOAA) NCEP-NCAR Reanalysis-1 Project were used after downscaling the global dataset to the scale of the temperature gages.

4.5. Process Representation

HEC-HMS provides a variety of methods for simulating precipitation-runoff processes, each representing a different aspect of the hydrologic cycle, such as canopy interception, surface

infiltration, runoff losses, runoff transformation, baseflow, and routing. The methods used in this study are discussed below:

4.5.1. Canopy Method: Simple Canopy

The canopy method in HEC-HMS models the interception of precipitation by vegetation (Bartles et al., 2022). The Simple Canopy approach was selected due to its ease of use and fewer input parameter requirements. In this method, rainfall is stored in the canopy until it reaches its maximum capacity. Once the canopy storage capacity is filled, any additional precipitation is assumed to run off the surface or infiltrate into the soil (Bartles et al., 2022).

4.5.2. Surface Method: Simple Surface

The surface method in HEC-HMS models the storage and infiltration of precipitation on the ground surface. The Simple Surface method was selected as it is a simple representation of soil surface and is most appropriate for use with the available data. This method accounts for depression storage by representing the accumulation of excess precipitation on the ground surface until its capacity is reached. When the storage capacity is reached, and the rate of precipitation through-fall exceeds the rate of infiltration, surface runoff begins (Bartles et al., 2022).

4.5.3. Loss Method: Soil Moisture Accounting (SMA)

Precipitation that is not intercepted by vegetation canopies and surface depressions may infiltrate into the soil or run off the surface. The loss method in HEC-HMS estimates the amount of precipitation that infiltrates the soil from the land surface. The Soil Moisture Accounting (SMA) method was selected for this study. SMA uses three layers to represent the continuous movement and storage of water within the soil profile: soil storage, upper groundwater, and lower groundwater. Water leaves the soil storage and enters the groundwater layer via percolation (Bartles et al., 2022). For simplicity, only one layer of groundwater was considered, with water

percolating out of the groundwater layer entering the baseflow. SMA requires specification of ten parameters: initial soil storage, initial groundwater storage, maximum infiltration rate, impervious area, maximum soil storage, tension storage, soil percolation rate, maximum groundwater storage, groundwater percolation rate, and groundwater coefficient.

4.5.3.1. Initial Soil Storage is the percentage of soil that is filled with water at the beginning of a simulation (Bartles et al., 2022).

4.5.3.2. Initial Groundwater Storage is the amount of water that is stored in the groundwater layer at the beginning of a simulation (Bartles et al., 2022).

4.5.3.3. Maximum Infiltration Rate is the highest rate at which water can enter the soil layer (Bartles et al., 2022).

4.5.3.4. Percent Impervious Area represents the fraction of subbasin covered by impervious surfaces. All precipitation in this area becomes excess precipitation and contributes to direct runoff (Bartles et al., 2022).

4.5.3.5. Maximum Soil Storage is the total available storage capacity in the soil layer, including both tension and gravity storage (Bartles et al., 2022).

4.5.3.6. Tension Storage is the water storage in the soil that does not drain under the effects of gravity and is only removed through ET. Percolation from the soil layer to the groundwater layer will only occur whenever the current soil storage exceeds the tension storage. Therefore, tension storage must be less than the soil storage (Bartles et al., 2022).

4.5.3.7. Soil Percolation Rate is the maximum rate at which water exits the soil layer and enters the groundwater layer (Bartles et al., 2022).

4.5.3.8. Maximum Groundwater Storage is the maximum water capacity that the groundwater layer can hold (Bartles et al., 2022).

4.5.3.9. Groundwater Percolation Rate determines the maximum percolation from groundwater layer out of the system. It is influenced by the bedrock material, its jointing and weathering (Woolridge et al., 2020).

4.5.3.10. Groundwater Coefficient is used as the linear reservoir time constant to transform water in storage to lateral subsurface flow, which then becomes available as baseflow. It is similar to the linear reservoir time constant in the baseflow method, which controls the rate at which the released subsurface flow is routed to the subbasin outlet (Bartles et al., 2022).

4.5.4. Transform Method: Clark's Unit Hydrograph

The Transform method in HEC-HMS converts excess precipitation occurring at any point in the subbasin into direct runoff or streamflow at the subbasin outlet. It considers the time-area distribution of the watershed and the storage characteristics (Bartles et al., 2022). The Clark's Unit Hydrograph method was used in this study because it considers natural storage in the subbasin through a linear reservoir. This method uses the concept of an instantaneous unit hydrograph to route excess precipitation to the subbasin outlet. It explicitly represents two crucial processes in transforming excess precipitation into runoff: translation (movement of excess precipitation from its origin throughout the drainage network to the watershed outlet) and attenuation (reduction of flow as it is stored across the entire watershed) (Clark, 1945).

4.5.5. Baseflow Method: Linear Reservoir

Baseflow is the continuous flow in perennial streams that occur even when there has been no recent precipitation. It is produced by the subsurface flow discharging into the stream. The actual subsurface flow is calculated by a baseflow method (Bartles et al., 2022). The Linear Reservoir Baseflow model was used in conjunction with the SMA model to simulate the baseflow because it is the only baseflow method in HEC-HMS that conserves mass within the subbasin. The

outflow from the groundwater layer of the SMA is the inflow to the linear reservoir. Only one reservoir was used in this study for simplicity.

4.5.6. Routing Method: Muskingum-Cunge

River routing involves transferring flow through channel reaches and is essential for combining flows from the upper and lower subbasins. Routing methods calculate a downstream hydrograph based on an upstream hydrograph (Bartles et al., 2022). The Muskingum-Cunge Routing method was selected for routing because it accounts for both the lag and attenuation of the hydrograph as it moves through the reach (Woolridge & Niemann, 2018). This makes it suitable for overbank flows during extreme events, and for a wide range of channel slopes and depths (Feldman, 2000).

4.6. Parameter Estimation

4.6.1. Canopy Method: Simple Canopy

The simple canopy model requires estimation of three parameters: initial canopy storage, maximum canopy storage, and crop coefficient. The parameters used for this method are presented in *Table 4.5*. The initial storage was set to zero, assuming there is no water present in the canopy before the start of the simulation. The maximum canopy storage depends on the vegetation cover type and is expected to vary with the density of vegetation cover (Sabol, 2008; Irvin et al., 2023). The land use/land cover data obtained from the FAO database at a spatial resolution of 30 arc-sec was used to identify the dominant vegetation cover type in each subbasin. The vegetation cover types were then compared to *Table 4.4: Common Canopy Storage Values (Zinke, 1967)*, and their corresponding storage values were used to represent the vegetation canopies in each subbasin. The default crop coefficient of 1.0 was used and calibrated later. The canopy was set to perform ET

during both dry and wet periods, and the tension reduction method was used as the uptake method for extraction of water from the soil.

Table 4.4: *Common canopy storage values (Zinke, 1967)*

Canopy description	Maximum storage (mm)
General Vegetation	1.3
Grasses and Deciduous Trees	2.0
Coniferous trees	2.5

Table 4.5: *Parameters for simple canopy method*

Subbasin	Initial storage (%)	Maximum storage (mm)	Crop coefficient
Subbasin-1	0	1.3	1
Subbasin-2	0	1.3	1
Subbasin-3	0	1.3	1
Subbasin-4	0	1.3	1
Subbasin-5	0	1.3	1
Subbasin-6	0	2.5	1
Subbasin-7	0	1.3	1
Subbasin-8	0	2.5	1
Subbasin-9	0	2.0	1
Subbasin-10	0	2.0	1
Subbasin-11	0	2.5	1
Subbasin-12	0	2.5	1
Subbasin-13	0	2.0	1

4.6.2. Surface Method: Simple Surface

The simple surface model requires estimation of two parameters: initial depression storage and maximum depression storage. The parameters used for the method are presented in *Table 4.6*. The initial storage was set to zero, assuming the surface is completely dry at the beginning of the simulation. The maximum depression storage represents the maximum amount of water that can be held on the soil surface before surface runoff begins. It is based on the physical surface characteristics of the subbasins. The storage values corresponding to the most dominant land cover type in each subbasin were taken from *Table 4.7: Common Depression Storage Values (Bennet, 1998)*, and calibrated later.

Table 4.6: *Parameters for simple surface method*

Subbasin	Initial storage (%)	Maximum storage (mm)	Subbasin	Initial storage (%)	Maximum storage (mm)
Subbasin-1	0	50.8	Subbasin-8	0	9.5
Subbasin-2	0	50.8	Subbasin-9	0	9.5
Subbasin-3	0	50.8	Subbasin-10	0	9.5
Subbasin-4	0	50.8	Subbasin-11	0	1.0
Subbasin-5	0	50.8	Subbasin-12	0	9.5
Subbasin-6	0	1.0	Subbasin-13	0	9.5
Subbasin-7	0	50.8			

Table 4.7: *Common depression storage values (Bennet, 1998)*

Surface description	Maximum storage (mm)
Most areas with impervious surface	4.8
Most areas with pervious surface	9.5
Flat agricultural land with Conservation tillage	50.8
Steep, Smooth slopes	1.0

4.6.3. Loss Method: Soil Moisture Accounting (SMA)

The SMA method parameters were estimated based on the soil data and are presented in *Table 4.8*.

4.6.3.1. Initial Soil Storage was estimated as the field capacity based on the soil type and calibrated later. The field capacity values were obtained from various USDA soil type following Saxton and Rawl (2006).

4.6.3.2. Initial Groundwater Storage was set to zero for simplicity and calibrated later.

4.6.3.3. Maximum Infiltration Rate, f was calculated using the Green-Ampt infiltration model (Green and Ampt, 1911):

$$f = K_{sat}\left(1 + \frac{\psi_f}{\delta}\right) \tag{4.2}$$

where K_{sat} = Saturated hydraulic conductivity

Ψ_f = Wetting front suction head

δ = Depth of wetting front selected

Values of K_{sat} and Ψ_f were estimated based on each subbasin's dominant soil texture using the texture class estimates proposed by Rawls et al. (1982). The depth of the wetting front, δ was chosen as 75 mm following Woolridge et al. (2020).

4.6.3.4. Percent Impervious Area was computed in ArcGIS using the FAO land use/land cover data. Total impervious area was calculated by dividing the total urban area by the total basin area. However, this method did not account for natural imperviousness, such as bedrock, or the fact that urban areas are typically not 100% impervious. Therefore, these values were calibrated.

4.6.3.5. Maximum Soil Storage, S_{max} was calculated using the equation suggested by Irvin et al. (2023). Specifically:

$$S_{max} = (1 - P_{GW})\, Z_{Soi}\, (\theta_{sat} - \theta_{wp}) \tag{4.3}$$

where P_{GW} = fraction of soil column above the restrictive layer dedicated to groundwater storage

Z_{soil} = Depth to any restrictive layer

θ_{sat} = Soil moisture content at saturation

θ_{wp} = Wilting point

Estimating P_{GW} is challenging as the thickness of the groundwater layer may vary between events. Thus, a value of P_{GW} = 0.10 was chosen, consistent with Irvin et. al (2021). Z_{soil} was used as 100 cm based on the soil profile layer depth used in ISRIC-WISE database. Values of θ_{sat} and θ_{wp} were estimated based on each subbasin's dominant soil texture and taken from the Texture Class Estimates proposed by Rawls et al., (1982).

4.6.3.6. Tension Storage, S_{ten} was estimated following Irvin et al. (2023). Specifically using:

$$S_{ten} = (1 - P_{GW})\, Z_{Soil}(\theta_{fld} - \theta_{wp}) \tag{4.4}$$

where θ_{fld} = field capacity; rest of the parameters are as defined for the previous equations.

4.6.3.7. Soil Percolation Rate was estimated assuming saturated conditions and gravity drainage (i.e., without a gradient in soil suction). Therefore, following Irvin et al. (2023), the percolation rate was assumed as K_{sat} of each subbasin's dominant soil texture, and calibrated.

4.6.3.8. Maximum Groundwater Storage, S_{GW} was estimated using the S_{GW} equation (Irvin et al., 2023):

$$S_{GW} = P_{GW} Z_{Soil} (\theta_{sat} - \theta_{wp}) \tag{4.5}$$

4.6.3.9. Groundwater Percolation Rate of 0.5 mm/h, as recommended by Woolridge et al. (2020) based on model performance was used and subsequently calibrated.

4.6.3.10. Groundwater Coefficient, T_{GW} of 20 h was assumed and subsequently calibrated.

Table 4.8: *Parameters for SMA method (GW is Groundwater)*

Subbasin	Initial soil content (%)	f (mm/hr)	Impervious (%)	S_{max} (mm)	S_{ten} (mm)	Soil percolation (mm/hr)	S_{GW} (mm)	GW percolation (mm/hr)	T_{GW} (hr)
Subbasin-1	34	16.0	0.04	237.6	126	2.3	26.4	0.5	20
Subbasin-2	34	16.0	0.38	237.6	126	2.3	26.4	0.5	20
Subbasin-3	21	102.5	1.26	317.7	99	25.9	35.3	0.5	20
Subbasin-4	34	16.0	0.05	237.6	126	2.3	26.4	0.5	20
Subbasin-5	34	16.0	0.25	237.6	126	2.3	26.4	0.5	20
Subbasin-6	34	16.0	0.00	237.6	126	2.3	26.4	0.5	20
Subbasin-7	36	6.3	0.01	184.5	81	0.6	20.5	0.5	20
Subbasin-8	34	16.0	0.00	237.6	126	2.3	26.4	0.5	20
Subbasin-9	36	6.3	0.00	184.5	81	0.6	20.5	0.5	20
Subbasin-10	36	6.3	0.02	184.5	81	0.6	20.5	0.5	20
Subbasin-11	34	16.0	0.00	237.6	126	2.3	26.4	0.5	20
Subbasin-12	34	16.0	0.00	237.6	126	2.3	26.4	0.5	20
Subbasin-13	34	16.0	0.03	237.6	126	2.3	26.4	0.5	20

4.6.4. Transform Method: Clark Unit Hydrograph

The translation of flow is provided as the time-area histogram given by (Bartles et al., 2022):

$$\frac{A_t}{A} = \begin{cases} 1.414\left(\frac{t}{T_c}\right)^{1.5} & for\ t \le \frac{T_c}{2} \\ 1 - 1.414\left(1 - \frac{t}{T_c}\right)^{1.5} & for\ t > \frac{T_c}{2} \end{cases} \tag{4.6}$$

where A_t = Cumulative watershed area contributing at time t

A = Total watershed area

T_c = Time of concentration

The Clark's method requires estimation of two parameters: Time of concentration, T_c and Storage coefficient, R. T_c represents the maximum travel time of excess precipitation from the furthest point in the basin to the outlet and is used in developing the translation hydrograph. It can be estimated using the watershed characteristics, and regression equation below (Bartles et al., 2022):

$$T_c = 2.2\left(\frac{L \times L_{ca}}{\sqrt{S_{10\text{ - }85}}}\right)^{0.3} \tag{4.7}$$

where L = Longest flow-path length

L_{ca} = Centroidal longest flow-path length

$S_{10\text{-}85}$ = Stream slope between points at 10- and 85-percent of total distance

R represents the extent to which attenuation occurs due to storage effects, and is commonly estimated by defining X as (Bartles et al., 2022):

$$X = \frac{R}{T_c + R} \tag{4.8}$$

Assuming X remains constant within a given region is the same as assuming (Irvin et al., 2023):

$$R = Z\,T_c \tag{4.9}$$

$$\text{where } Z \equiv \frac{X}{1-X} \tag{4.10}$$

This approach assumes that R increases with increasing subbasin size, consistent with Clark (1945), who considered the basin storage to occur mainly in the channels (Irvin et al., 2023). For simplicity, Z was set to 1, and R was set equal to T_c, and subsequently calibrated. *Table 4.9* provides the parameters used for Clark's method.

Table 4.9: *Parameters for Clark's unit hydrograph*

Subbasin	T_c (hr)	R (hr)	Subbasin	T_c (hr)	R (hr)
Subbasin-1	79	79	Subbasin-8	73	73
Subbasin-2	65	65	Subbasin-9	19	19
Subbasin-3	41	41	Subbasin-10	71	71
Subbasin-4	42	42	Subbasin-11	66	66
Subbasin-5	48	48	Subbasin-12	68	68
Subbasin-6	27	27	Subbasin-13	112	112
Subbasin-7	60	60			

4.6.5. Baseflow Method: Linear Reservoir

The parameters for linear reservoir were the same as those used for the SMA model. The estimated parameters are presented in *Table 4.10*.

Table 4.10: *Parameters for linear reservoir (GW is Groundwater)*

Subbasin	GW initial ($m^3/s/km^2$)	T_{GW} (hr)	Subbasin	GW initial ($m^3/s/km^2$)	T_{GW} (hr)
Subbasin-1	0	20	Subbasin-8	0	20
Subbasin-2	0	20	Subbasin-9	0	20
Subbasin-3	0	20	Subbasin-10	0	20
Subbasin-4	0	20	Subbasin-11	0	20
Subbasin-5	0	20	Subbasin-12	0	20
Subbasin-6	0	20	Subbasin-13	0	20
Subbasin-7	0	20			

4.6.6. Routing Method: Muskingum-Cunge

The Muskingum-Cunge routing method requires estimation of channel length, channel slope, channel roughness, floodplain roughness, and cross-section geometry. Channel length and slope were determined from the reach characteristics in HEC-HMS. The eight-point shape cross-section option was used to represent the channel and floodplain geometry, which was added as paired data in HEC-HMS. The cross-sections of the main channel and overbanks were developed using the DEM and "Interpolate Line function" in ArcGIS 3D Analyst. The main channel part of the cross-section was assumed to be rectangular, and the stream depth was estimated by substituting the average annual peak flow into Manning's equation. The estimated parameters for

Muskingum-Cunge method are presented in *Table 4.11*. Manning's roughness value of 0.035 was assigned for the main channel, following Chow's (1959) recommendation for major streams with irregular and rough sections. A roughness value of 0.04 was assigned to both the left and right bank floodplains, corresponding to land cover ranging from cultivated areas to scattered brush. The Manning's roughness coefficients were calibrated later.

Table 4.11: *Parameters for Muskingum-Cunge method*

Reach	Length (m)	Slope (m/m)	Manning's n	Left Manning's n	Right Manning's n
Reach-1	7608	0.0026	0.035	0.04	0.04
Reach-2	18599	0.0005	0.035	0.04	0.04
Reach-3	17269	0.0012	0.035	0.04	0.04
Reach-4	20286	0.0132	0.035	0.04	0.04
Reach-5	16878	0.0012	0.035	0.04	0.04
Reach-6	33613	0.0016	0.035	0.04	0.04
Reach-7	6185	0.0036	0.035	0.04	0.04
Reach-8	82587	0.0003	0.035	0.04	0.04
Reach-9	59731	0.0003	0.035	0.04	0.04
Reach-10	106170	0.0004	0.035	0.04	0.04

4.7. Reservoir

Presently, there are seven operational dams in the basin, constructed and made operational between 2000 and 2012. In HEC-HMS, dams were added to the model one by one, based on its reported completion date. The simulations involved the combination of a routing method and a storage method, which are discussed below:

4.7.1. Routing Method: Outflow Curve Routing

The reservoir routing uses the Modified Puls Routing method (also known as Level Pool Routing), which is based on the principles of conservation of mass, and a storage-discharge relationship to route flow from a reservoir.

4.7.2. Storage Method: Storage-Discharge

The initial storage of a dam represents the amount of water stored in it at the start of the simulation. Due to the lack of data on the specific start of operation dates for each dam, it was assumed that all dams began operating on January 1 of the year they were completed. The initial storage for each dam was calculated as the total volume of flow in January of the particular year, except for the two run-of-river dams (Sesan 3 and Sesan 3A), whose initial storages were set to zero due to their insignificant storage capacities. The calculated initial storage values for the dams are presented in *Table 4.12*. The storage-discharge relationship for each dam was developed externally assuming a linear relationship between their active storage and design flow.

Table 4.12: *Dam initial storage values*

Sl.	Reservoir	Completed year	Initial storage (1000 m^3)
1	Yali	2001	47,528
2	Plei Krong	2009	43,448
3	Sesan 4	2010	40,257
4	Sesan 4A	2011	15,722
5	Upper Kontum	2011	4,510

4.8. Flow Simulations before Parameter Calibration

The flow simulation periods were divided into three distinct time periods: i. Pre-dam period (before dams were constructed in the river basin) ii. Post-dam period (after the construction of dams), and iii. Future period (for forecasting flow in the future).

4.8.1. Pre-dam Simulation

A pre-dam model was set up using historical data from before dam construction began in the river basin (specifically, prior to 2001) and the parameters from Section 4.6. Streamflows were simulated at two streamflow gages, Kontum and Vouen Sai. The daily simulated streamflows were compared with the daily observed streamflows for 1985-2000 at Kontum and for 1965-1969 at Vouen Sai. The simulation periods were based on the availability of observed streamflow at each

streamflow gage. *Figures 4.2* and *4.3* presents streamflow comparisons in Kontum and Vouen Sai, respectively, before model calibration.

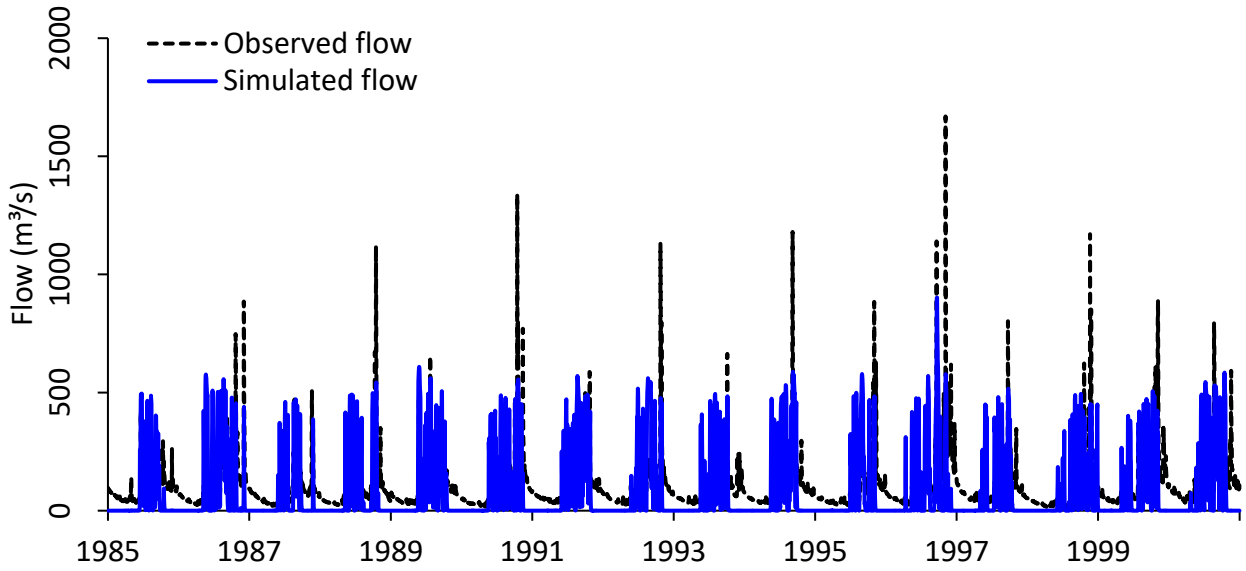

Figure 4.2: *Daily streamflow hydrographs for at Kontum before calibration*

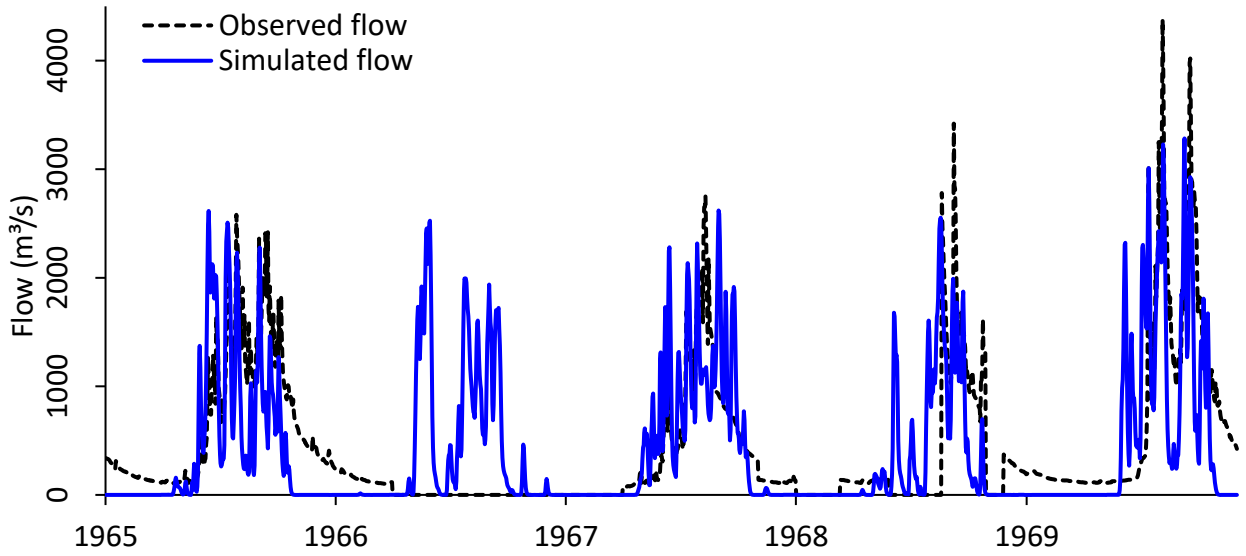

Figure 4.3: *Daily streamflow hydrographs for at Vouen Sai before calibration*

4.8.2. Calibration and Evaluation of Pre-dam Model

Before calibration, a sensitivity analysis was conducted by perturbing parameter values significantly to identify sensitive parameters affecting the model response. Once the sensitive parameters were identified, manual calibration was performed starting from the most upstream subbasin and progressing downstream. Calibration and evaluation of the pre-dam model was conducted at the two streamflow gages: Kontum and Vouen Sai. Based on the availability of observed streamflows, at Kontum, calibration was performed for a ten-year period from 1985 to 1995, with evaluation (or validation) for a five-year period from 1996 to 2000. At Vouen Sai, calibration was performed from 1965 to 1968, and evaluation (or validation) during 1969. Subsequently, automatic calibration was attempted using the Simplex method, which considers multiple parameters simultaneously. The objective function was set to minimize the mean of squared residuals for subbasin flows. However, despite employing multiple initial/base points and ranges, automatic calibration did not yield satisfactory results. Therefore, parameter values obtained from the manual calibration process were retained.

The calibrated parameters for different processes are presented in *Tables 4.13 to 4.17.* The calibrated parameter values are realistic and fall within the expected ranges. For example, the calibrated Manning's roughness value of 0.06, falls within the range of values for major rivers (> 30 m), which is 0.025-0.06 for regular section with no boulders or brush, and 0.035-0.10 for irregular and rough sections (Chow, 1959). The value indicates a relatively rough channel, which is consistent with the meandering nature of Sesan River and the presence of vegetation. The calibrated crop coefficient values of (0.5-0.8) are realistic, given the dominance of evergreen forest in the Sesan basin. These values align with the coefficients of 0.15, 0.79, and 0.15 for the initial, middle, and final growth stages of evergreen forest reported by Corbari et al. (2017).

Table 4.13: *Calibrated parameters for simple canopy method*

Subbasin	Initial storage (%)	Maximum storage (mm)	Crop coefficient
Subbasin-1	50	0.64	0.5
Subbasin-2	50	1.27	0.8
Subbasin-3	50	0.64	0.5
Subbasin-4	50	0.64	0.5
Subbasin-5	50	0.64	0.5
Subbasin-6	50	1.27	0.5
Subbasin-7	50	0.64	0.5
Subbasin-8	50	1.27	0.5
Subbasin-9	50	1.01	0.5
Subbasin-10	50	1.01	0.5
Subbasin-11	50	1.27	0.5
Subbasin-12	50	1.27	0.5
Subbasin-13	50	1.01	0.5

Table 4.14: *Calibrated parameters for simple surface method*

Subbasin	Initial storage (%)	Maximum storage (mm)	Subbasin	Initial storage (%)	Maximum storage (mm)
Subbasin-1	50	2.4	Subbasin-8	50	0.4
Subbasin-2	50	5.0	Subbasin-9	50	0.4
Subbasin-3	50	2.4	Subbasin-10	50	2.4
Subbasin-4	50	2.4	Subbasin-11	50	0.12
Subbasin-5	50	2.4	Subbasin-12	50	0.4
Subbasin-6	50	0.12	Subbasin-13	50	2.4
Subbasin-7	50	2.4			

Table 4.15: *Calibrated parameters for SMA method*

Subbasin	Initial soil content (%)	f (mm/hr)	Impervious (%)	S_{max} (mm)	S_{ten} (mm)	Soil percolation (mm/hr)	S_{GW} (mm)	GW percolation (mm/hr)	T_{GW} (hr)
Subbasin-1	70	1.52	5.5	51.7	1.6	0.9	1500	0.3	1050
Subbasin-2	68	4.00	8.5	116.2	6.3	0.9	1200	0.3	1500
Subbasin-3	68	2.54	5.5	60.0	1.6	0.9	1200	0.3	1000
Subbasin-4	68	1.52	5.5	51.7	1.6	0.9	1120	0.3	1312
Subbasin-5	68	1.52	5.5	51.7	1.6	0.9	1120	0.3	1000
Subbasin-6	68	1.52	5.5	51.7	1.6	0.9	1120	0.3	1500
Subbasin-7	72	0.38	5.5	45.0	1.6	0.9	984	0.3	1000
Subbasin-8	68	1.52	5.5	51.7	1.6	0.9	1120	0.3	1200
Subbasin-9	72	0.38	5.5	45.0	1.6	0.9	984	0.3	1200
Subbasin-10	72	0.38	5.5	45.0	1.6	0.9	984	0.3	1280
Subbasin-11	68	1.52	5.5	51.7	1.6	0.9	1120	0.3	1280
Subbasin-12	68	1.52	5.5	51.7	1.6	0.9	1120	0.3	1280
Subbasin-13	68	1.52	5.5	75.0	1.6	0.9	800	0.3	1500

Since the basin is in a tropical region with dense vegetation, it is reasonable to use higher initial storage values, as dense vegetation reduces evaporation from the soil, increasing soil moisture content at the start of the simulation. The other parameters for SMA are also realistic for the basin's soil type, which is dominated by clay loam and clay. The maximum infiltration rates are within the ranges recommended by Sabol (2008) for these soil groups. Additionally, the small soil and groundwater percolation rates are consistent with the soil texture. A higher groundwater coefficient indicates a higher time constant, which is also reasonable given the soil texture. The calibrated values of time of concentration and storage coefficient for Clark's Unit Hydrograph are within the recommended ranges of 0.1-500 hr and 0 hr-150 hr, respectively, by Bartles et al. (2022).

Table 4.16: *Calibrated Parameters for Clark's unit hydrograph*

Subbasin	*Tc* (hr)	*R* (hr)	Subbasin	*Tc* (hr)	*R* (hr)
Subbasin-1	25.4	27.0	Subbasin-8	40.2	77.8
Subbasin-2	14.4	46.0	Subbasin-9	10.8	24.8
Subbasin-3	28.8	54.0	Subbasin-10	25.8	47.8
Subbasin-4	30.2	56.2	Subbasin-11	23.6	43.8
Subbasin-5	14.6	34.6	Subbasin-12	23.4	45.8
Subbasin-6	19.8	36.8	Subbasin-13	23.0	45.0
Subbasin-7	31.8	63.8			

Table 4.17: *Calibrated parameters for linear reservoir*

Subbasin	GW initial ($m^3/s/km^2$)	GW coefficient (hr)	Subbasin	GW initial ($m^3/s/km^2$)	GW coefficient (hr)
Subbasin-1	0.02	1000	Subbasin-8	0.02	800
Subbasin-2	0.03	1400	Subbasin-9	0.02	960
Subbasin-3	0.02	1000	Subbasin-10	0.02	1024
Subbasin-4	0.02	1000	Subbasin-11	0.02	1024
Subbasin-5	0.02	1200	Subbasin-12	0.02	1024
Subbasin-6	0.02	1000	Subbasin-13	0.02	800
Subbasin-7	0.02	800			

4.8.3. Post-dam Simulation

The pre-dam calibrated and evaluated model was used as the starting point, and then the seven operational dams were progressively added to the model based on their respective years of completion. The post-dam calibration of the dams' storage function was conducted at Vouen Sai only, as all the dams are located upstream of this point. Streamflow observations were available from 2002 to 2014. Dams were added to the model one by one based on its completion year, and its storage function was calibrated for the period before the next dam was added. For instance, Yali dam, the first one constructed in the basin, started operating in 2002. Therefore, only Yali dam was added to the model and simulated for four years until the second dam in the basin (Sesan 3) was added in 2006.

4.8.4. Future period Simulation

The calibrated and evaluated pre-dam and post-dam models were fed with the projected meteorological data from the climate change scenarios, to forecast flows for future periods both with dams and without dams. The comparisons and impact analysis are discussed in the Results chapter.

4.8.5. Evaluation of Model Performance

Model evaluation was conducted using both graphical techniques and quantitative statistics, following the recommendations of Moriasi et al. (2007). Graphical techniques included time series plots of daily, monthly, and annual values, which allowed for visual comparison. The slope and y-intercept of the best-fit regression line in the correlation chart were used to indicate the match between observed and simulated values. A slope of 1 and a y-intercept of 0 indicate a perfect match. The quantitative statistics included the coefficient of determination (R^2), Nash Sutcliffe efficiency (NSE), percent bias (PBIAS), and Root Mean Square Error-observations

Standard deviation Ratio (RSR). The evaluation was conducted based on threshold ranges for daily flows recommended by Moriasi et al. (2007), as presented in *Table 4.18.*

Table 4.18: *Performance rating threshold range for daily flows (Moriasi et al., 2007)*

Performance Rating	R^2	NSE	RSR	PBIAS
Very Good	$0.65 < R^2 \leq 1.00$	$0.65 < NSE \leq 1.00$	$0.00 < RSR \leq 0.60$	$PBIAS < \pm 15$
Good	$0.55 < R^2 \leq 0.65$	$0.55 < NSE \leq 0.65$	$0.60 < RSR \leq 0.70$	$\pm 15 < PBIAS \leq \pm 20$
Satisfactory	$0.40 < R^2 \leq 0.55$	$0.40 < NSE \leq 0.55$	$0.70 < RSR \leq 0.80$	$\pm 20 < PBIAS \leq \pm 30$
Unsatisfactory	$R^2 \leq 0.40$	$NSE \leq 0.40$	$RSR > 0.80$	$PBIAS \geq \pm 30$

4.8.5.1. Coefficient of determination (R^2) is the squared value of the Pearson's correlation coefficient (R) and indicates the degree of linear relationship between simulated and observed data. It represents the proportion of variance explained by the model (Moriasi et al., 2015). R^2 and R are widely used benchmarks but are sensitive to extreme values and do not account for additive and proportional differences between observed and model simulated data. R^2 ranges from 0 to 1, with higher values indicating less error. R^2 is computed using the equation below (Moriasi et al., 2015):

$$R^2 = \left[\frac{\sum_{i=1}^{n}(O_i - \bar{O})(S_i - \bar{S})}{\sqrt{\sum_{i=1}^{n}(O_i - \bar{O})^2}\sqrt{\sum_{i=1}^{n}(S_i - \bar{S})^2}} \right]^2 \quad (4.11)$$

where O_i and S_i are i^{th} observed and i^{th} model simulated values, respectively

$\bar{O}$ and $\bar{S}$ are the mean of observed and model simulated values, respectively

n is the total number of time steps.

4.8.5.2. Nash-Sutcliffe efficiency (NSE) is a normalized statistic used to assess the goodness of fit between the observed and simulated data in hydrological modeling (Nash and Sutcliffe, 1970). It compares the residual variance to the observed data variance. NSE is robust for

continuous long-term simulations, but sensitive to extreme values (Moriasi et al., 2015). NSE ranges from -∞ to 1, with 1 being the optimal value. It is computed using the equation below:

$$NSE = 1 - \frac{\sum_{i=1}^{n}(O_i - S_i)^2}{\sum_{i=1}^{n}(O_i - \bar{O})^2} \quad (4.12)$$

where O_i and S_i are i[th] observed and i[th] model simulated values, respectively

$\bar{O}$ is the mean of observed values

n is the total number of time step

4.8.5.3. Percent bias (PBIAS) measures the average tendency of simulated data to be larger or smaller than observed data and is expressed as a percentage (Gupta et al., 1999). PBIAS ranges from -∞ to ∞, with 0 being the optimal value, which indicates no average tendency to over- or under-estimate the observations. It can be computed using the equation below (Moriasi et al., 2007):

$$PBIAS = \frac{\sum_{i=1}^{n} O_i - S_i}{\sum_{i=1}^{n} O_i} \; x \; 100 \quad (4.13)$$

where O_i and S_i are i[th] observed and i[th] model simulated values, respectively

n is the total number of time step

4.8.5.4. Root Mean Square Error-Observations Standard Deviation Ratio (RSR) is a standardized error index statistic that measures the model's performance by normalizing the RMSE with the standard deviation (SD) of observed data (Moriasi et al., 2007). RSR is the ratio of RMSE to SD, and its values range from 0 (indicating perfect model simulation) to ∞. RSR gives more weight to high values compared to low values due to the squared difference values in the numerator and denominator. The equations for RMSE, SD and RSR are given below:

$$RMSE = \sqrt{\frac{\sum_{i=1}^{n}(O_i - S_i)^2}{n}} \quad (4.14)$$

$$SD = \sqrt{\frac{\sum_{i=1}^{n}(O_i - \bar{O})^2}{n}} \tag{4.15}$$

$$RSR = \frac{RMSE}{SD} = \frac{\sqrt{\sum_{i=1}^{n}(O_i - S_i)^2}}{\sqrt{\sum_{i=1}^{n}(O_i - \bar{O})^2}} \tag{4.16}$$

where O_i and S_i are ith observed and ith model simulated values, respectively

$\bar{O}$ is the mean of observed values

n is the total number of time step

Chapter 5

Methodology: Climate Change Projection

This chapter outlines the steps, methods, and tools used to project future climate change based on three daily climatic variables: precipitation, minimum temperature, and maximum temperature. The projection covered the period from 2025 to 2100, divided into three 25-year periods: Near Future (2025-2050), Mid-Future (2051-2075), and Far Future (2076-2100), with respect to the baseline period of 30 years (1984-2014). Climate models from the CMIP- 6 were employed under SSP2-4.5 and SSP5-8.5 scenarios. These projections were downscaled and adjusted for biases before being used in the HEC-HMS model for projecting streamflows. To address uncertainties in climate response and future emissions, multiple climate models were used, as discussed below.

5.1. Selection of Climate Models

In climate change studies, the selection of climate models is guided by several criteria, including Vintage, Resolution, Validity, and Representativeness of the results, as established by Smith and Humes (1998). Newer models are preferred over older ones as they incorporate the latest scientific advancements. Higher spatial resolution models offer better climate representation, especially in heterogeneous terrains where climate and topography can vary significantly over small distances. The validity of a climate model is assessed by how well it replicates past or present climate compared to observed data.

Three ESMs from CMIP-6, namely, EC-Earth 3, EC-Earth 3-CC, NorESM 2-MM, were selected for this study. These ESMs ranked among the Top 5 for South and Southeast Asia based

on spatial resolution and correlation with observed data metrics (Iqbal et al., 2021; Khadka et al., 2022). *Table 5.1* provides an overview of the selected ESMs' key characteristics.

Table 5.1: *Characteristics of selected ESMs*

Features	CMIP-6 ESMs		
	EC-Earth 3	EC-Earth 3-CC	NorESM 2-MM
Research Institute	EC-Earth-Consortium		Norwegian Climate Center
Vintage	2020	2021	2019
Grid Resolution	1° x 0.75°	0.9° x 0.9°	0.9° x 1.25°
Driving GCM Model	EC-Earth 2	EC-Earth 2	NorESM 1

5.2. Selection of Emission Scenarios

Future climate projections were conducted under two distinct emission scenarios SSP2-4.5 (medium forcing level) and SSP5-8.5 (high forcing level). SSP2 represents the most plausible scenario, while SSP5 represents a more pessimistic future (IPCC AR6, 2021).

5.2.1. SSP2-4.5 (Middle of the Road)

The SSP2-4.5 scenario projects a future with moderate global population growth and slow and uneven progress towards sustainability (Riahi et al., 2017). Social, economic, and technological trends are expected to follow historical patterns, with no notable shifts. While there will be some improvements in resource and energy use, environmental systems will still experience degradation. CO_2 emissions are projected to remain at current levels, failing to reach net-zero by 2100. As a result, the average temperature is projected to increase by about 2.12 °C with a radiative forcing of 4.5 W/m^2 by the end of the century (IPCC, 2021).

5.2.2. SSP5-8.5 (Fossil-fueled Development)

The SSP5 scenario projects a future with high challenges to mitigation and low challenges to adaptation. It is characterized by an energy-intensive, fossil fuel-based economy that places increasing reliance on competitive markets, innovation, and participatory societies to drive rapid

technological progress and human capital development. However, this growth is fueled by exploiting fossil fuels and energy-intensive lifestyles (Riahi et al., 2017). By 2100, this scenario projects an average temperature increases of about 2.76 °C with a radiative forcing of 8.5 W/m^2 (IPCC, 2021).

5.3. Downscaling of ESM data

5.3.1. Statistical Downscaling

The ESM climate data were downloaded from the World Climate Research Programme (WCRP) CMIP6 website: https://esgf-node.llnl.gov/projects/cmip6/. Statistical downscaling was performed using the "raster" package in R, along with basic R functions such as "extract()", to derive finer resolution data from the coarser resolution ESM data. Downscaling was carried out specifically for six rainfall and four temperature gages located within and around the basin.

5.4. Bias Correction

5.4.1. QM

To address systematic biases in the climate model simulations, bias corrections or adjustments are applied. For this study, the QM method was selected. QM is a statistical method that corrects bias in the simulated data from a GCM by matching the cumulative distribution function (CDF) of a model's output to the CDF of the observed data. This is done by comparing the model simulated data to the observed data for a historical period (hindcast). The difference between the simulated and observed data is then used to adjust the simulated data for the forecast period. The adjustment is applied to each quantile of the simulated data, ensuring that the bias-corrected data has the same statistical properties as the observed data. The equation of QM is as follows (Heo et al., 2019; Gudmundsson et al., 2012):

$$Q_m(t) = F_o^{-1}\,[F_s[Q_s(t)]] \tag{5.1}$$

where $Q_m(t)$ and $Q_s(t)$ are the t^{th} bias-corrected data and model simulated data, respectively

F_s and F_o^{-1} are the CDF of raw model data and inverse CDF of observed data, respectively. QM can effectively remove model biases for the mean, interannual variability, and extreme events (Tong et al., 2021), and is a more sophisticated approach for bias correcting stochastic variables, such as precipitation (Racines et al., 2015). Shrestha et al. (2017) found that QM outperformed the linear scaling method in bias correcting precipitation projections for four Asian cities (Bangkok, Bandung, Ho Chi Minh, and Lahore). QM method was implemented in R language using an automated looping program developed by Shrestha (2017), which uses "qmap" package.

5.4.2. Performance Evaluation of QM

The performance of QM in correcting the bias was assessed using R^2, RMSE and PBIAS. These metrics assess how well the bias-corrected data matches the observed data. However, while QM aims to improve the accuracy of the model simulations, its performance depends on the quality of the input model data.

5.5. Spatial Distribution of Climatic Variables

The downscaled and bias-corrected climate data obtained at the meteorological gages were interpolated across the entire Sesan basin using the Thiessen polygon method. *Figure 5.1* (left) and (right) illustrate the division of Thiessen polygons and their corresponding weights for the rainfall and temperature gages, respectively. These polygon weights were applied to the time series climate data from each gage, and the resulting weighted data were then aggregated to calculate the average climate conditions for the entire basin. The Thiessen polygon method ensured a more comprehensive representation of basin-wide climate conditions, given the limited number of meteorological gages present in the basin. Basin average climate data were calculated from the ensemble of the three ESMs.

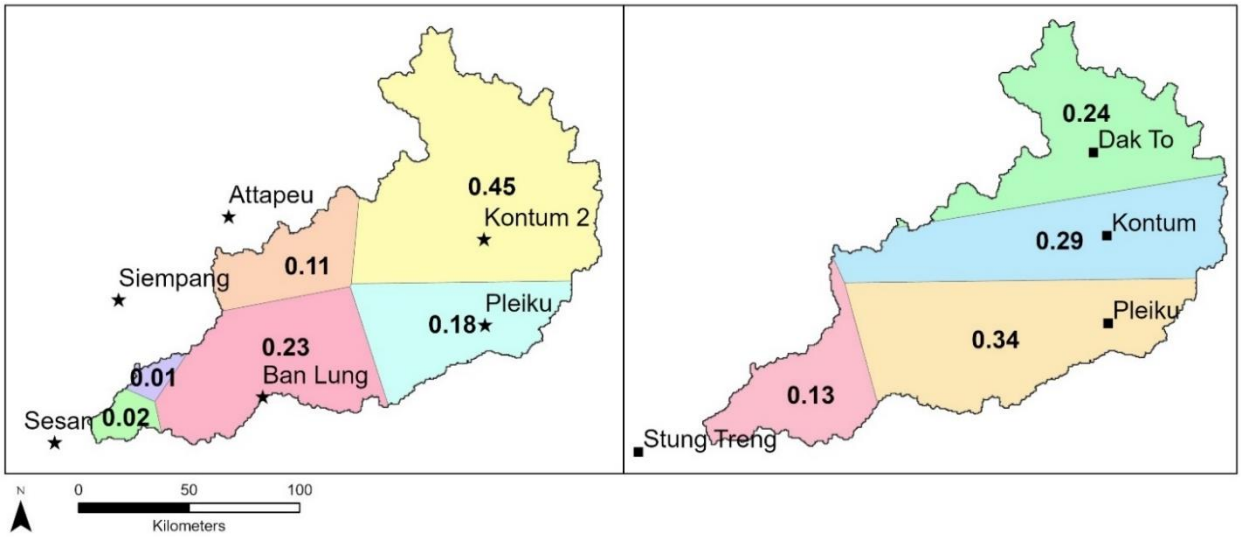

Figure 5.1: *Thiessen polygon for rainfall gages (left) and temperature gages (right)*

Chapter 6

Methodology: Hydrologic Alteration

This chapter discusses the computation of hydrologic alteration using the RVA/IHA.

6.1. IHA

The IHA program assesses 67 ecologically relevant statistics derived from daily streamflow data. These statistics are divided into 33 IHA metrics (represented by five flow characteristics-magnitude, frequency, duration, timing, and rate of change) and 34 Environmental Flow Components (EFC) metrics (represented by five types of flow events-low flows, extreme low flows, high flow pulses, small floods, and large floods) (The Nature Conservancy, 2009). This study focused on the 33 IHA metrics because they describe the flow characteristics rather than the flow event types, which are described by the EFC metrics. *Table 6.1* summarizes the IHA metrics, as outlined by Richter et al. (1996).

6.2. RVA

Richter et al. (1996) found that the RVA, which includes 33 IHA metrics is a valuable tool for assessing hydrologic alterations between time periods before and after an impact (such as addition of dams or climate change). RVA quantifies the alteration of flow regimes by comparing the statistical distribution of hydrologic metrics from a pre-impact period to the statistical distribution of the same metrics from a post-impact period, using the pre-impact distribution as a reference (Xue et al., 2017). Richter et al., (1997) suggests that water managers should strive to keep the distribution of annual values of the IHA metrics as close to the pre-impact distributions as possible. RVA is based on the idea that river flow regimes have a natural range of variability,

and that this variability is essential for maintaining healthy river ecosystems (Acuña, 2020).

Table 6.1: *Summary of IHA metrics and their characteristics (Richter et al., 1996)*

IHA Group	Hydrologic Parameters
Group 1: Magnitude and timing of monthly flow conditions	Mean for each calendar month
Group 2: Magnitude and duration of annual extremes	Annual 1-day minimum Annual 3-day minimum Annual 7-day minimum Annual 30-day minimum Annual 90-day minimum Annual 1-day maximum Annual 3-day maximum Annual 7-day maximum Annual 30-day maximum Annual 90-day maximum Number of zero-flow days Base flow index: Ratio of annual 7-day minimum flow to annual mean flow
Group 3: Timing of extremes	Julian date of each annual 1-day maximum Julian date of each annual 1-day minimum
Group 4: Magnitude and frequency of high and low pulses	Number of low pulses within each water year Mean duration of low pulses (days) Number of high pulses within each water year Mean duration of high pulses (days)
Group 5: Frequency and rate of changes	Rise rates: Mean of all positive differences between consecutive daily values. Fall rates: Mean of all negative differences between consecutive daily values. Number of hydrologic reversals (Frequency of flow direction shifts from rising to falling or vice versa)

RVA targets are set to define the desired range of variability for each hydrologic metric (Zuo & Liang, 2015). The management objective is to attain the targeted range at the same frequency as occurred in the natural or pre-impact flow regime. In a parametric analysis, the RVA target range is typically defined as ±1 standard deviation from the mean, and in a non-parametric analysis, the RVA target range is typically defined using percentiles, such as the 25th and 75th percentiles (Richter et al., 1998). To ensure reliable results, the Nature Conservancy recommends

using at least twenty years of daily records for both pre-impact and post-impact periods (Richter et al., 1997; Huh et al., 2005).

This study used parametric analysis in RVA to study the hydrologic alteration from dams and climate change. Due to limited availability of observed streamflow, this study relied on the data simulated by the calibrated HEC-HMS models (described in the preceding chapters). Measures of the central tendency (mean and standard deviation) were computed from the annual series for each IHA metric to characterize interannual variation, separately for the pre- and post-impact periods. IHA metric values from the pre-impact period were used as a benchmark to assess the extent of alteration from natural flow regimes. Following Richter et al. (1997), the RVA target range were selected as ± 1 standard deviation (SD) from the mean for each 33 IHA metric from the pre-impact period. In cases where skewness in the distribution of the pre-impact annual values led the mean -1 SD values to fall below the pre-impact low range limits, the 25th percentile level was used as a default.

The RVA outputs a series of hydrologic alteration factors, which represent the degree of change in each hydrologic metric. The degree of hydrologic alteration, D_i for each metric is calculated as the difference between the observed frequency (i.e., the number of years during a post-impact period where a specific hydrologic index falls within the RVA target range) and the expected frequency (i.e., the expected number of years during a post-impact period where the same hydrologic index falls within the RVA target range) divided by the expected frequency (Richter et al, 1997; Sharma et al., 2021). The equation is:

$$D_i = \left[\frac{N_o - N_e}{N_e}\right] \tag{6.1}$$

where N_o is observed frequency

N_e is expected frequency

Positive values of hydrologic alteration factors indicate an increased frequency of values in the RVA target range, while negative values indicate a decreased frequency. This means that annual metric values fell within the RVA target window more often or less often than expected, respectively (Richter et al., 1998). The overall average hydrologic alteration was computed by averaging the absolute values of deviation of each metric. Richter et al. (1998) grouped the range of the average hydrologic alteration into three classes with equal ranges: 0-33% (low alteration), 34-67% (moderate alteration), and 68-100% (high alteration).

6.3. Comparison of Hydrologic Alterations

The deviations in the hydrologic regime from the pre-impact to post-impact periods were evaluated by contrasting the simulated streamflow for the two periods. Results from RVA/IHA were used to quantify the extent of hydrologic alteration. The following comparisons were made:

i. To determine the hydrologic alterations due to dams only, simulated streamflows without and with dams for the BL period were compared. This comparison examined the difference between the natural flow without dams and the flow after the addition of dams.

ii. To assess the hydrologic alterations due to climate change only, simulated streamflows without dams during the BL and future periods were compared. This comparison examined the difference between flows without dams during the BL period, which had no impact from climate change to the projected future flows that considered climate change.

iii. To assess the combined impacts from dams and climate change, simulated streamflows without dams for the BL period were compared to simulated streamflows with dams for the future periods. This comparison examined the difference between the natural flow in the BL period without dams versus the future flow considering both climate change and dams in the river basin.

Chapter 7

Results and Discussion

This chapter contains of the findings and analysis of this study presented as three main sections:

i. Results of calibration and evaluation of hydrologic model.

ii. Results of climate change projection.

iii. Comparisons of hydrologic alteration under hydropower dams operation, potential climate change and the combined impact of both.

7.1. Calibration and Evaluation of HEC-HMS

Hydrologic simulation was divided into pre-dam period (before dam construction) and post-dam period (after dam constructions), for which separate models were built, calibrated and evaluated (validated).

7.1.1. Calibration and Evaluation of Pre-dam Model

The pre-dam model was calibrated and evaluated (validated) at the two streamflow gages, Kontum and Vouen Sai. At Kontum, calibration was performed for ten years from 1985 to 1995, and evaluation was performed for five years from 1996 to 2000. *Figure 7.1* shows the daily simulated (blue line) and observed (dotted black line) streamflows at Kontum during the calibration and evaluation periods. Simulated streamflow tends to overestimate the flow during the seasonal recession limb, which is the period between the end of the wet season and the beginning of the dry season. The hydrograph shows the highest flows in 1996 and the lowest flow in 1967, indicating a period of intense flow followed by a dry spell. The correlation charts in *Figures 7.2 (a) and (b)* show a positive correlation between the observed and simulated values both during calibration and evaluation periods. There is better agreement between the simulation and

observations during low flows than high flows. Since the simulated flow values in *Figure 7.2* tend to be below the 1:1 line, the model tends to underestimate the observed flows.

At Vouen Sai, calibration was performed for four years from 1965 to 1968, and evaluation was performed during 1969. Hydrographs in *Figure 7.3* show the daily streamflow variation over the period of five years. The simulated streamflow consistently follows the observed streamflow pattern but tends to be higher than the observed streamflow during the recession limbs. This could occur in part because observations are missing during two recessions, which reduces the role of the recessions in the performance metrics used during calibration. *Figures 7.4 (a) and (b)* show a positive correlation between the observed and simulated values at Vouen Sai during calibration and evaluation, respectively. The correlation coefficient for the evaluation period is 0.61, which is slightly higher than the 0.56 for the calibration period. This indicates a moderate to good degree of accuracy in the model's streamflow simulation during both periods. However, the model tends to underestimate the high observed flows and overestimate the low observed flows, as evident from the regression lines in the plots.

7.1.2. Performance Metrics of Pre-dam Model

Table 7.1 shows the statistical performance metrics for the pre-dam model at both streamflow gages. The evaluation was based on the threshold ranges for daily flows recommended by Moriasi et al. (2007), where satisfactory values were considered to be above 0.4 for R^2 and NSE 0.4, and below 0.8 for RSR and ± 30 for PBIAS. Overall, all performance metrics at both gages exceeded these levels, indicating that the calibrated pre-dam model effectively simulates streamflow with a satisfactory to a good degree of accuracy. The model's simulations may be biased due to inaccuracies in its representation of physical processes or limitations in the input data, such as precipitation and temperature data. Precipitation is a key input to the model, and any

errors in the precipitation data will be propagated into the model outputs. The limited number of rainfall gages available in such a large watershed could have caused discrepancies, as precipitation can vary substantially over short distances. Additionally, groundwater-surface water interactions were excluded from the model due to insufficient data and computational challenges. As a result, the model only considered direct runoff from rainfall. Groundwater recharge during the wet season provides a sustained source of flow during the dry season, which could explain the disagreements seen in the seasonal recessions.

Table 7.1: *Summary of statistical performance metrics for the pre-dam model*

Performance Metric	Kontum		Vouen Sai	
	Calibration	Evaluation	Calibration	Evaluation
R^2	0.47	0.46	0.56	0.61
NSE	0.41	0.41	0.51	0.59
RSR	0.77	0.77	0.70	0.64
PBIAS	6.3%	-4.4%	14.1%	4.5%

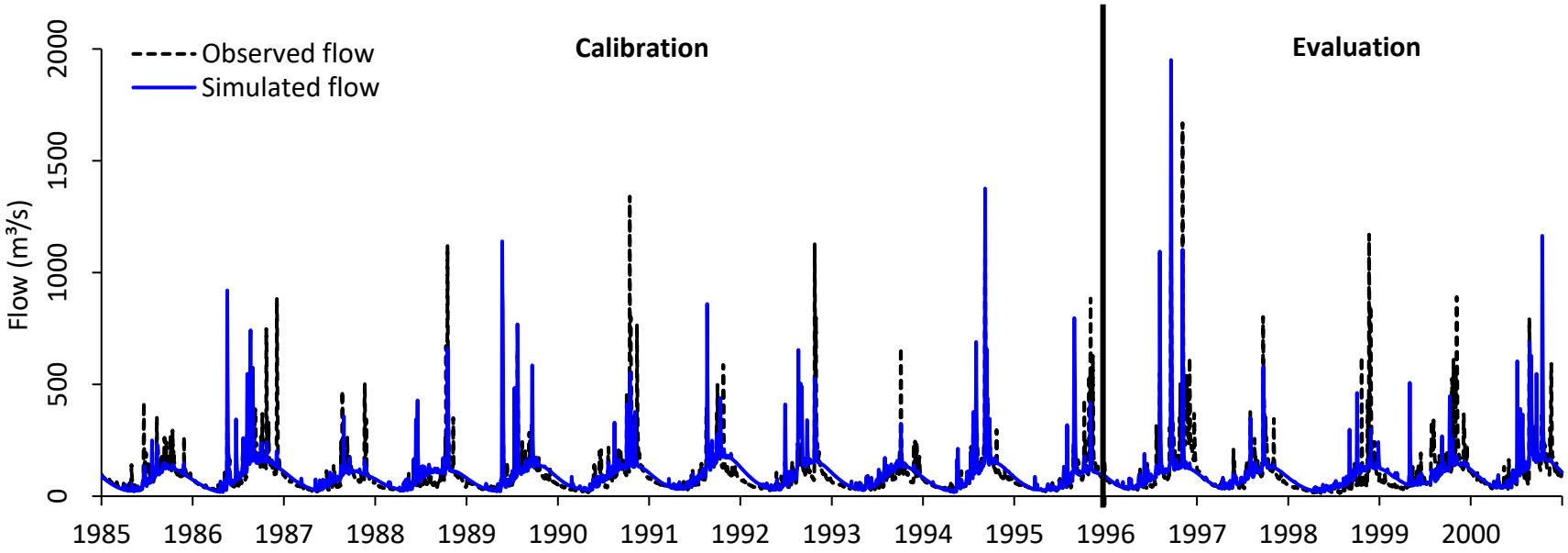

Figure 7.1: *Daily streamflow hydrographs for calibration and evaluation at Kontum Station*

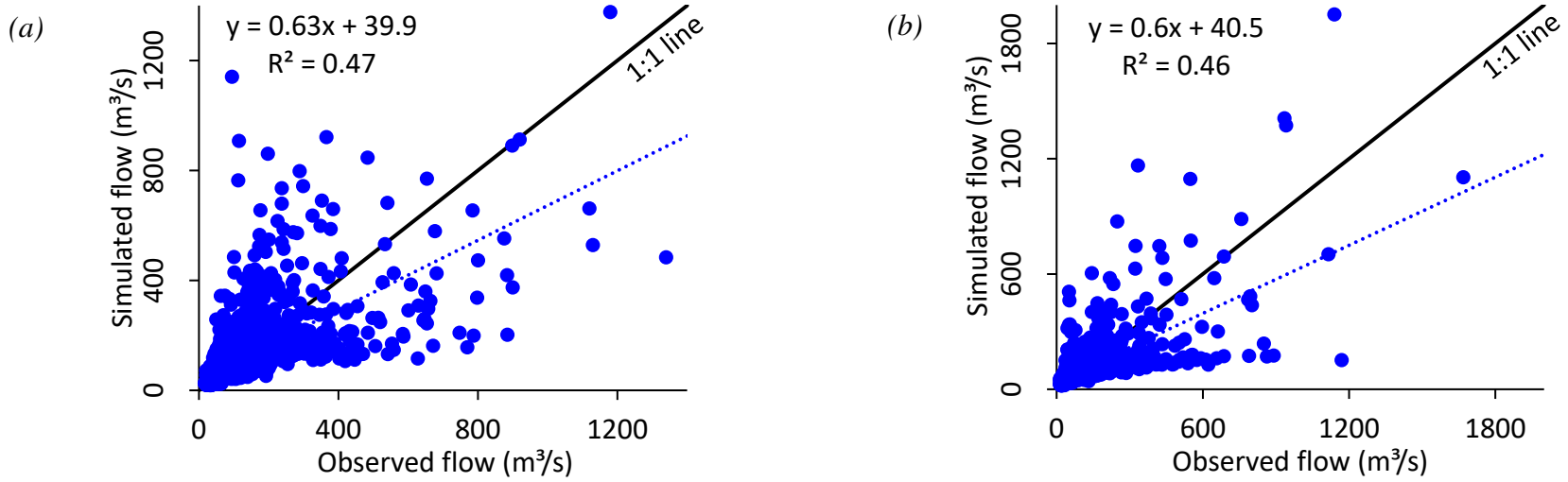

Figure 7.2: *Correlation charts for (a) calibration and (b) evaluation at Kontum Station*

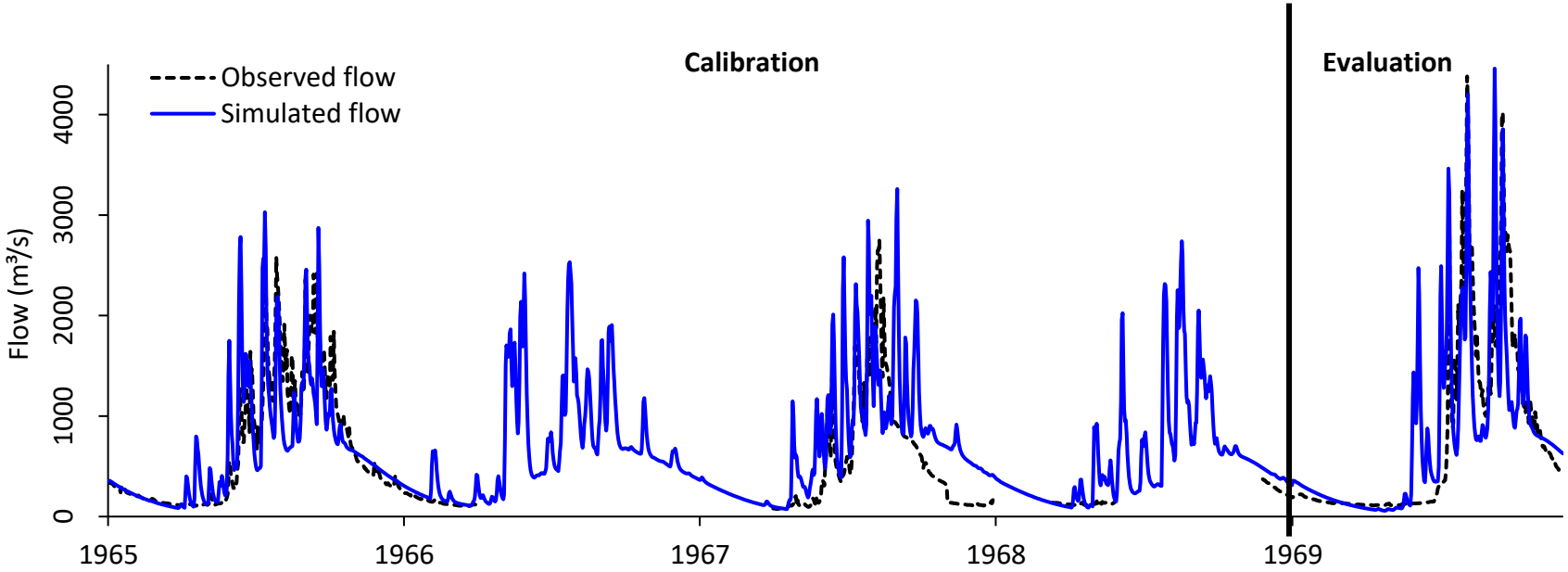

Figure 7.4: *Daily streamflow hydrographs for calibration and evaluation at Vouen Sai Station*

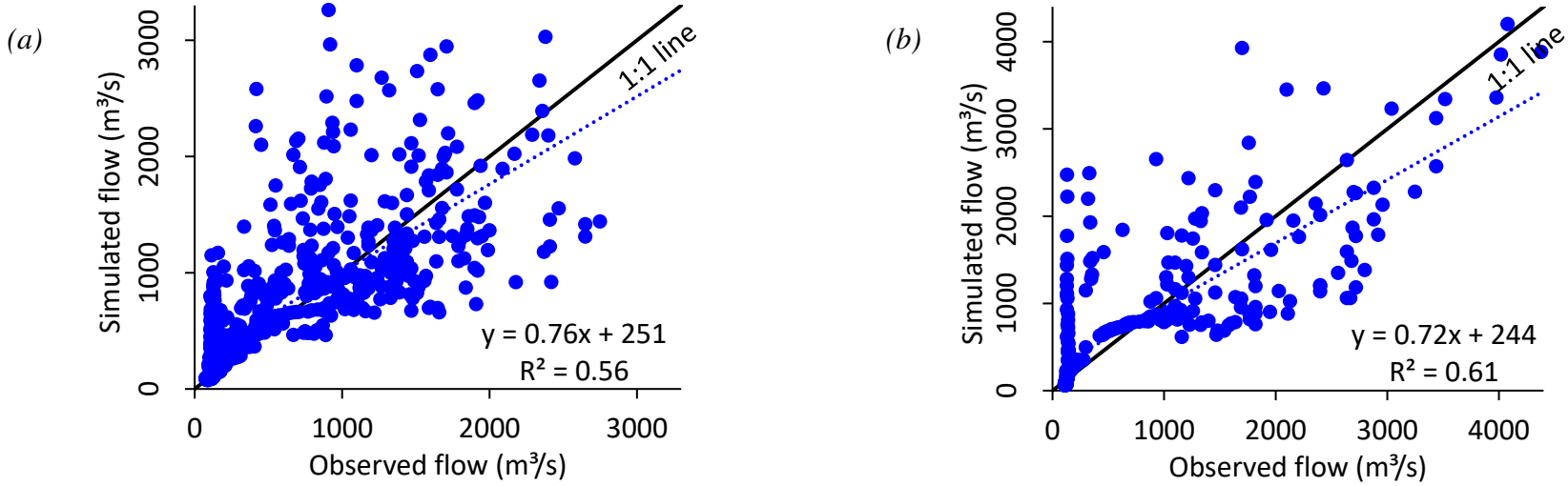

Figure 7.3: *Correlation charts for (a) calibration and (b) evaluation at Vouen Sai Station*

7.1.3. Calibration of Post-dam Model

The post-dam model was calibrated at Vouen Sai only, as all the dams in the basin are located upstream of this point. Dams were added to the model incrementally in the order of their completion dates, and their storage curves were calibrated before adding the next dam. *Figure 7.5 (a to f)* shows the calibration results for each dam addition. Since the larger dams in the basin are seasonal storage dams, which store water during the wet season and release it during the dry season, the hydrographs show visible reductions in peak flows (maximum streamflow during wet season) and visible increases in low flows (minimum streamflow during dry season).

Figure 7.6 shows the model simulated and observed streamflow for the entire period after addition of dams. The simulated streamflow aligns with the observed streamflow patterns and reproduces low flows, except in 2010 and 2011, during which the simulated flow overestimates the observed data. This mismatch could be due to potential inaccuracies in the observed streamflow or unusual reservoir releases. Overall, the observed and simulated values for the post-dam model show a positive correlation of 0.56. However, the model tends to underestimate the observed streamflow, particularly the high flows. This is evident from the correlation chart in *Figure 7.7,* where the simulated values are mostly below the 1:1 correlation line. *Table 7.2* shows the model performance metrics of the post-dam model, which indicate a moderate to good level of accuracy in the model's streamflow simulation.

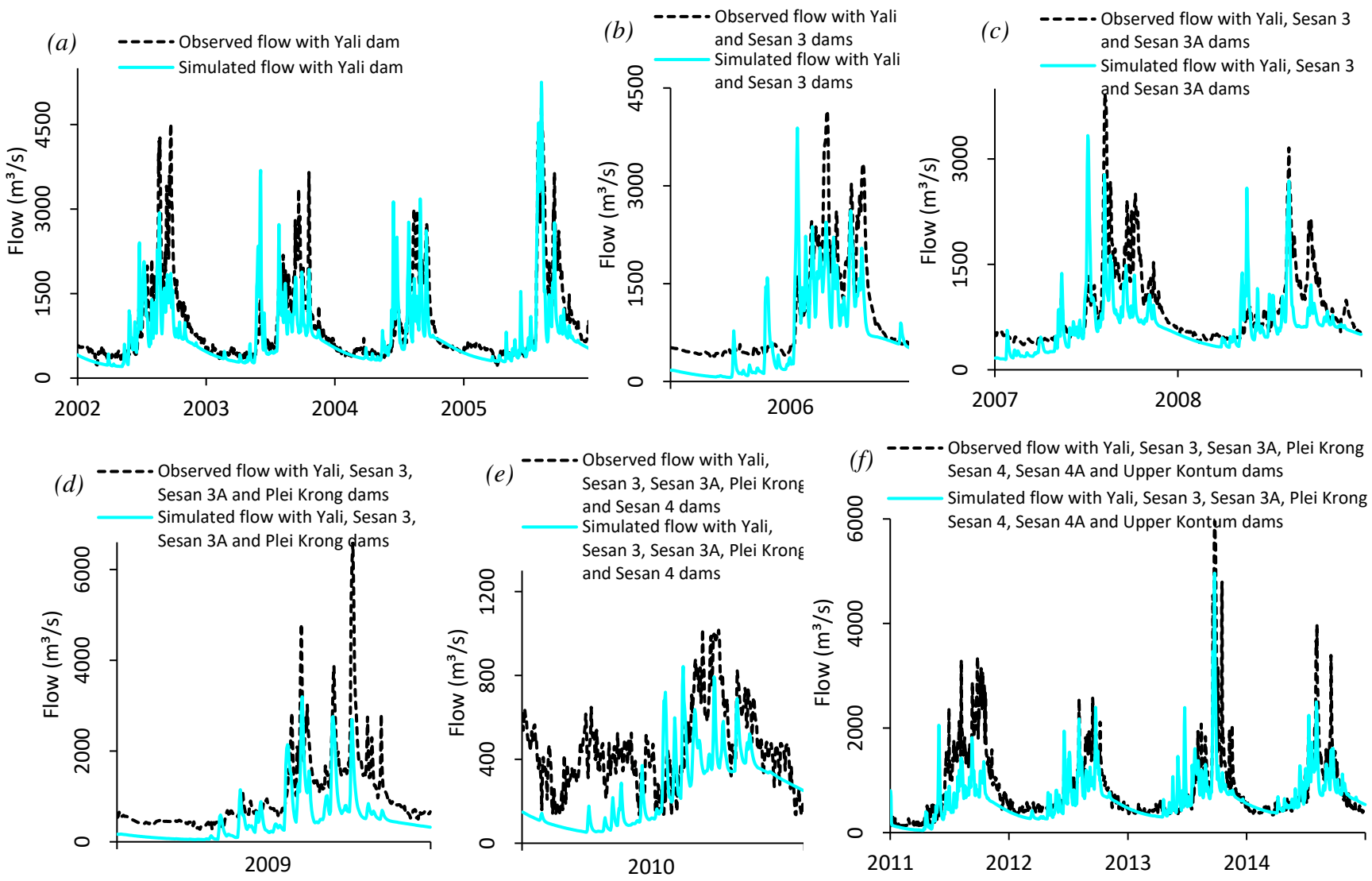

Figure 7.5: *Calibration of daily streamflow with phase-wise addition of dams at Vouen Sai Station (a) Yali dam-2002 to 2005 (b) Yali and Sesan 3-2006 (c) Yali, Sesan 3 and Sesan 3A-2007 to 2008 (d) Yali, Sesan 3, Sesan 3A and Plei Krong-2009 (e) Yali, Sesan 3, Sesan 3A, Plei Krong and Sesan 4-2010 (f) Yali, Sesan 3, Sesan 3A, Plei Krong, Sesan 4, Sesan 4A and Upper Kontum-2011 to 2014*

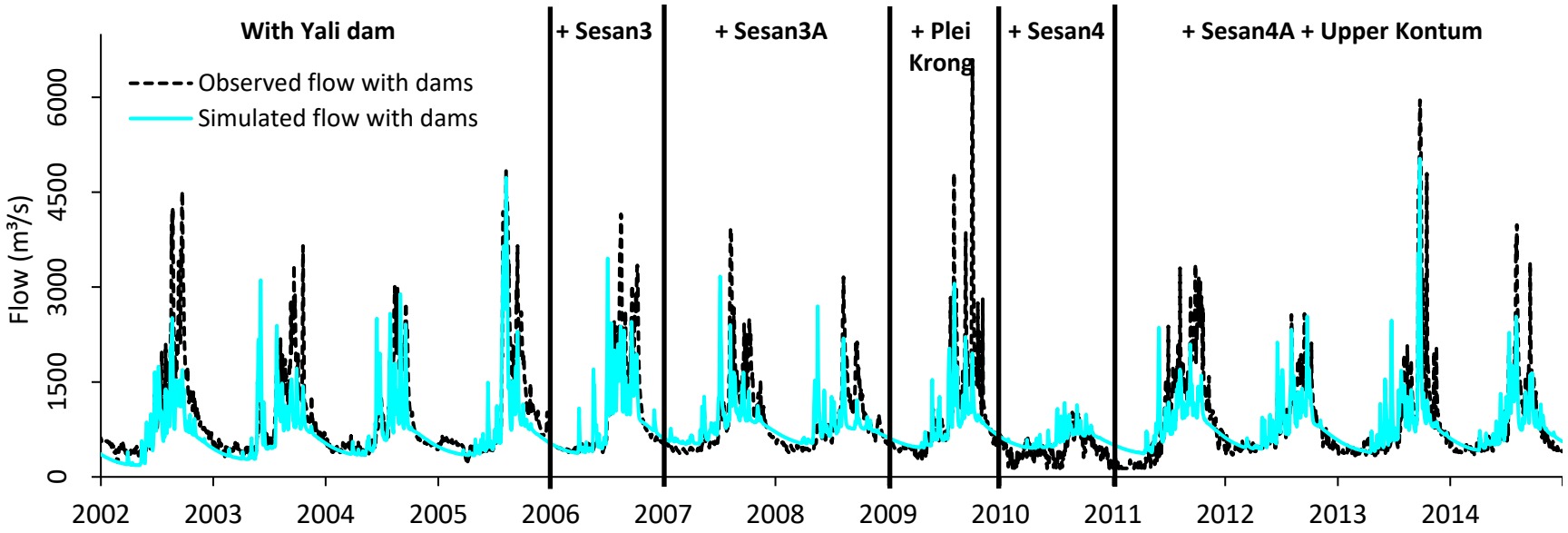

Figure 7.6: *Comparison of daily observed and simulated streamflow after calibration of all dams at Vouen Sai Station*

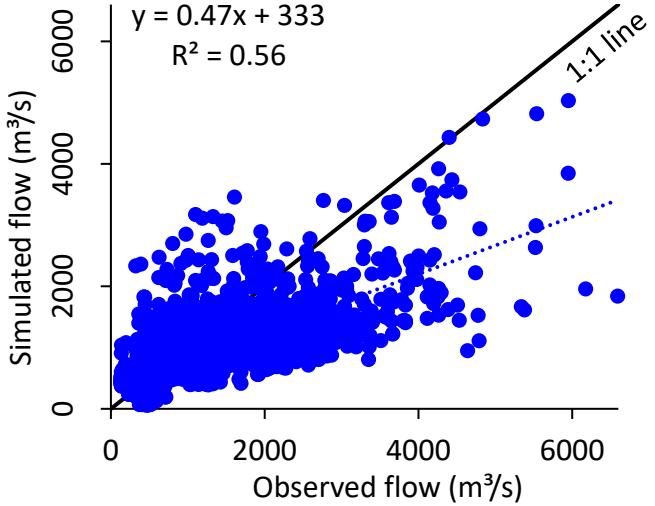

Figure 7.7: *Correlation of post-dam simulated and observed values*

Table 7.2: *Summary of statistical performance metrics for the post-dam model*

Performance Metric	Calibration
R^2	0.56
NSE	0.51
RSR	0.70
PBIAS	-15.9

7.2. Climate change projections

Climate projections were based on three daily climatic variables: precipitation, minimum temperature, and maximum temperature. Future climate projections were conducted for 2025-2100, relative to BL period (1984-2014), and under SSP2-4.5 and SSP5-8.5 scenarios. The effectiveness of the Quantile Mapping bias correction in adjusting anomalies in the downscaled ESM data was assessed using several evaluation metrics, including R^2, RMSE and PBIAS. These metrics were used to compare the raw (i.e., before bias correction) and corrected (i.e., after bias correction) data in the BL period. The results, presented in *Table 7.3*, show improvements in the corrected dataset compared to the raw dataset. Further, the biased-corrected ESM data at each meteorological gage was multiplied by the corresponding Thiessen polygon weights (presented in *Figure 5.1*) to compute the average climate conditions across the basin. Finally, the average of the projections from the three GCMs was calculated and used as input to the HEC-HMS models.

Table 7.3: *Performance evaluation of QM bias correction*

Precipitation						
Climate Model	R^2		RMSE (mm)		PBIAS (%)	
	Raw	Corrected	Raw	Corrected	Raw	Corrected
EC-Earth3	0.09	0.03	13.98	10.74	4.66	-0.09
EC-Earth3-CC	0.08	0.04	13.75	10.91	-1.08	0.06
Nor-ESM2-MM	0.03	0.02	15.20	12.22	4.50	-0.13
Minimum temperature						
Climate Model	R^2		RMSE (°C)		PBIAS (%)	
	Raw	Corrected	Raw	Corrected	Raw	Corrected
EC-Earth3	0.48	0.46	2.09	2.09	3.78	0.00
EC-Earth3-CC	0.49	0.45	1.96	2.10	1.88	0.00
Nor-ESM2-MM	0.45	0.41	2.33	2.19	-3.52	0.00
Maximum temperature						
Climate Model	R^2		RMSE (°C)		PBIAS (%)	
	Raw	Corrected	Raw	Corrected	Raw	Corrected
EC-Earth3	0.27	0.25	2.92	2.22	1.92	0.00
EC-Earth3-CC	0.26	0.26	2.98	2.20	1.27	0.00
Nor-ESM2-MM	0.15	0.24	3.62	2.26	0.73	0.00

7.2.1. Precipitation

Figure 7.8 shows the average annual precipitation projected by the ESMs under the two SSP scenarios. The annual average precipitation in the BL period is 2120 mm (represented by dotted black line). The blue lines represent projections by the ESMs under SSP2-4.5 and the red lines represent the projections under SSP5-8.5. All the three ESMs exhibit a similar trend of increasing future precipitation, with the magnitude of increase greater under SSP5-8.5 than under SSP2-4.5. The average precipitation projections increase by 7%, 4%, and 13% under SSP2-4.5, and 7%, 14%, and 29% under SSP5-8.5 in the NF, MF, and FF, respectively. The most substantial precipitation anomalies occur in the FF under both SSP scenarios.

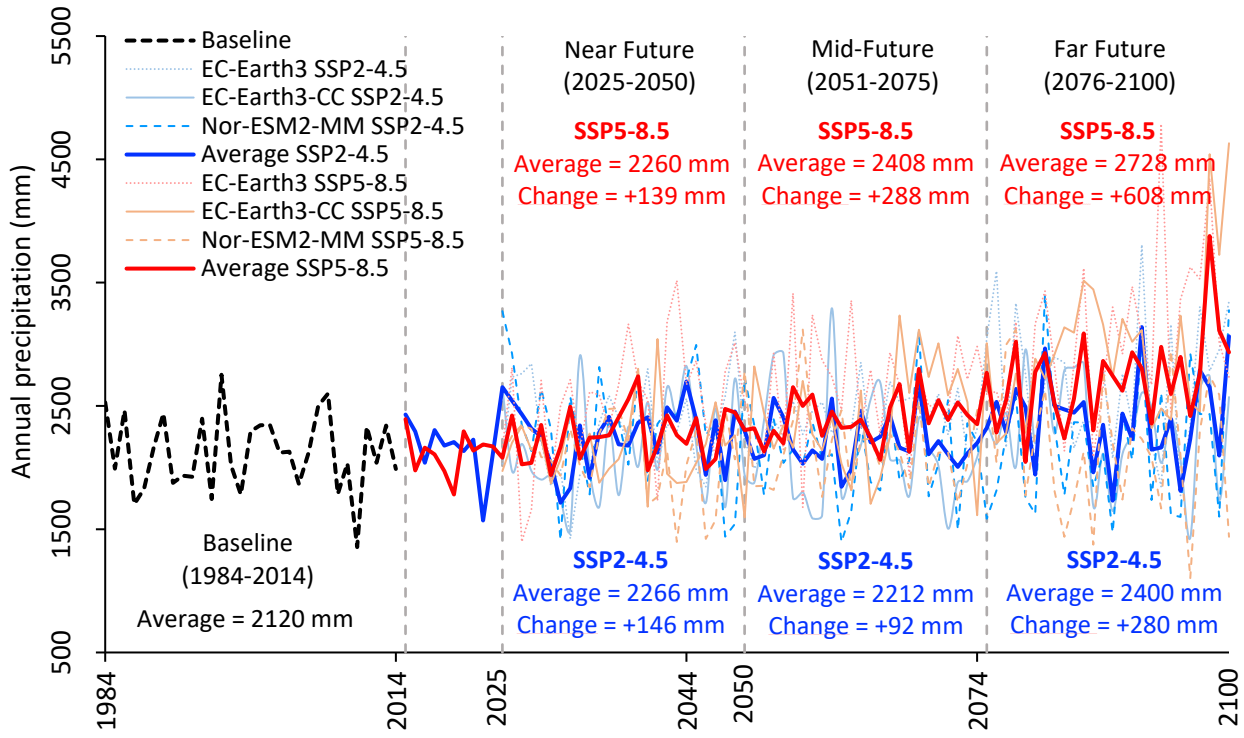

Figure 7.8: *Average annual precipitation under SSP2-4.5 and SSP5-8.5, and changes relative to BL*

7.2.2. Minimum Temperature

Figure 7.9 shows the annual minimum temperature projected by the ESMs under the two SSP scenarios. The projections show a steady increase in the minimum temperature under both

SSP scenarios, with a greater increase under SSP5-8.5. The increases are 8%, 13%, and 16% under SSP2-4.5, and 10%, 18%, and 26% under SSP5-8.5, in the NF, MF, and FF, respectively. While the projections under the two scenarios are similar during the NF, the divergence between them widens progressively from the MF to FF periods.

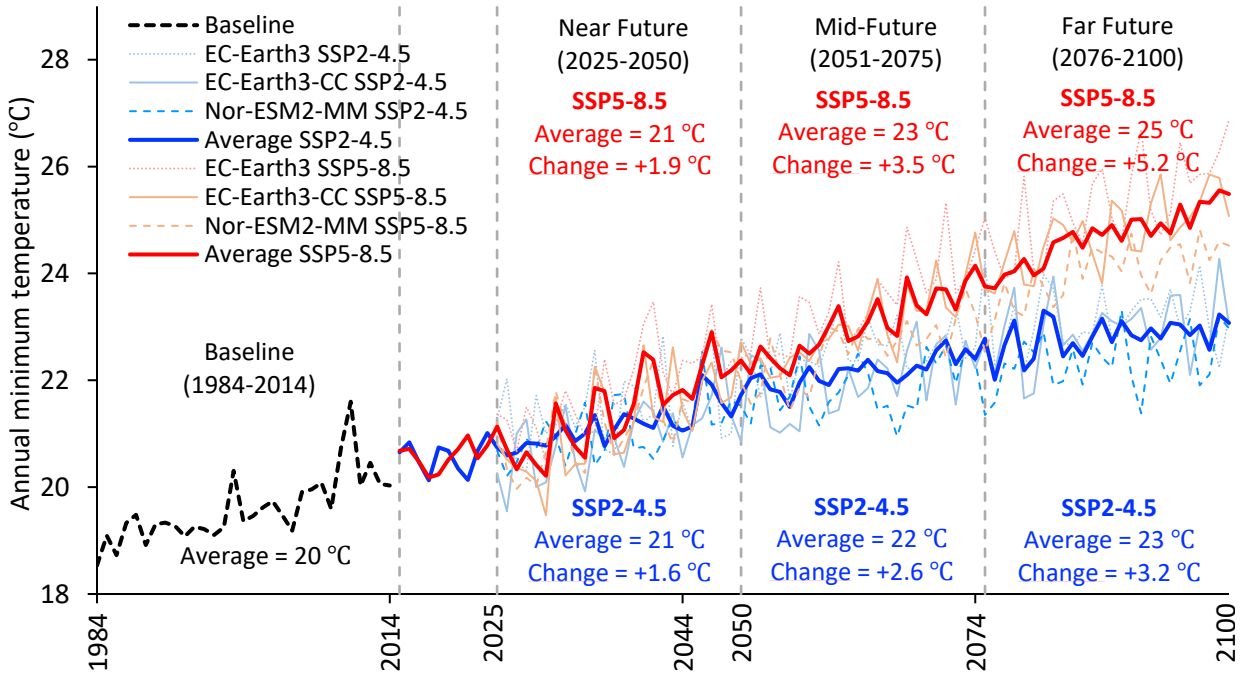

Figure 7.9: *Annual minimum temperature under SSP2-4.5 and SSP5-8.5, and changes relative to BL*

7.2.3. Maximum Temperature

Figure 7.10 shows the annual maximum temperature projected by the ESMs under the two SSP scenarios. The projections show a steady increase in the maximum temperature under both SSP scenarios, with a greater increase under SSP5-8.5. The increases are 3%, 5%, and 7% under SSP2-4.5, and 3%, 7%, and 12% under SSP5-8.5, in the NF, MF, and FF, respectively. The projections in the NF display an almost overlapping pattern, however, the divergence between the two scenarios gradually increases from the MF to FF periods.

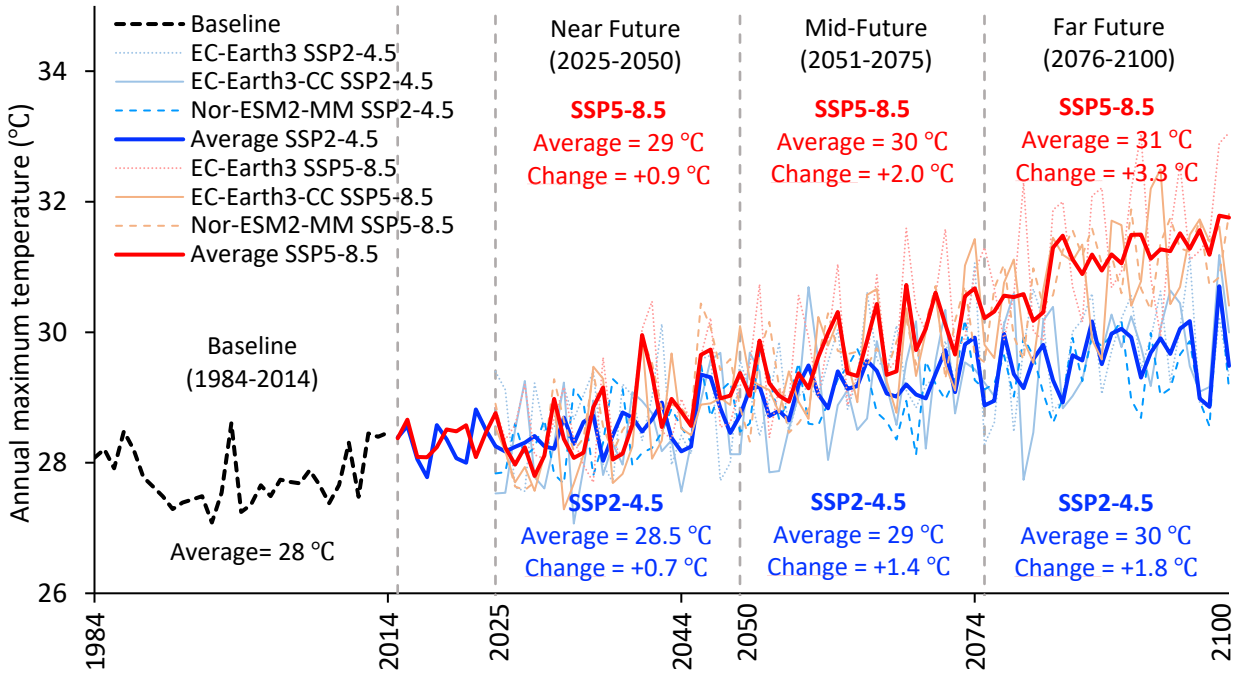

Figure 7.10: *Annual maximum temperature under SSP2-4.5 and SSP5-8.5, and changes relative to BL*

7.3. Comparisons of Hydrologic Alteration

7.3.1. Impact of Dams only

7.3.1.1. Analysis at Vouen Sai Station-Dams Impact Analysis

Figure 7.13 (top and bottom) shows a comparison of daily streamflow at Vouen Sai, split into two time periods: 1984-2000 and 2001-2014, for clarity. The addition of dams significantly alters the hydrograph's characteristics, particularly by smoothing out its peaks and troughs. Four of the seven dams in the basin have relatively higher reservoir storage capacities and function as seasonal storage facilities, accumulating excess water during the wet season and gradually releasing it during the dry seasons. *Figure 7.11 shows the* seasonal streamflow hydrographs, which highlight the operational strategy of the dams as a distinct reduction of high flows and a concurrent rise of low flows are seen. The average simulated peak flow without dams is 1563 m³/s, while with dams, the peak flow is reduced to 1228 m³/s (a 21% reduction). Conversely, the lowest average

monthly flow increases from 199 m³/s to 438 m³/s after the addition of dams (a 55% increase). *Figure 7.12* shows the impact of dams on the annual flow patterns. Both hydrographs show a consistent pattern of high and low flows, except in the initial years, when the average simulated flows with dams are comparatively lower than flows without dams. This is likely due to the dam-filling phase, during which less streamflow was released. To focus on the ongoing impacts of the dams rather than their impacts during filling, the initial two years were excluded from the comparative analysis in the RVA/IHA.

After excluding the initial two years (1984 and 1985) the remaining daily simulated streamflow from 1986 to 2014 were used in the RVA/IHA. The scenario without dam was defined as the pre-impact period, and the period with dam was considered the post-impact period. The results of RVA/IHA at Vouen Sai are presented in *Table 7.4*. Dams have a greater impact on the magnitude of streamflow than on the timing of flows, and they have a greater impact on low flows than on high flows. This is evident from the RVA/IHA results. For example, dams have a significant impact on the magnitude of monthly flows during the dry season (January-April), where the deviation is high (-75 to -93%). However, they have a lesser impact during the wet season (May-December), where the deviation is low to moderate (0 to 67%). Negative deviations indicate a decreased frequency during the post-dam period relative to the pre-dam period. This means that the magnitude of monthly flow values fell within the RVA target window less often than expected. Similarly, dams have a significant impact on the magnitude of low flows than on high flows since dams store water during wet season and release it during dry season. This is evident from the RVA/IHA results for minimum extremes such as the 1-day, 3-day, 7-day, 30-day, and 90-day minimums, where the deviation is very high (-91 to -100%). This reduces the seasonal variability of flow and decreases the frequency of high flows and low flow extremes. Moreover, high flows

are more variable between years than low flows. This means that the dam's reduced flows are still more likely to fall within the range of natural variability of high flows. However, the dam's reduced flows are more likely to fall outside of the range of natural variability of low flows. The overall degree of hydrologic alteration, calculated as the average of absolute deviations of all parameters is 43%, which falls under "moderate" category.

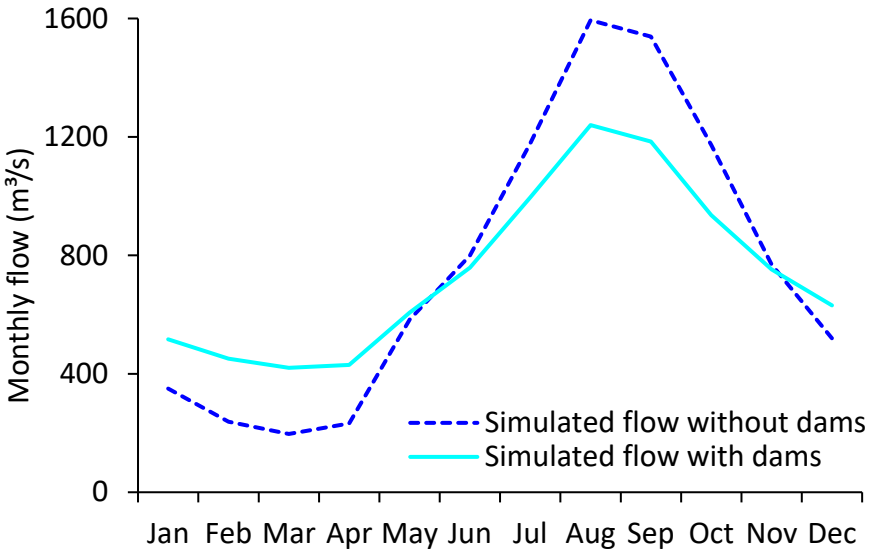

Figure 7.11: *Average monthly streamflow comparison at Vouen Sai-Dams impact analysis*

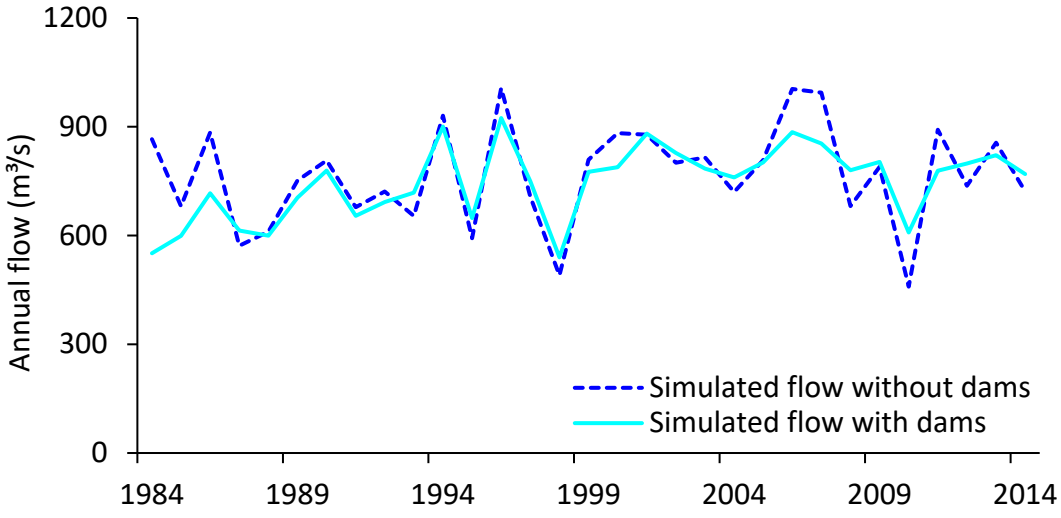

Figure 7.12: *Average annual streamflow comparison at Vouen Sai-Dams impact analysis*

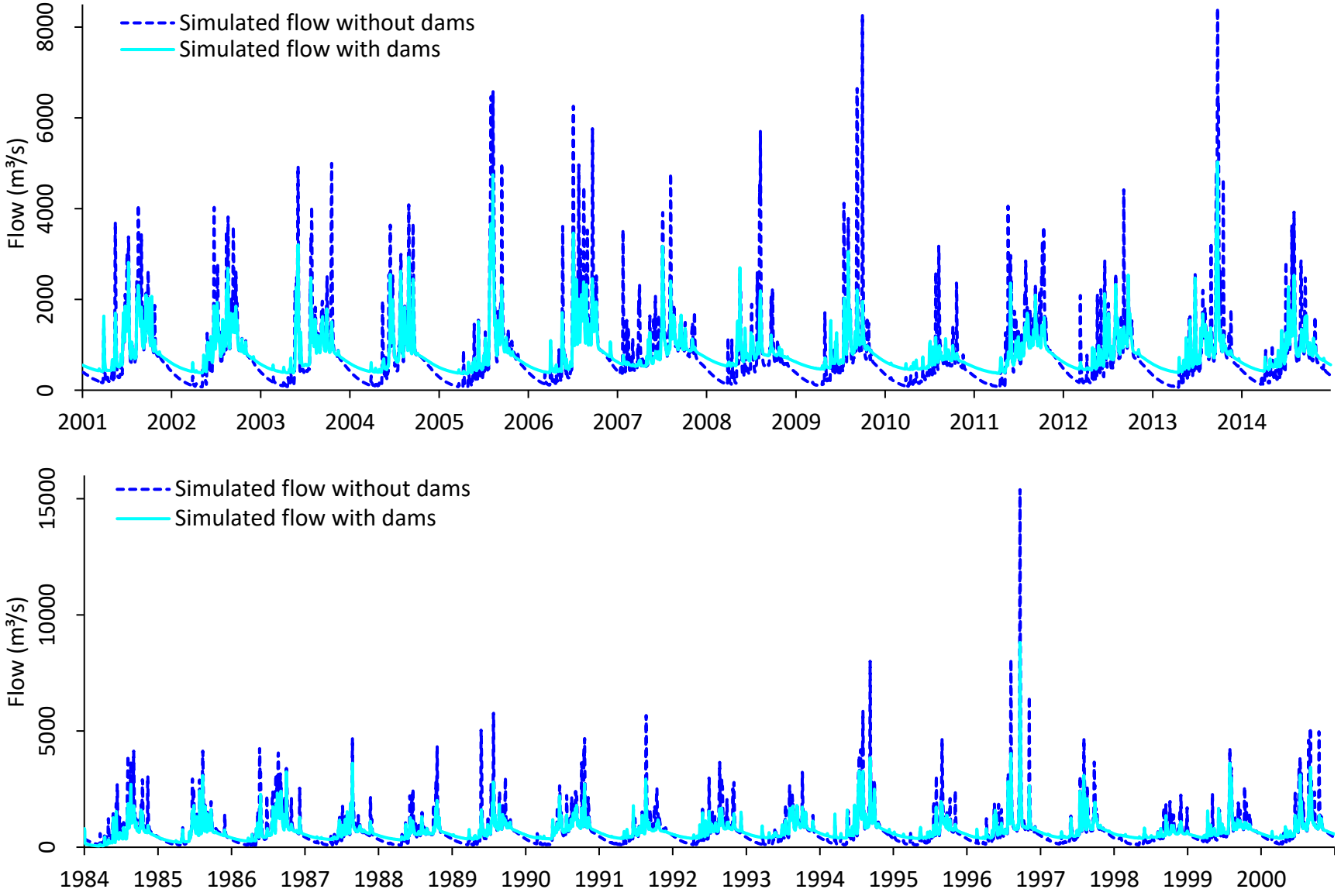

Figure 7.13: *Daily streamflow comparison at Vouen Sai, 1984 to 2000 (top) and 2001 to 2014 (bottom)-Dams impact analysis*

Table 7.4: *Results of RVA/IHA at Vouen Sai-Dams impact analysis*

Parameter	Mean without RV	Mean with RV	RVA Boundaries Low	RVA Boundaries High	Expected Count	Observed Count	D_i (%)	IHA Class
Parameter Group #1: Magnitude of monthly flows (m^3/s)								
January	350	517	255	445	28	2	-93	H
February	238	452	182	339	22	2	-91	H
March	197	420	135	314	22	2	-91	H
April	233	429	147	374	20	5	-75	H
May	583	607	261	905	22	28	27	L
June	800	756	447	1153	18	30	67	M
July	1178	994	664	1693	25	24	-4	L
August	1594	1238	1097	2092	24	21	-13	L
September	1539	1188	932	2146	24	24	0	L
October	1173	937	816	1531	21	25	19	L
November	769	755	583	956	23	29	26	L
December	520	632	419	620	24	13	-46	M
Parameter Group #2: Magnitude and duration of annual extreme flows and baseflow conditions (m^3/s)								
1-day minimum	115	376	84	172	22	0	-100	H
3-day minimum	117	377	87	175	22	0	-100	H
7-day minimum	123	379	91	184	22	0	-100	H
30-day minimum	151	393	115	237	22	1	-95	H
90-day minimum	209	424	155	320	22	2	-91	H
1-day maximum	5217	3072	2851	7584	26	15	-42	M
3-day maximum	4633	2792	2658	6608	27	14	-48	M
7-day maximum	3659	2317	2218	5100	25	13	-48	M
30-day maximum	2174	1518	1568	2781	24	10	-58	M
90-day maximum	1597	1213	1234	1959	21	13	-38	M
Number of zero days	0	0	0	0	31	31	0	L
Base flow index	0.2	0.5	0.1	0.2	24	1	-96	H
Parameter Group #3: Timing of annual extreme flows (Julian day)								
Date of minimum	103	111	82	125	24	20	-17	L
Date of maximum	236	228	194	278	22	23	5	L
Parameter Group #4: Frequency and duration of high and low pulses								
Low pulse count	4	0	2	5	22	2	-91	H
Low pulse duration	26	21	13	39	24	2	-92	H
High pulse count	7	4	5	9	24	13	-46	M
High pulse duration	6	4	4	7	20	14	-30	L
Parameter Group #5: Rate and frequency of flow changes								
Rise rate	217	116	154	280	23	4	-83	H
Fall rate	-77	-38	-100	-55	20	3	-85	H
Number of reversals	59	59	51	67	22	25	14	L
Average D_i (%)							**43**	**M**

7.3.1.2. Analysis at Basin Outlet-Dams Impact Analysis

The effects of the dams on the hydrologic regime seen at the basin outlet closely resemble the effects observed at Vouen Sai. This similarity can be attributed to the absence of significant alterations between the two points, as there are minimal differences in the geographical area, and no major additional dams that cause abrupt changes within this stretch. This geographical difference is illustrated in *Figure 4.1.* Comparisons of simulated streamflows with- and without dams are depicted on daily, monthly, and annual scales in *Figures 7.14, 7.15* and *7.16,* respectively. Again, the reduction of high flows and concurrent increase of low flows are clearly apparent in the hydrographs. Overall, the percentage differences between the with dam and without dam scenarios are smaller at the basin outlet than at Vouen Sai. At the outlet, the maximum average monthly flow without dams reaches 1760 m^3/s, whereas the peak flow with dams is 1430 m^3/s, (a 19% reduction in the average peak flow). The lowest average monthly flow rises from 211 m^3/s to 451 m^3/s after dam incorporation (a 53% increase). *Figure 7.16* illustrates the impact of dam incorporation on the annual flow patterns. The average annual flow without dams subtly exceeds that with dams, with a marginal difference of around 1%.

The results of the RVA/IHA for the outlet are presented in *Table 7.5*. The deviations observed in the IHA metrics at the outlet mirror those at Vouen Sai. The overall degree of hydrologic alteration is 38% and falls under the "moderate" category. This is a slight reduction compared to the alteration observed at Vouen Sai (43%) and could be because the basin outlet is further downstream of Vouen Sai. There is a 106 km reach after Vouen Sai that is undisturbed by dams, which could provide more opportunities for the streamflow to attenuate and become more similar to the BL natural flow.

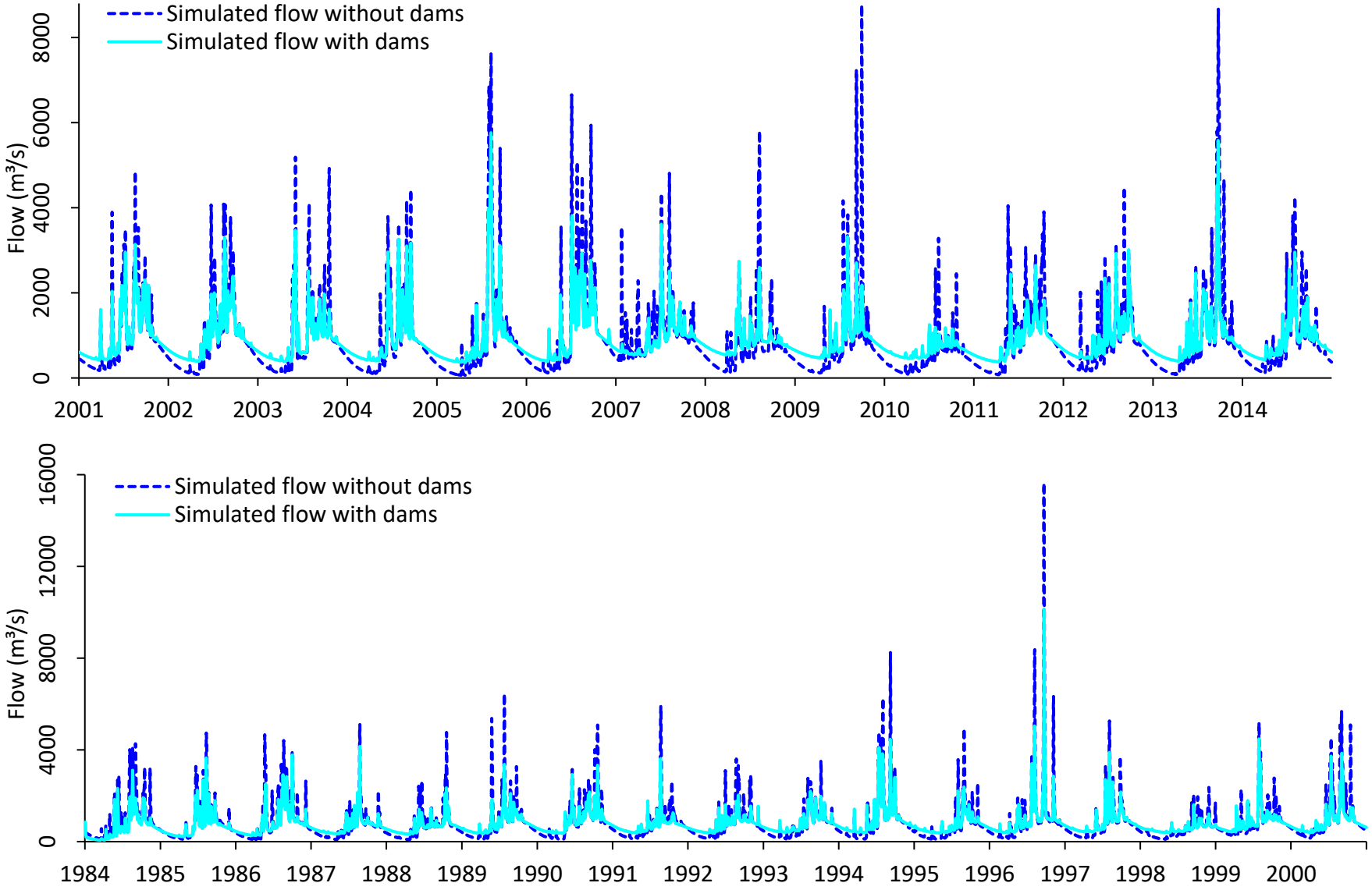

Figure 7.14: *Daily streamflow comparison at basin outlet, 1984 to 2000 (top) and 2001 to 2014 (bottom)-Dam impact analysis*

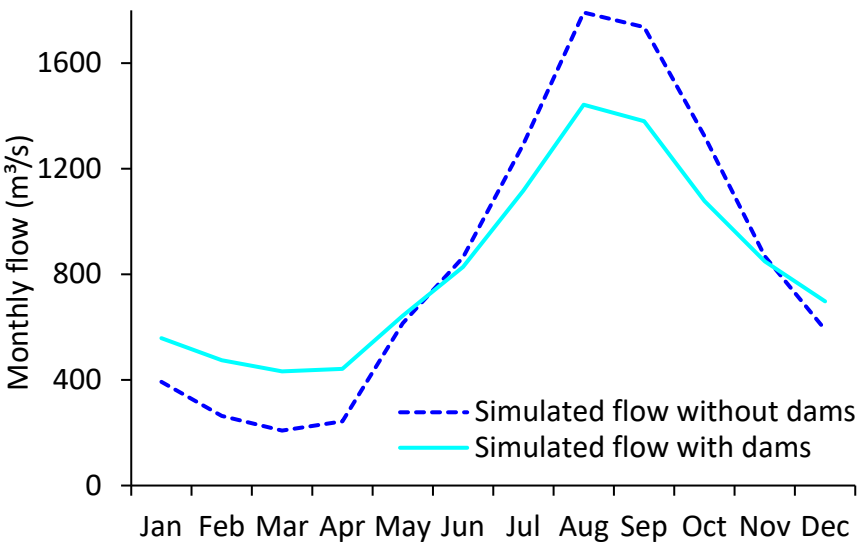

Figure 7.15: *Average monthly streamflow comparison at basin outlet-Dam impact analysis*

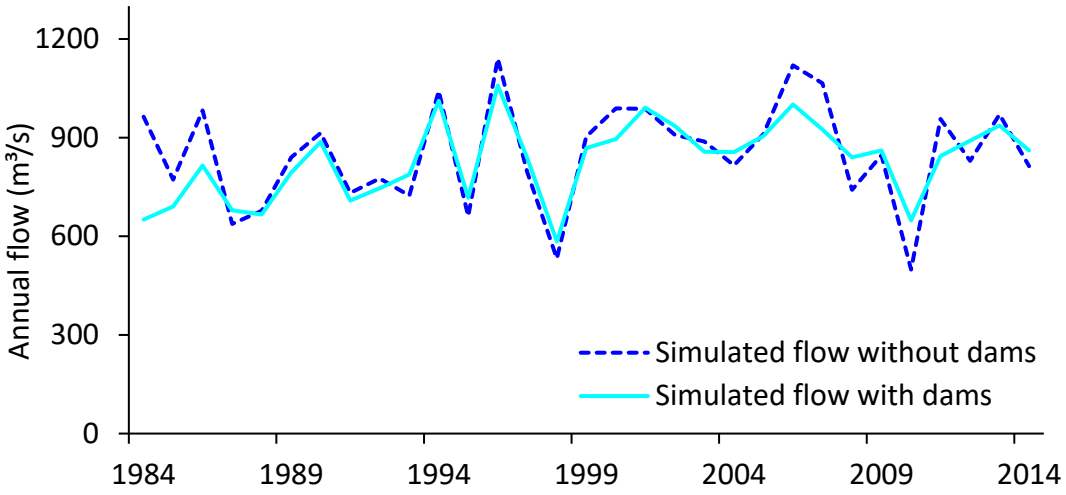

Figure 7.16: *Average annual streamflow comparison at basin outlet-Dam impact analysis*

Table 7.5: *Results of RVA/IHA at basin outlet-Dams impact analysis*

Parameter	Mean without RV	Mean with RV	RVA Boundaries Low	RVA Boundaries High	Expected Count	Observed Count	D_i (%)	IHA Class
Parameter Group #1: Magnitude of monthly flows (m^3/s)								
January	393	559	294	492	27	2	-93	H
February	264	476	160	367	28	2	-93	H
March	208	433	146	319	22	2	-91	H
April	243	441	151	392	20	7	-65	M
May	615	643	278	951	22	28	27	L
June	865	825	475	1254	20	28	40	M
July	1293	1114	711	1875	23	24	4	L
August	1792	1440	1229	2354	24	24	0	L
September	1737	1384	1045	2429	24	24	0	L
October	1324	1079	928	1720	21	25	19	L
November	868	851	674	1063	23	29	26	L
December	590	699	483	697	25	13	-48	M
Parameter Group #2: Magnitude and duration of annual extreme flows and baseflow conditions (m^3/s)								
1-day minimum	126	385	90	190	22	0	-100	H
3-day minimum	129	386	95	193	22	0	-100	H
7-day minimum	134	388	106	202	22	0	-100	H
30-day minimum	163	404	124	252	22	1	-95	H
90-day minimum	224	438	165	337	22	2	-91	H
1-day maximum	5562	3559	3159	7964	26	18	-31	L
3-day maximum	5049	3309	2865	7233	25	19	-24	L
7-day maximum	4074	2797	2469	5679	25	18	-28	L
30-day maximum	2438	1785	1743	3134	25	13	-48	M
90-day maximum	1786	1406	1364	2207	21	18	-14	L
Number of zero days	0	0	0	0	31	31	0	L
Base flow index	0	0	0	0	26	1	-96	H
Parameter Group #3: Timing of annual extreme flows (Julian day)								
Date of minimum	103	111	82	125	24	22	-8	L
Date of maximum	235	231	193	276	23	24	4	L
Parameter Group #4: Frequency and duration of high and low pulses								
Low pulse count	4	0	2	5	17	3	-82	H
Low pulse duration	29	22	16	42	21	2	-90	H
High pulse count	6	4	4	8	16	11	-31	L
High pulse duration	7	5	4	9	23	19	-17	L
Parameter Group #5: Rate and frequency of flow changes								
Rise rate	215	120	152	278	24	6	-75	H
Fall rate	-78	-42	-101	-55	20	5	-75	H
Number of reversals	55	54	46	64	22	24	9	L
Average D_i (%)							**38**	**M**

7.3.2. Impact of Potential Climate Change only

7.3.2.1. Analysis at Vouen Sai Station-Climate Change Impact Analysis

Figure 7.17 presents the average monthly streamflow at Vouen Sai for the three future periods (NF, MF and FF) under the climate change scenarios along with the BL natural flow conditions. In the NF period, the increases were limited mainly to September for both scenarios. However, in the MF and FF, the impact of climate change grew to impact much of the year. The hydrographs observed under both climate change scenarios maintain a similar pattern as the BL hydrograph, albeit with higher peak flows than the BL conditions.

The flows under the SSP5-8.5 scenario demonstrate a more pronounced impact compared to those under the SSP2-4.5. The BL average flow is 728 m^3/s, and the projected average flows for the future periods increase by 2% each in NF and MF, and by 13% in FF under SSP2-4.5, and 3% in NF, 12% in MF and 29% in FF under SSP5-8.5 scenario. Seasonal peak flow relative to BL is projected to increase by 7%, 14% and 18%, under SSP2-4.5, and by 11%, 30% and 35% under SSP5-8.5, during NF, MF and FF, respectively. Projected increases in streamflow are likely due to projected increases in precipitation. The increasing trend in projected streamflow from NF to FF periods follows the same pattern as the increasing trend in projected precipitation. Another notable alteration due to climate change is the timing of the seasonal peak flow. While the peak flow in the BL occurs in August, the peak flow during both the NF and MF periods shifts to September under both SSP scenarios. For the FF, under SSP2-4.5, the peak flow timing aligns with the baseline timing of August. However, under the SSP5-8.5 scenario, the peak flow timing shifts to September. The shifts in peak flow timing are likely due to increased temperature from climate change, which can increase PET and change the seasonal precipitation cycle. The uncertainties in precipitation patterns under climate change contribute to the uncertainty in peak flow timing.

The daily simulated streamflow data for the climate change scenarios were utilized in the RVA/IHA. The results of the analysis of the daily streamflow at Vouen Sai are presented in *Table 7.6*. In general, the observed alterations across all metrics ranged from low to moderate levels, apart from high alteration in the magnitude of monthly flows during January and December. However, in contrast to the high impact of dams seen on annual extreme flow conditions, the impacts due to climate change were low in the NF and MF, and escalated to a medium level of alteration in the FF. The overall hydrologic alterations increase from 19% in NF to 24% in FF under SSP2-4.5, and from 16% to 25% under SSP5-8.5, indicating an increasing impact of climate change as we move further into the future. All these alterations remain within the "low" category.

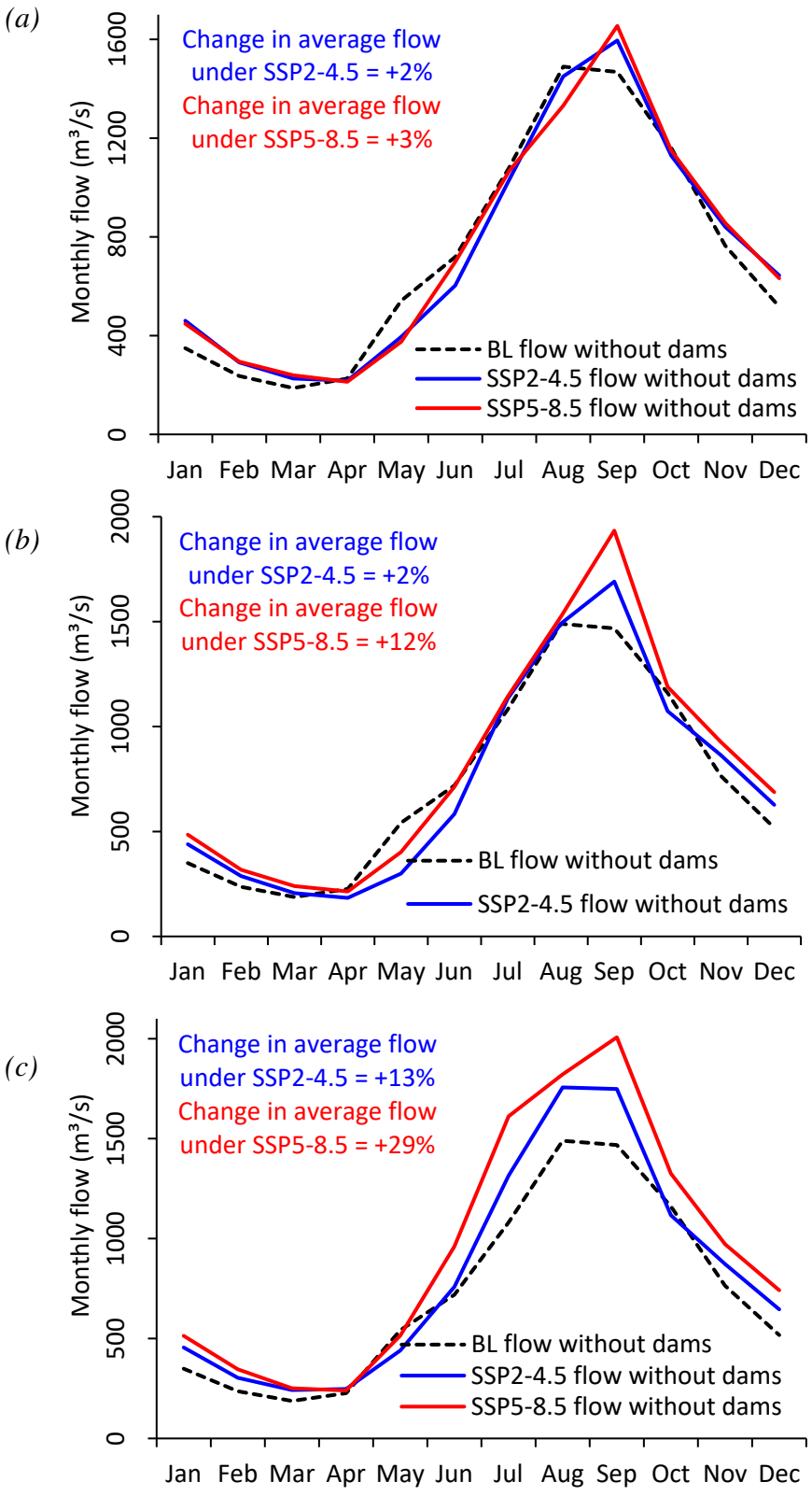

Figure 7.17: *Average monthly streamflow comparisons, and changes relative to BL at Vouen Sai (a) NF (b) MF (c) FF-Climate change impact analysis*

Table 7.6: *Results of RVA/IHA at Vouen Sai-Climate change impact analysis*

Parameter	BL Vs. NF				BL Vs. MF				BL Vs. FF			
	SSP2-4.5		SSP5-8.5		SSP2-4.5		SSP5-8.5		SSP2-4.5		SSP5-8.5	
	D_i (%)	IHA Class	D_i (%)	IHA Class	D_i (%)	IHA Class	D_i (%)	IHA Class	D_i (%)	IHA Class	D_i (%)	IHA Class
Parameter Group #1												
January	-36	M	-45	M	-34	L	-78	H	-60	M	-78	H
February	3	L	-2	L	13	L	-38	M	-10	L	-38	M
March	25	L	8	L	42	M	24	L	-6	L	24	L
April	19	L	1	L	24	L	5	L	-26	L	5	L
May	-3	L	2	L	-29	L	18	L	-47	M	18	L
June	2	L	2	L	12	L	-11	L	-17	L	-11	L
July	14	L	24	L	3	L	-48	M	-17	L	-48	M
August	14	L	3	L	24	L	-15	L	-4	L	-15	L
September	19	L	19	L	-3	L	-25	L	2	L	-25	L
October	37	M	49	M	49	M	12	L	36	M	12	L
November	25	L	14	L	13	L	-21	L	13	L	-21	L
December	-43	M	-48	M	-26	L	-70	H	-60	M	-70	H
Parameter Group #2												
1-day minimum	-35	M	-24	L	1	L	-49	M	-72	H	-49	M
3-day minimum	-30	L	-24	L	-4	L	-55	M	-66	M	-55	M
7-day minimum	-30	L	-24	L	-4	L	-61	M	-66	M	-61	M
30-day minimum	-13	L	-13	L	7	L	-21	L	-55	M	-21	L
90-day minimum	14	L	3	L	18	L	18	L	-27	L	18	L
1-day maximum	1	L	-13	L	-5	L	-14	L	14	L	-14	L
3-day maximum	1	L	-8	L	-5	L	-14	L	5	L	-14	L
7-day maximum	9	L	-11	L	3	L	-7	L	3	L	-7	L
30-day maximum	4	L	-12	L	-8	L	-30	L	2	L	-30	L
90-day maximum	31	L	14	L	18	L	-53	M	12	L	-53	M
Number of zero days	0	L	0	L	0	L	0	L	0	L	0	L
Base flow index	-38	M	-33	L	-1	L	-45	M	-40	M	-45	M
Parameter Group #3												
Date of minimum	-22	L	-22	L	-28	L	-28	L	-62	M	-28	L
Date of maximum	-1	L	4	L	14	L	24	L	-7	L	24	L
Parameter Group #4												
Low pulse count	-25	L	-16	L	-28	L	-28	L	-28	L	-28	L
Low pulse duration	-51	M	-19	L	-44	M	-44	M	-49	M	-44	M
High pulse count	32	L	39	M	17	L	31	L	17	L	31	L
High pulse duration	26	L	13	L	31	L	-2	L	11	L	-2	L
Parameter Group #5												
Rise rate	-78	H	-57	M	-55	M	-21	L	-27	L	-21	L
Fall rate	-17	L	-28	L	-26	L	18	L	12	L	18	L
Number of reversals	4	L	-16	L	-7	L	-7	L	-23	L	-7	L
Average D_i (%)	**19**	**L**	**16**	**L**	**16**	**L**	**25**	**L**	**24**	**L**	**25**	**L**

7.3.2.2. Analysis at Basin Outlet-Climate Change Impact Analysis

Figure 7.18 shows the average monthly streamflow at the basin outlet for three future periods (NF, MF and FF) under climate change scenarios, along with the BL natural flow conditions. The flow patterns mirror those observed at Vouen Sai, with the only difference being increased flow magnitudes. During all time periods, the average monthly flows at the outlet exceed those observed at Vouen Sai. The BL average flow at the outlet is 819 m^3/s, and the projected average flows for the future periods increase by 2% each in NF and MF, and by 15% in FF under SSP2-4.5, and 3% in NF, 13% in MF and 34% in FF under SSP5-8.5. Seasonal peak flow relative to BL is projected to increase by 9%, 15% and 20%, under SSP2-4.5, and by 13%, 33% and 40% under SSP5-8.5, during NF, MF and FF, respectively. The timing of peak flows at the outlet also mirrors that observed at Vouen Sai.

Similarly, the RVA/IHA results at the basin outlet, as presented in *Table 7.7*, closely resemble those observed at Vouen Sai. The degree of hydrologic alteration at the basin outlet is slightly less intense than at Vouen Sai, possibly due to the presence of a 2,540 km^2 subbasin and a 106 km reach between the two points. The larger area of the subbasin could mean more spatial averaging of hydrological processes, which could help to smooth out the effects of climate change and reduce alteration at the basin outlet. The overall hydrologic alterations increase from 17% in NF to 23% in FF under SSP2-4.5, and from 14% to 24% under SSP5-8.5. All these alterations remain within the "low" category.

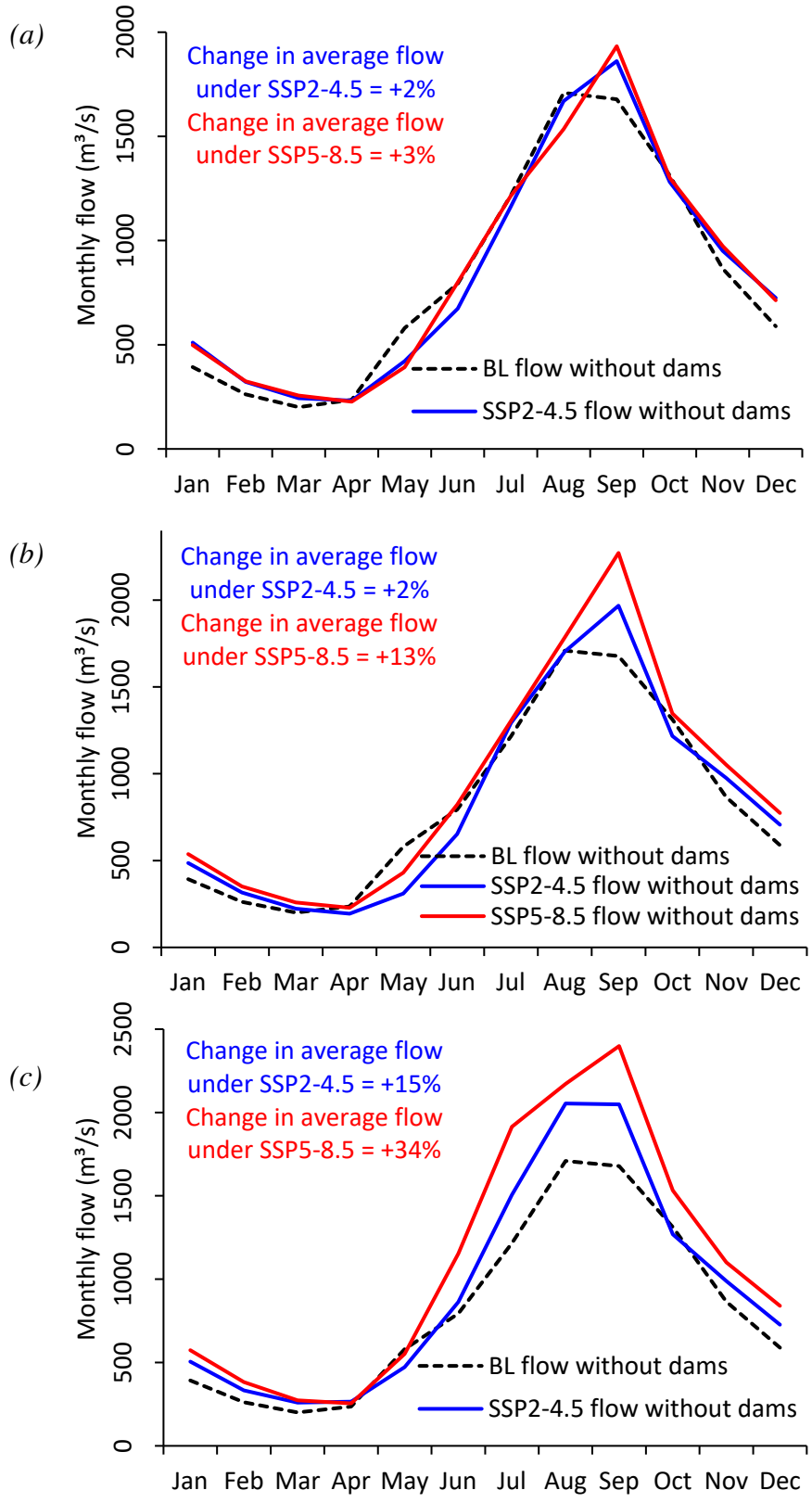

Figure 7.18: *Average monthly streamflow comparisons, and changes relative to BL at basin outlet (a) NF (b) MF (c) FF-Climate change impact analysis*

Table 7.7: *Results of RVA/IHA at basin outlet-Climate change impact analysis*

Parameter	BL Vs. NF				BL Vs. MF				BL Vs. FF			
	SSP2-4.5		SSP5-8.5		SSP2-4.5		SSP5-8.5		SSP2-4.5		SSP5-8.5	
	D_i (%)	IHA Class	D_i (%)	IHA Class	D_i (%)	IHA Class	D_i (%)	IHA Class	D_i (%)	IHA Class	D_i (%)	IHA Class
Parameter Group #1												
January	-34	L	-47	M	-31	L	-59	M	-59	M	-77	H
February	3	L	-8	L	13	L	-4	L	-15	L	-44	M
March	14	L	8	L	30	L	-6	L	-29	L	0	L
April	19	L	1	L	24	L	24	L	-32	L	5	L
May	1	L	1	L	-32	L	-32	L	-38	M	18	L
June	-8	L	-2	L	1	L	1	L	-21	L	-15	L
July	14	L	24	L	3	L	14	L	-28	L	-48	M
August	9	L	-7	L	13	L	8	L	-8	L	-25	L
September	19	L	14	L	-8	L	-8	L	-3	L	-30	L
October	31	L	42	M	42	M	42	M	30	L	6	L
November	19	L	4	L	8	L	-25	L	2	L	-25	L
December	-43	M	-48	M	-26	L	-65	M	-60	M	-75	H
Parameter Group #2												
1-day minimum	-30	L	-24	L	-4	L	-21	L	-66	M	-49	M
3-day minimum	-30	L	-24	L	-4	L	-21	L	-66	M	-55	M
7-day minimum	-30	L	-24	L	-4	L	-4	L	-66	M	-61	M
30-day minimum	-2	L	-13	L	7	L	13	L	-55	M	-21	L
90-day minimum	3	L	-8	L	18	L	13	L	-27	L	13	L
1-day maximum	-3	L	-7	L	-8	L	-13	L	6	L	-17	L
3-day maximum	1	L	1	L	0	L	-9	L	5	L	-14	L
7-day maximum	9	L	9	L	3	L	-12	L	-2	L	-7	L
30-day maximum	19	L	-7	L	-3	L	8	L	2	L	-46	M
90-day maximum	25	L	8	L	13	L	1	L	7	L	-49	M
Number of zero days	0	L	0	L	0	L	0	L	0	L	0	L
Base flow index	-40	M	-36	M	-5	L	-5	L	-43	M	-33	L
Parameter Group #3												
Date of minimum	-38	M	-28	L	-40	M	-40	M	-65	M	-26	L
Date of maximum	4	L	9	L	24	L	13	L	8	L	19	L
Parameter Group #4												
Low pulse count	35	M	-5	L	-17	L	7	L	7	L	-1	L
Low pulse duration	-48	M	-22	L	-41	M	-8	L	-46	M	-35	M
High pulse count	19	L	19	L	-12	L	31	L	-5	L	-34	M
High pulse duration	9	L	-16	L	19	L	14	L	-7	L	-33	L
Parameter Group #5												
Rise rate	-59	M	-38	M	-41	M	2	L	-14	L	-8	L
Fall rate	-9	L	-26	L	-23	L	24	L	6	L	0	L
Number of reversals	9	L	-6	L	-17	L	9	L	-17	L	-2	L
Average D_i (%)	**17**	**L**	**14**	**L**	**14**	**L**	**15**	**L**	**23**	**L**	**24**	**L**

7.3.3. Combined Impacts of Dams and Potential Climate Change

7.3.3.1. Analysis at Vouen Sai Station-Combined Impact Analysis

Figure 7.19 shows the average monthly streamflows at Vouen Sai across three future periods (NF, MF and FF) under the combined influence of dams and climate change, as well as the BL natural flow conditions. Dams have a clear impact on the flow patterns during the NF period, smoothing peaks and increasing low flows. Seasonal peak flows decrease by 21% and 19% under SSP2-4.5 and SSP5-8.5, respectively, while the lowest flows increase by 129% and 124%, respectively. However, climate change becomes more influential in the MF and FF periods, particularly in terms of seasonal peak flows, which start to increase compared to NF, and even surpass BL levels by 1% in FF under SSP5-8.5. The shift of peak flow timing from August in the BL to September under climate change scenarios is evident across all time periods. The lowest flows in the MF and FF consistently increase ranging from 134% to 182%.

Table 7.8 shows the results of RVA/IHA for the combined impact scenario at Vouen Sai. The combined scenario shows high negative deviations in nearly all metrics, especially in NF, compared to the individual scenarios. Interestingly, the combined scenario shows a decreasing trend in overall alteration from NF to FF, in contrast to the increasing trend observed in the climate change-only scenario. This overall alteration shifts from 60% in NF to 53% in FF under SSP2-4.5, and from 60% in NF to 49% in FF under SSP5-8.5. This may be because dams and climate change have opposing effects on high flows. This suggests that the inclusion of dams could be mitigating the impacts of climate change, especially for high flows, although it introduces its own level of alterations. Overall, the combined impact of dams and climate change is seen to induce greater alterations in the NF compared to MF and FF periods. The overall ranges of hydrologic alteration fall within the higher end of the "moderate" category.

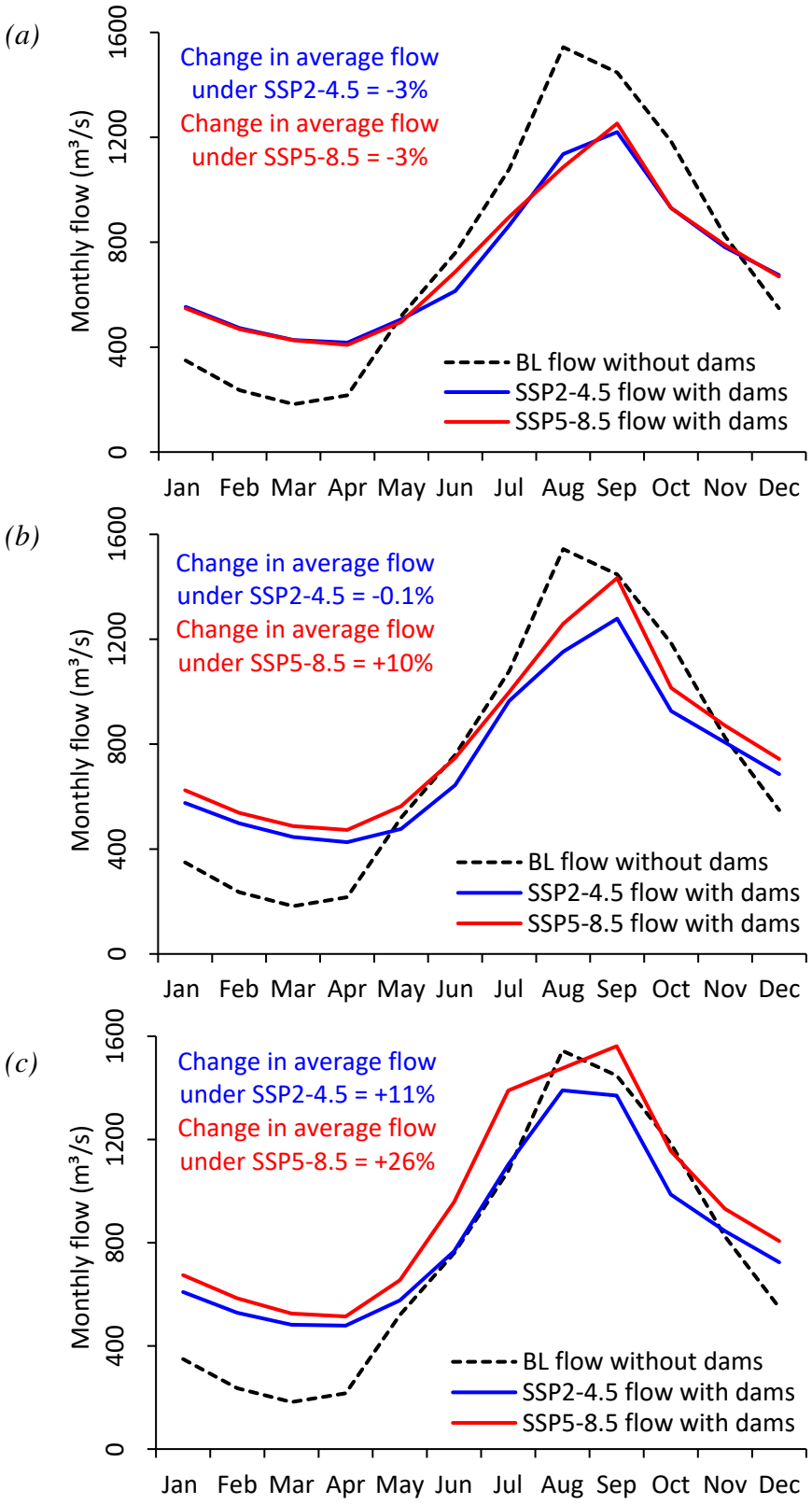

Figure 7.19: *Average monthly streamflow comparisons, and changes relative to BL at Vouen Sai (a) NF (b) MF (c) FF-Combined impact analysis*

Table 7.8: *Results of RVA/IHA at Vouen Sai-Combined impact analysis*

Parameter	BL Vs. NF				BL Vs. MF				BL Vs. FF			
	SSP2-4.5		SSP5-8.5		SSP2-4.5		SSP5-8.5		SSP2-4.5		SSP5-8.5	
	D_i (%)	IHA Class	D_i (%)	IHA Class	D_i (%)	IHA Class	D_i (%)	IHA Class	D_i (%)	IHA Class	D_i (%)	IHA Class
Parameter Group #1												
January	-96	H	-96	H	-100	H	-100	H	-100	H	-100	H
February	-100	H	-95	H	-100	H	-100	H	-100	H	-100	H
March	-95	H	-95	H	-100	H	-100	H	-100	H	-100	H
April	-76	H	-76	H	-100	H	-100	H	-88	H	-100	H
May	35	M	30	L	41	M	30	L	30	L	35	M
June	52	M	66	M	65	M	72	H	52	M	31	L
July	0	L	19	L	19	L	19	L	19	L	-21	L
August	-25	L	-40	M	-33	L	-17	L	9	L	-17	L
September	14	L	19	L	29	L	29	L	29	L	19	L
October	31	L	31	L	48	M	48	M	36	M	48	M
November	35	M	24	L	35	M	19	L	29	L	-8	L
December	-75	H	-75	H	-95	H	-100	H	-90	H	-100	H
Parameter Group #2												
1-day minimum	-100	H	-100	H	-100	H	-100	H	-100	H	-100	H
3-day minimum	-100	H	-100	H	-100	H	-100	H	-100	H	-100	H
7-day minimum	-100	H	-100	H	-100	H	-100	H	-100	H	-100	H
30-day minimum	-100	H	-95	H	-100	H	-100	H	-100	H	-100	H
90-day minimum	-95	H	-95	H	-100	H	-100	H	-100	H	-100	H
1-day maximum	-86	H	-82	H	-71	H	-52	M	-43	M	-28	L
3-day maximum	-87	H	-82	H	-72	H	-54	M	-40	M	-27	L
7-day maximum	-86	H	-86	H	-70	H	-40	M	-21	L	-16	L
30-day maximum	-75	H	-70	H	-64	M	-33	L	-17	L	-12	L
90-day maximum	-66	M	-66	M	-59	M	-11	L	-6	L	12	L
Number of zero days	0	L	0	L	0	L	0	L	0	L	0	L
Base flow index	-95	H	-100	H	-100	H	-100	H	-100	H	-100	H
Parameter Group #3												
Date of minimum	-40	M	-40	M	-54	M	-43	M	-54	M	-17	L
Date of maximum	35	M	19	L	35	M	35	M	18	L	13	L
Parameter Group #4												
Low pulse count	-95	H	-89	H	-100	H	-100	H	-100	H	-100	H
Low pulse duration	-95	H	-95	H	-100	H	-100	H	-100	H	-100	H
High pulse count	-90	H	-55	M	-85	H	-43	M	-54	M	-2	L
High pulse duration	-23	L	-46	M	-13	L	-19	L	5	L	-26	L
Parameter Group #5												
Rise rate	-100	H	-100	H	-95	H	-100	H	-95	H	-78	H
Fall rate	-100	H	-100	H	-100	H	-100	H	-100	H	-81	H
Number of reversals	19	L	-24	L	-21	L	7	L	-21	L	-10	L
Average *Di* (%)	**60**	**M**	**60**	**M**	**62**	**M**	**56**	**M**	**53**	**M**	**49**	**M**

7.3.3.2. Analysis at Basin Outlet (Sink)-Combined Impact Analysis

Figure 7.20 shows the average monthly streamflows at the basin outlet across three future periods (NF, MF and FF) under the combined influence of dams and climate change, as well as the BL natural flow conditions. The flow patterns are similar to those observed at Vouen Sai, but with higher flow magnitudes. Dams have a clear impact on the flow patterns during the NF period, smoothing peaks and increasing low flows. In the NF, seasonal peak flows decrease by 14% and 12% under SSP2-4.5 and SSP5-8.5, respectively, while the lowest flows increase by 118% and 113%. However, climate change becomes more influential in the MF and FF periods, particularly in terms of seasonal peak flows, which start to increase compared to NF, and even surpass BL levels by 2% and 13% in MF and FF, respectively under SSP5-8.5. The shift of peak flow timing from August in the BL to September under climate change scenarios is evident across all time periods. The lowest flows in the MF and FF consistently increase ranging from 120% to 167%.

Table 7.9 shows the results of RVA/IHA for the combined impact scenario at the basin outlet. These results are similar to those seen in Vouen Sai, but slightly lower. The overall degree of hydrologic alteration decreased from 53% in NF to 48% in FF under SSP2-4.5, and from 53% in NF to 45% in FF under SSP5-8.5. This may be due to the presence of a subbasin and a reach between the two points, since a larger area of the subbasin could help to smooth out the effects of climate change and reduce alteration at the basin outlet. The ranges of alteration fall within the "moderate" category.

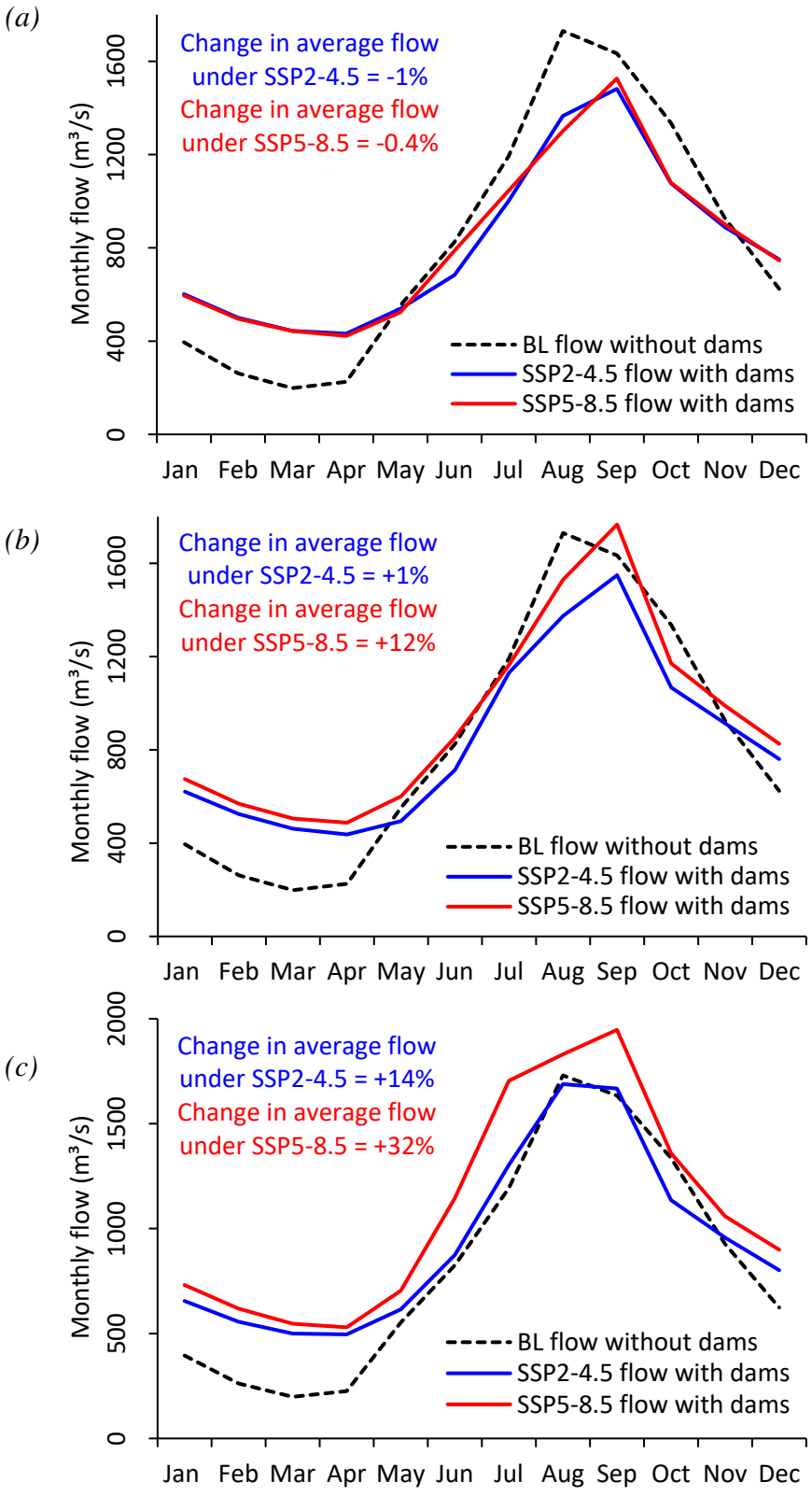

Figure 7.20: *Average monthly streamflow comparisons, and changes relative to BL at basin outlet (a) NF (b) MF (c) FF-Combined impact analysis*

Table 7.9: *Results of RVA/IHA at basin outlet-Combined impact analysis*

Parameter	BL Vs. NF				BL Vs. MF				BL Vs. FF			
	SSP2-4.5		SSP5-8.5		SSP2-4.5		SSP5-8.5		SSP2-4.5		SSP5-8.5	
	D_i (%)	IHA Class	D_i (%)	IHA Class	D_i (%)	IHA Class	D_i (%)	IHA Class	D_i (%)	IHA Class	D_i (%)	IHA Class
Parameter Group #1												
January	-100	H	-96	H	-100	H	-100	H	-100	H	-100	H
February	-100	H	-96	H	-100	H	-100	H	-100	H	-100	H
March	-95	H	-95	H	-100	H	-100	H	-100	H	-100	H
April	-64	M	-70	H	-88	H	-100	H	-88	H	-100	H
May	35	M	35	M	41	M	27	L	30	L	30	L
June	31	L	43	M	49	M	47	M	30	L	5	L
July	19	L	35	M	29	L	28	L	24	L	-30	L
August	-11	L	-21	L	-12	L	3	L	14	L	-12	L
September	24	L	24	L	29	L	23	L	24	L	14	L
October	31	L	36	M	48	M	48	M	36	M	42	M
November	35	M	24	L	35	M	15	L	24	L	-19	L
December	-71	H	-76	H	-90	H	-100	H	-85	H	-100	H
Parameter Group #2												
1-day minimum	-100	H	-100	H	-100	H	-100	H	-100	H	-100	H
3-day minimum	-100	H	-100	H	-100	H	-100	H	-100	H	-100	H
7-day minimum	-100	H	-95	H	-100	H	-100	H	-100	H	-100	H
30-day minimum	-100	H	-95	H	-100	H	-100	H	-100	H	-100	H
90-day minimum	-95	H	-95	H	-100	H	-100	H	-100	H	-100	H
1-day maximum	-54	M	-59	M	-62	M	-23	L	-5	L	0	L
3-day maximum	-43	M	-38	M	-55	M	-7	L	4	L	4	L
7-day maximum	-43	M	-52	M	-45	M	-13	L	9	L	-1	L
30-day maximum	-52	M	-38	M	-55	M	-1	L	4	L	-11	L
90-day maximum	-38	M	-38	M	-29	L	18	L	30	L	18	L
Number of zero days	0	L	0	L	0	L	0	L	0	L	0	L
Base flow index	-95	H	-100	H	-100	H	-100	H	-100	H	-100	H
Parameter Group #3												
Date of minimum	-35	M	-35	M	-48	M	-48	M	-59	M	-17	L
Date of maximum	35	M	9	L	29	L	28	L	13	L	13	L
Parameter Group #4												
Low pulse count	-93	H	-86	H	-100	H	-100	H	-100	H	-100	H
Low pulse duration	-94	H	-94	H	-100	H	-100	H	-100	H	-100	H
High pulse count	-70	H	-25	L	-77	H	-13	L	9	L	-23	L
High pulse duration	4	L	-17	L	-19	L	1	L	2	L	2	L
Parameter Group #5												
Rise rate	-100	H	-100	H	-95	H	-100	H	-85	H	-59	M
Fall rate	-100	H	-100	H	-100	H	-100	H	-88	H	-50	M
Number of reversals	-8	L	-30	L	-32	L	-23	L	-27	L	-10	L
Average *Di* (%)	**53**	**M**	**53**	**M**	**59**	**M**	**50**	**M**	**48**	**M**	**45**	**M**

Chapter 8

Conclusion and Recommendations

This study assessed alterations in the hydrologic regime of the Sesan River caused by hydropower dams and potential climate change. Calibrated and evaluated HEC-HMS models were used to simulate streamflows under different scenarios. Climate change projections were based on the daily precipitation, minimum temperature, and maximum temperature, which were estimated from an ensemble of three ESMs under SSP2-4.5 and SSP5-8.5 scenarios. Results indicated a consistent rise in future precipitation and temperatures under both SSP scenarios. Precipitation showed increases of 7%, 4%, and 13% under SSP2-4.5, and 7%, 14%, and 29% under SSP5-8.5 in the NF, MF, and FF periods, respectively. The minimum temperature showed increases of 8%, 13%, and 16% under SSP2-4.5, and 10%, 18%, and 26% under SSP5-8.5. Maximum temperatures showed increases of 3%, 5%, and 7% under SSP2-4.5, and 3%, 7%, and 12% under SSP5-8.5.

Hydrologic alterations were assessed at the Vouen Sai Station and the basin outlet, under three primary scenarios: hydropower dam operations only, climate change impact only, and the combined impact of dams and climate change. The alterations were quantified using the RVA/IHA. The addition of dams significantly altered the hydrograph characteristics by attenuating and smoothing its peaks and troughs. High flows during the wet season experienced a reduction of 21% at Vouen Sai and 19% at the outlet, while low flows increased by 55% at Vouen Sai and 53% at the outlet. The overall degree of hydrologic alteration from the hydropower dams in the basin was 43% at Vouen Sai and 38% at the outlet, both of which fall in the "moderate" category.

Climate change most noticeably increased high flow rates during wet months, with the impact limited to September in the NF, but impacting much of the year in the MF and FF periods.

At Vouen Sai, the future average flow increased by 2-13% under SSP2-4.5, and 3-29% under SSP5-8.5. Seasonal peak flow increased by 7-18% under SSP2-4.5, and 11-35% under SSP5-8.5. At the basin outlet, the future average flow increased by 2-15% under SSP2-4.5, and 3-34% under SSP5-8.5. Seasonal peak flow increased by 9- 20% under SSP2-4.5, and by 13-40% under SSP5-8.5. These increases in streamflow are likely due to projected increases in precipitation. The increasing trend in projected streamflow from NF to FF periods follows the same pattern as the increasing trend in projected precipitation. Another notable alteration due to climate change was the shift in the timing of peak flow, from August in the BL to September in the future periods. The shifts in peak flow timing are likely due to increased temperature from climate change, which can increase PET and change the seasonal precipitation cycle. The uncertainties in precipitation patterns under climate change contribute to the uncertainty in peak flow timing. At Vouen Sai, the overall degree of alteration spanned 19-24% under SSP2-4.5, and 16-25% under SSP5-8.5. At the basin outlet, the alterations spanned 17-23% under SSP2-4.5, and 14-24% under SSP5-8.5. All these alterations fall in the "low" category.

The combined impact of dams and climate change exceeded that of the individual scenarios, however, it showed a decreasing trend in the overall alteration from NF to FF, in contrast to the increasing trend under climate change only scenario. At Vouen Sai, the degree of alteration decreased from 60% in NF to 53% in FF under SSP2-4.5 and from 60% to 49% under SSP5-8.5. Similarly, at the outlet, it decreased from 53% to 48% under SSP2-4.5 and from 53% to 45% under SSP5-8.5. This is likely because dams and climate change have opposing effects on high flows. Therefore, the results suggest that dams mitigate the impacts of climate change, especially for high flows, although they introduce their own level of alterations. All these alterations fall in the "moderate" category.

8.1. Scope and Limitations

This study acknowledges the following scope and limitations:

i. This study assumes that the hydrologic model parameters remain constant during forecasts, neglecting potential changes to the watershed (e.g., wildfires, changes in forest species, etc.) due to climate change.

ii. The study area is limited to Sesan River Basin only.

iii. Limited to existing hydropower dams only.

iv. Limited length of available pre- and post-dam streamflow records.

v. Climate change analysis is based on only three climatic variables: precipitation, minimum and maximum temperature.

vi. Does not account for groundwater interactions or inter-basin transfers.

vii. Assumed values of Manning's *n* were used.

8.2. Recommendations

Building upon the limitations of this research. here are some recommendations for future studies:

i. Hydrologic alteration assessment considering changes in land use and land cover, and groundwater interactions.

ii. Incorporate multiple dam operation rule curves for existing and planned dams.

iii. Explore potential impacts of altered streamflow regimes on hydropower generation, fisheries, agriculture, sediment and nutrients transport, geomorphology, and water quality.

iv. Evaluate tradeoffs and synergies between hydropower generation and environmental flow requirements.

References

Acuña, V., Jorda-Capdevila, D., Vezza, P., De Girolamo, A. M., McClain, M. E., Stubbington, R., ... & Datry, T. (2020). Accounting for flow intermittency in environmental flows design. *Journal of Applied Ecology, 57(4), 742-753.*

Almazroui, M., Saeed, S., Saeed, F., Islam, M. N., & Ismail, M. (2020). Projections of Precipitation and Temperature over the South Asian Countries in CMIP6. *Earth Systems and Environment*, *4*(2), 297-320. https://doi.org/10.1007/s41748-020-00157-

Amatya, D. M., Harrison, C. A., & Trettin, C. C. (2014). Comparison of potential evapotranspiration (PET) using three methods for a grass reference and a natural forest in coastal plain of South Carolina.

Arnold, J. G., Moriasi, D. N., Gassman, P. W., Abbaspour, K. C., White, M. J., Srinivasan, R., ... & Jha, M. K. (2012). SWAT: Model use, calibration, and validation. *Transactions of the ASABE, 55*(4), 1491-1508.

Arthington, A. H., Bhaduri, A., Bunn, S. E., Jackson, S. E., Tharme, R. E., Tickner, D., ... & Ward, S. (2018). The Brisbane declaration and global action agenda on environmental flows (2018). *Frontiers in Environmental Science, 6,* 45.

Asch, R. G., Pilcher, D. J., Rivero-Calle, S., & Holding, J. M. (2016). Demystifying Models: Answers to Ten Common Questions That Ecologists Have About Earth System Models. *Limnology and Oceanography Bulletin*, *25*(3), 65-70. https://doi.org/10.1002/lob.10113

Aslam, R. A., Shrestha, S., & Pandey, V. P. (2018). Groundwater vulnerability to climate change: A review of the assessment methodology. *Science of the Total Environment*, *612*, 853-875

Bajwa, H., & Tim, U. (2002, July). Toward immersive virtual environments for GIS-based Floodplain modeling and Visualization. In *Proceedings of 22nd ESRI user Conference* (pp. 7-23).

Baran, E., & Myschowoda, C. (2009). Dams and fisheries in the Mekong Basin. *Aquatic Ecosystem Health & Management*, *12*(3), 227-234.

Bartles, M., Brauer, T., Ho, D., Fleming, M., Karlovits, G., Pak, J., Van, N., & Willis, J. (2022). Hydrologic Modeling System HEC-HMS: Technical Reference Manual (CPD-74B). U.S. Army Corps of Engineers, Institute for Water Resources, Hydrologic Engineering Center (CEIWR-HEC).

Bergström, S. (1976). Development and application of a conceptual runoff model for Scandinavian catchments.

Carpenter, D. H., & Hayes, D. C. (1996). *Low-flow characteristics of streams in Maryland and Delaware* (Vol. 94, No. 4020). US Geological Survey.

Cavendish, M. G., & Duncan, M. I. (1986). Use of the instream flow incremental methodology: a tool for negotiation. *Environmental Impact Assessment Review*, *6*(4), 347-363.

Chow, V. T. (1959). *Open-channel hydraulics McGraw-Hill Book Company, 1959*. ISBN 07-010776-9.

Christensen, J. H., Boberg, F., Christensen, O. B., & Lucas-Picher, P. (2008). On the need for bias correction of regional climate change projections of temperature and precipitation. *Geophysical Research Letters*, *35*(20). https://doi.org/10.1029/2008GL035694

Clark, C. O. (1945). Storage and the unit hydrograph. *Transactions of the American Society of Civil Engineers*, *110*(1), 1419-1446.

Constable, D. (2015). Atlas of the 3S Basins. Bangkok, Thailand: IUCN & Swiss Agency for Development and Cooperation

Corbari, C., Ravazzani, G., Galvagno, M., Cremonese, E., & Mancini, M. (2017). Assessing crop coefficients for natural vegetated areas using satellite data and eddy covariance stations. *Sensors, 17*(11), 2664.

Devi, G. K., Ganasri, B., & Dwarakish, G. (2015). A Review on Hydrological Models. *Aquatic Procedia*, *4*, 1001-1007. https://doi.org/10.1016/j.aqpro.2015.02.126

Dusting, A., Broadhurst, B., Nichols, S., & Dyer, F. (2017). Act environmental flow guidelines: review Prepared for: Environment, Planning and Sustainable Development Directorate, ACT Government Document history and status Final-revised Act environmental flow guidelines: review. In *Review of the ACT Water Resources Environmental Flow Guidelines*.

Energy Exascale Earth System Model-E3SM Project. (2023). E3SM's Single-Column Model Offers a New Frontier for Model Validation. E3SM Project. https://e3sm.org/e3sms-single-column-model-offers-a-new-frontier-for-model-validation/

Feldman, A. D. (2000). Hydrologic Modeling System Technical Reference Manual. Institute for Water Resources, Hydrologic Engineering Center, Davis, CA.

Flato, G., J. Marotzke, B. Abiodun, P. Braconnot, S.C. Chou, W. Collins, P. Cox, F. Driouech, S. Emori, V. Eyring, C. Forest, P. Gleckler, E. Guilyardi, C. Jakob, V. Kattsov, C. Reason, and M. Rummukainen, 2013: Evaluation of climate models. In *Climate Change 2013: The Physical Science Basis. Contribution of Working Group I to the Fifth Assessment Report of the Intergovernmental Panel on Climate Change*. T.F. Stocker, D. Qin, G.-K. Plattner,

M. Tignor, S.K. Allen, J. Doschung, A. Nauels, Y. Xia, V. Bex, and P.M. Midgley, Eds., Cambridge University Press, pp. 741-882, doi:10.1017/CBO9781107415324.020

Gao, W., Zhang, X., Yang, L., & Liu, H. (2010, July). An improved Sobel edge detection. In *2010 3rd International conference on computer science and information technology* (Vol. 5, pp. 67-71). IEEE.

Green, W. H., & Ampt, G. A. (1911). Studies on Soil Phyics. *The Journal of Agricultural Science*, *4*(1), 1-24.

Gudmundsson, L., Bremnes, J. B., Haugen, J. E., & Skaugen, T. E. (2012). Downscaling RCM precipitation to the station scale using quantile mapping-a comparison of methods. *Hydrology & Earth System Sciences Discussions*, *9*(5), 6185-6201.

Gunawardana, S. K., Shrestha, S., Mohanasundaram, S., Salin, K. R., & Piman, T. (2021). Multiple drivers of hydrological alteration in the transboundary Srepok River Basin of the Lower Mekong Region. *Journal of Environmental Management*, *278*, 111524. https://doi.org/10.1016/j.jenvman.2020.111524

Gutowski Jr., W. J., Decker, S. G., Donavon, R. A., Pan, Z., Arritt, R. W., & Takle, E. S. (2003). Temporal-Spatial Scales of Observed and Simulated Precipitation in Central U.S. Climate. *Journal of Climate*, *16*(22), 3841-3847. https://doi.org/10.1175/1520-0442(2003)016<3841:TSOOAS>2.0.CO;2

Hajima, Tomohiro & Kawamiya, M. & Watanabe, Michio & Kato, Etsushi & Tachiiri, Kaoru & Sugiyama, Masahiro & Watanabe, Shingo & Okajima, Hideki & Ito, Akinori. (2014). Modeling in Earth system science up to and beyond IPCC AR5. *Progress in Earth and Planetary Science.* 1:29. 10.1186/s40645-014-0029-y.

Hargreaves, G. H., & Allen, R. G. (2003). History and evaluation of Hargreaves evapotranspiration equation. *Journal of irrigation and drainage engineering*, *129*(1), 53-63.

Hartmann, D. (2016). *Global Physical Climatology* (2nd ed.). Elsevier. https://books.google.com/books/about/Global_Physical_Climatology.html?id=RsScBAAAQBAJ

Hecht, J. S., Lacombe, G., Arias, M. E., Dang, T. D., & Piman, T. (2019). Hydropower dams of the Mekong River basin: A review of their hydrological impacts. *Journal of Hydrology*, *568*, 285-300. https://doi.org/10.1016/j.jhydrol.2018.10.045

Heo, J. H., Ahn, H., Shin, J. Y., Kjeldsen, T. R., & Jeong, C. (2019). Probability distributions for a quantile mapping technique for a bias correction of precipitation data: A case study to precipitation data under climate change. *Water*, *11*(7), 1475.

Hoang, L. P., Lauri, H., Kummu, M., Koponen, J., Van Vliet, M. T. H., Supit, I., Leemans, R., Kabat, P., & Ludwig, F. (2016). Mekong River flow and hydrological extremes under climate change. *Hydrology and Earth System Sciences*, *20*(7), 3027-3041. https://doi.org/10.5194/hess-20-3027-2016

Hong Troung et al. 2013. Basin Profile of the Upper Sesan River. Project report: Challenge Program on Water & Food Mekong project MK3 "Optimizing the management of a cascade of reservoirs at the catchment level". ICEM - International Centre for Environmental Management, Hanoi Vietnam, 2013

Hortle, K. G. (2007). Consumption and the yield of fish and other aquatic animals from the Lower Mekong Basin. *MRC technical paper, 16,* 1-88.

Horton, P., Schaefli, B., & Kauzlaric, M. (2022). Why do we have so many different hydrological models? A review based on the case of Switzerland. Wiley Interdisciplinary Reviews: *Water, 9(1), e1574.*

Huh, S., Dickey, D. A., Meador, M. R., & Ruhl, K. E. (2005). Temporal analysis of the frequency and duration of low and high streamflow: years of record needed to characterize streamflow variability. *Journal of Hydrology*, *310*(1-4), 78-94.

Intralawan, A., Wood, D., Frankel, R., Costanza, R., & Kubiszewski, I. (2018). Tradeoff analysis between electricity generation and ecosystem services in the Lower Mekong Basin. *Ecosystem Services*, *30*, 27-35.

IPCC, 2007: Climate Change 2007 - The Physical Science Basis: Working Group I Contribution to the Fourth Assessment Report of the IPCC. Cambridge University Press. https://books.google.co.th/books?id=8-m8nXB8GB4C

IPCC, 2014: Climate Change 2014: Synthesis Report. Contribution of Working Groups I, II and III to the Fifth Assessment Report of the Intergovernmental Panel on Climate Change; IPCC: Geneva, Switzerland, 2014; p. 151. ISBN 978-92-9169-143-2.

IPCC, 2018: Summary for Policymakers. In: Global Warming of 1.5°C. An IPCC Special Report on the impacts of global warming of 1.5°C above pre-industrial levels and related global greenhouse gas emission pathways, in the context of strengthening the global response to the threat of climate change, sustainable development, and efforts to eradicate poverty [Masson-Delmotte, V., P. Zhai, H.-O. Pörtner, D. Roberts, J. Skea, P.R. Shukla, A. Pirani, W. Moufouma-Okia, C. Péan, R. Pidcock, S. Connors, J.B.R. Matthews, Y. Chen, X. Zhou, M.I. Gomis, E. Lonnoy, T. Maycock, M. Tignor, and T. Waterfield (eds.)].

Cambridge University Press, Cambridge, UK and New York, NY, USA, pp. 3-24, doi:10.1017/9781009157940.001

IPCC, 2023: Climate Change 2023: Synthesis Report. Contribution of Working Groups I, II and III to the Sixth Assessment Report of the Intergovernmental Panel on Climate Change [Core Writing Team, H. Lee and J. Romero (eds.)]. IPCC, Geneva, Switzerland, pp. 35-115, doi: 10.59327/IPCC/AR6-9789291691647

IPCC, 2023: Summary for Policymakers. In: Climate Change 2023: Synthesis Report. Contribution of Working Groups I, II and III to the Sixth Assessment Report of the Intergovernmental Panel on Climate Change [Core Writing Team, H. Lee and J. Romero (eds.)]. IPCC, Geneva, Switzerland, pp. 1-34, doi: 10.59327/IPCC/AR6-9789291691647.001

Iqbal, Z., Shahid, S., Ahmed, K., Ismail, T., Ziarh, G. F., Chung, E. S., & Wang, X. (2021). Evaluation of CMIP6 GCM rainfall in mainland Southeast Asia. *Atmospheric Research*, *254*. https://doi.org/10.1016/j.atmosres.2021.105525

Irvin IV, B. C., Niemann, J. D., Perry, M. A., Bauer, K. E., & McCormick III, W. T. (2023). Parameter estimation for models of major rainfall induced floods in ungaged mountain basins of Colorado. *Journal of Hydrology: Regional Studies, 45,* 101300.

Karakoyun, Y., Dönmez, A. H., & Yumurtacı, Z. (2018). Comparison of environmental flow assessment methods with a case study on a runoff river-type hydropower plant using hydrological methods. *Environmental monitoring and assessment, 190, 1-15*.

Khadka, D., Babel, M. S., Abatan, A. A., & Collins, M. (2022). An evaluation of CMIP5 and CMIP6 climate models in simulating summer rainfall in the Southeast Asian monsoon

domain. *International Journal of Climatology*, *42*(2), 1181-1202. https://doi.org/10.1002/joc.7296

King, J. M., & Brown, C. (2018). Environmental flow assessments are not realizing their potential as an aid to basin planning. *Frontiers in Environmental Science*, *6*(OCT). https://doi.org/10.3389/fenvs.2018.00113

Koren, V., Smith, M., Wang, D., & Zhang, Z. (2000). 2.16 Use of soil property data in the derivation of conceptual rainfall-runoff model parameters. In *Proceedings of the 15th Conference on Hydrology, American Meteorological Society, Long Beach, California* (pp. 103-106).

Krysanova, V., & White, M. (2015). Advances in water resources assessment with SWAT—an overview. *Hydrological Sciences Journal*, *60*(5), 771-783.

Kuti, I. A., & Ewemoje, T. A. (2021). Modelling of sediment yield using the soil and water assessment tool (SWAT) model: a case study of the Chanchaga Watersheds, Nigeria. *Scientific African*, *13*, e00936.

Lauri, H., de Moel, H., Ward, P. J., Räsänen, T. A., Keskinen, M., & Kummu, M. (2012). Future changes in Mekong River hydrology: impact of climate change and reservoir operation on discharge. *Hydrology and Earth System Sciences, 16*(12), 4603-4619. https://doi.org/10.5194/hess-16-4603-2012

Leander, R., & Buishand, T. A. (2007). Resampling of regional climate model output for the simulation of extreme river flows. *Journal of hydrology, 332(3-4), 487-496*.

Lebel, L., Garden, P., & Imamura, M. (2005). The politics of scale, position, and place in the governance of water resources in the Mekong region. *Ecology and society*, *10*(2).

Lough, J. M., Wigley, T. M. L., & Palutikof, J. P. (1983). Climate and climate impact scenarios for Europe in a warmer world. *Journal of Applied Meteorology and Climatology*, *22*(10), 1673-1684.

Luo, M., Liu, T., Meng, F., Duan, Y., Frankl, A., Bao, A., & De Maeyer, P. (2018). Comparing bias correction methods used in downscaling precipitation and temperature from regional climate models: a case study from the Kaidu River Basin in Western China. *Water, 10(8), 1046.*

Luo, X., Fan, X., Li, Y., & Ji, X. (2020). Bias correction of a gauge-based gridded product to improve extreme precipitation analysis in the Yarlung Tsangpo-Brahmaputra River basin. *Natural Hazards and Earth System Sciences, 20(8), 2243-2254.*

MacKay, R., & Khalil, M. (1991). Theory and development of a one-dimensional time dependent radiative convective climate model. *Chemosphere*, *22*(3-4), 383-417. https://doi.org/10.1016/0045-6535(91)90326-9

Maraun, D., Wetterhall, F., Ireson, A. M., Chandler, R. E., Kendon, E. J., Widmann, M., Brienen, S., Rust, H. W., Sauter, T., Themeßl, M., C. Venema, V. K., Chun, K. P., Goodess, C. M., Jones, R. G., Onof, C., Vrac, M., & Thiele-Eich, I. (2010). Precipitation downscaling under climate change: Recent developments to bridge the gap between dynamical models and the end user. *Reviews of Geophysics*, *48*(3). https://doi.org/10.1029/2009RG000314

Mendez, M., & Maathuis, B. (2020). Performance Evaluation of Bias Correction Methods for Climate Change Monthly Precipitation Projections over Costa Rica. *Water*, *12*(2), 482. https://doi.org/10.3390/w12020482

Meynell, P., Carew-Reid, J., Räsänen, T., Tilleard, S., & Ketelsen, T. (2014). Exploring environmental flows: Case study of the Lower Se San River. Project report: Challenge

Program on Water & Food Mekong project MK3 “Optimizing the management of a cascade of reservoirs at the catchment level”. ICEM-International Centre for Environmental Management, Hanoi, Vietnam.

Middelkoop, H., Daamen, K., Gellens, D., Grabs, W., Kwadijk, J. C., Lang, H., Parmet, B. W., Schädler, B., Schulla, J., & Wilke, K. (2001). Impact of Climate Change on Hydrological Regimes and Water Resources Management in the Rhine Basin. *Climatic Change*, *49*(1), 105-128. https://doi.org/10.1023/A:1010784727448

Milly, P. C., Betancourt, J., Falkenmark, M., Hirsch, R. M., Kundzewicz, Z. W., Lettenmaier, D. P., & Stouffer, R. J. (2008). Stationarity is dead: Whither water management?. *Science, 319*(5863), 573-574.

Mohammed, I. N., Bolten, J. D., Souter, N. J., Shaad, K., & Vollmer, D. (2022). Diagnosing challenges and setting priorities for sustainable water resource management under climate change. *Scientific Reports*, *12*. https://doi.org/10.1038/s41598-022-04766-2

Moriasi, D. N., Arnold, J. G., Van Liew, M. W., Bingner, R. L., Harmel, R. D., & Veith, T. L. (2007). Model evaluation guidelines for systematic quantification of accuracy in watershed simulations. *Transactions of the ASABE*, *50*(3), 885-900.

Moriasi, D. N., Zeckoski, R. W., Arnold, J. G., Baffaut, C., Malone, R. W., Daggupati, P., ... & Douglas-Mankin, K. R. (2015). Hydrologic and water quality models: Key calibration and validation topics. *Transactions of the ASABE*, *58*(6), 1609-1618.

Moss, R.H., Edmonds, J.A., Hibbard, K.A., Manning, M.R., Rose, S.K., Van Vuuren, D.P., Carter, T.R., Emori, S., Kainuma, M., Kram, T., Meehl, G.A., Mitchell, J.F.B., Nakicenovic, N., Riahi, K., Smith, S.J., Stouffer, R.J., Thomson, A.M., Weyant, J.P., Wilbanks, T.J., 2010.

The next generation of scenarios for climate change research and assessment. *Nature 463,* 747-756 https://doi.org/10.1038/nature08823

MRC (Mekong River Commission), 2010. State of the Basin Report 2010. Vientiane, Mekong River Commission. Available here: http://www.mrcmekong.org/assets/ Publications/basin reports/MRC-SOB-report-2010full-report.pdf.

MRC (Mekong River Commission), 2023. Mekong dam database. Website: https://www.mrcmekong.org/our-work/topics/hydropower/

MRC. (2017). Transboundary Water Resources Management Issues in the Sesan and Srepok River Basins of Cambodia and Viet Nam. Vientiane: MRC Secretariat. https://doi.org/10.52107/mrc.ajg7fp

Nash, J. E., & Sutcliffe, J. V. (1970). River flow forecasting through conceptual models part I—A discussion of principles. *Journal of hydrology*, *10*(3), 282-290.

National Oceanic and Atmospheric Administration. (2023). *Active Storage Capacity. Glossary of Hydrologic Terms.* https://www.noaa.gov/

Navarro-Racines, C. E., & Tarapues Montenegro, J. E. (2015). Bias-correction in the CCAFS-Climate Portal: A description of methodologies.

Ngo, L. A., Masih, I., Jiang, Y., & Douven, W. (2018). Impact of reservoir operation and climate change on the hydrological regime of the Sesan and Srepok Rivers in the Lower Mekong Basin. *Climatic change, 149,* 107-119. https://doi.org/10.1007/s10584-016-1875-y.

Nilsson, C., Reidy, C. A., Dynesius, M., & Revenga, C. (2005). Fragmentation and flow regulation of the world's large river systems. *Science*, *308*(5720), 405-408.

Nystrom, E. A., & Burns, D. A. (2011). TOPMODEL Simulations of Streamflow and Depth to Water Table in Fishing Brook Watershed, New York, 2007-09. *US Department of the Interior, US Geological Survey.*

O'Neill, B. C., Tebaldi, C., Van Vuuren, D. P., Eyring, V., Friedlingstein, P., Hurtt, G., ... & Sanderson, B. M. (2016). The scenario model intercomparison project (ScenarioMIP) for CMIP6. *Geoscientific Model Development, 9*(9), 3461-3482. https://doi.org/10.5194/gmd-9-3461-2016

Palmer, M. A., Lettenmaier, D. P., Poff, N. L., Postel, S. L., Richter, B., & Warner, R. (2009). Climate change and river ecosystems: protection and adaptation options. *Environmental management*, *44*, 1053-1068.

Parry, M. L., Carter, T. R., & Konijn, N. T. (1988). *The climatology of droughts and drought prediction* (pp. 305-323). Springer Netherlands.

Pearse-Smith, S. W. D. (2012). The impact of continued Mekong Basin hydropower development on local livelihoods. *Consilience,* (7), 73-86.

Phung, D., Nguyen-Huy, T., Tran, N. N., Tran, D. N., Doan, V. Q., Nghiem, S., Nguyen, N. H., Nguyen, T. H., & Bennett, T. (2021). Hydropower dams, river drought and health effects: A detection and attribution study in the lower Mekong Delta Region. *Climate Risk Management*, *32*, 100280. https://doi.org/10.1016/j.crm.2021.100280

Piman, T., Cochrane, T. A., & Arias, M. E. (2016). Effect of proposed large dams on water flows and hydropower production in the Sekong, Sesan and Srepok rivers of the Mekong Basin. *River research and applications*, *32*(10), 2095-2108.

Piman, T., Cochrane, T. A., Arias, M. E., Green, A., & Dat, N. D. (2013). Assessment of flow changes from hydropower development and operations in Sekong, Sesan, and Srepok rivers

of the Mekong basin. *Journal of Water Resources Planning and Management*, *139*(6), 723-732.

Piman, T., Lennaerts, T., & Southalack, P. (2013). Assessment of hydrological changes in the lower Mekong Basin from Basin-Wide development scenarios. *Hydrological Processes*, *27*(15), 2115-2125.

Poff, N. L., & Zimmerman, J. K. (2010). Ecological responses to altered flow regimes: a literature review to inform the science and management of environmental flows. *Freshwater biology*, *55*(1), 194-205. https://doi.org/10.1111/j.1365-2427.2009.02272.x

Poff, N. L., Allan, J. D., Bain, M. B., Karr, J. R., Prestegaard, K. L., Richter, B. D., ... & Stromberg, J. C. (1997). The natural flow regime. *BioScience*, *47*(11), 769-784.

Pokhrel, Y., Burbano, M., Roush, J., Kang, H., Sridhar, V., & Hyndman, D. W. (2018). A review of the integrated effects of changing climate, land use, and dams on Mekong river hydrology. *Water, 10*(3), 266. https://doi.org/10.3390/w10030266.

Pokhrel, Y., Shin, S., Lin, Z., Yamazaki, D., & Qi, J. (2018). Potential Disruption of Flood Dynamics in the Lower Mekong River Basin Due to Upstream Flow Regulation. *Scientific Reports*, *8*(1), 1-13. https://doi.org/10.1038/s41598-018-35823-4

Praskievicz, S., & Chang, H. (2009). A review of hydrological modelling of basin-scale climate change and urban development impacts. *Progress in Physical Geography*. https://doi.org/10.1177/0309133309348098

Qian, W., & Chang, H. H. (2021). Projecting health impacts of future temperature: a comparison of quantile-mapping bias-correction methods. *International Journal of Environmental Research and Public Health, 18*(4), 1992.

Räsänen, T. A., Koponen, J., Lauri, H., & Kummu, M. (2012). Downstream hydrological impacts of hydropower development in the Upper Mekong Basin. *Water Resources Management, 26,* 3495-3513. https://doi.org/10.1007/s11269-012-0087-0

Räty, O., Räisänen, J., & Ylhäisi, J. S. (2014). Evaluation of delta change and bias correction methods for future daily precipitation: intermodel cross-validation using ENSEMBLES simulations. *Climate dynamics*, *42*, 2287-2303.

Rawls, W. J., Brakensiek, D. L., & Saxtonn, K. E. (1982). Estimation of soil water properties. *Transactions of the ASAE*, *25*(5), 1316-1320.

Riahi, K., Van Vuuren, D. P., Kriegler, E., Edmonds, J., O'neill, B. C., Fujimori, S., ... & Tavoni, M. (2017). The Shared Socioeconomic Pathways and their energy, land use, and greenhouse gas emissions implications: An overview. *Global environmental change, 42,* 153-168.

Richter, B. D. & Thomas, G. A. (2007). Restoring environmental flows by modifying dam operations. *Ecology and Society, 12*(1).

Richter, B. D., Baumgartner, J. V., Braun, D. P., & Powell, J. (1998). A spatial assessment of hydrologic alteration within a river network. *Regulated Rivers: Research & Management: An International Journal Devoted to River Research and Management, 14*(4), 329-340.

Richter, B. D., Baumgartner, J. V., Powell, J. & Braun, D. P. (1996). A method for assessing hydrologic alteration within ecosystems. *Conservation Biology, 10 (4),* 1163-1174.

Richter, B., Baumgartner, J., Wigington, R., & Braun, D. (1997). How much water does a river need?. *Freshwater biology*, *37*(1), 231-249.

Rienecker, M. M., Suarez, M. J., Gelaro, R., Todling, R., Bacmeister, J., Liu, E., ... & Woollen, J. (2011). MERRA: NASA's modern-era retrospective analysis for research and applications. *Journal of climate*, *24*(14), 3624-3648.

Rounsevell, M. D., & Metzger, M. J. (2010). Developing qualitative scenario storylines for environmental change assessment. *Wiley interdisciplinary reviews: climate change*, *1*(4), 606-619.

Sabol, G. V. (2008). Hydrologic Basin response parameter estimation guidelines [Dam Safety Report, State of Colorado].

Santoso, H., Idinoba, M., & Imbach, P. A. (2008). Climate Scenarios: What we need to know and how to generate them. *Working paper no. 45. Bogor, Indonesia: Center for International Forestry Research (CIFOR). 27 p.*

Satianesan, Y., Tan, W. L., & Ling, L. (2022, December). Assessment of Various Rainfall Bias Correction Techniques in Peninsular Malaysia. *In International Conference on Mathematical Sciences and Statistics 2022* (ICMSS 2022) (pp. 114-129). Atlantis Press.

Saxton, K. E., & Rawls, W. J. (2006). Soil water characteristic estimates by texture and organic matter for hydrologic solutions. *Soil science society of America Journal, 70(5),* 1569-1578

Schmidli, J., Frei, C., & Vidale, P. L. (2006). Downscaling from GCM precipitation: a benchmark for dynamical and statistical downscaling methods. *International Journal of Climatology: A Journal of the Royal Meteorological Society*, *26*(5), 679-689.

Seaby, L., Refsgaard, J., Sonnenborg, T., Stisen, S., Christensen, J., & Jensen, K. (2013). Assessment of robustness and significance of climate change signals for an ensemble of distribution-based scaled climate projections. *Journal of Hydrology*, *486*, 479-493. https://doi.org/10.1016/j.jhydrol.2013.02.015

Shrestha, A. B., & Aryal, R. (2011). Climate change in Nepal and its impact on Himalayan glaciers. *Regional Environmental Change*, *11*(1), 65-77. https://doi.org/10.1007/s10113-010-01749

Shrestha, M., Acharya, S. C., & Shrestha, P. K. (2017). Bias correction of climate models for hydrological modelling-are simple methods still useful? *Meteorological Applications*, *24*(3), 531-539. https://doi.org/10.1002/met.1655

Shrestha, S., Bae, D. H., Hok, P., Ghimire, S., & Pokhrel, Y. (2021). Future hydrology and hydrological extremes under climate change in Asian river basins. *Scientific Reports*, *11*(1), [17089]. https://doi.org/10.1038/s41598-021-96656-2

Shrestha, S., Shrestha, M., & Babel, M. S. (2017). *Assessment of climate change impact on water diversion strategies of Melamchi Water Supply Project in Nepal*. 311-323. https://doi.org/10.1007/s00704-015-1713-6

Sitterson, J., Knightes, C., Parmar, R., Wolfe, K., Avant, B., & Muche, M. (2018). An overview of rainfall-runoff model types.

Smakhtin, V., & Weragala, N. (2005). *An assessment of hydrology and environmental flows in the Walawe river basin, Sri Lanka*. IWMI.

Sorooshian, S., Hsu, K. L., Coppola, E., Tomassetti, B., Verdecchia, M., & Visconti, G. (Eds.). (2008). *Hydrological modelling and the water cycle: coupling the atmospheric and hydrological models* (Vol. 63). Springer Science & Business Media.

Soukhaphon, A., Baird, I. G., & Hogan, Z. S. (2021). The Impacts of Hydropower Dams in the Mekong River Basin: A Review. *Water*, *13*(3), 265. https://doi.org/10.3390/w13030265

Tabari, H., Paz, S. M., Buekenhout, D., and Willems, P. (2021). Comparison of statistical downscaling methods for climate change impact analysis on precipitation-driven drought.

Hydrology and Earth System Sciences, 25, 3493-3517. https://doi.org/10.5194/hess-25-3493-2021

Tennant, D. L. (1976). Instream flow regimens for fish, wildlife, recreation and related environmental resources. *Fisheries*, *1*(4), 6-10.

Teutschbein, C., & Seibert, J. (2012). Bias correction of regional climate model simulations for hydrological climate-change impact studies: Review and evaluation of different methods. *Journal of Hydrology*, *456-457*, 12-29. https://doi.org/10.1016/j.jhydrol.2012.05.052

Tharme, R. E. (1996). Review of international methodologies for the quantification of the instream flow requirements of rivers. *Water Law Review: final report for policy development, South African Department of Water Affairs and Forestry. Freshwater Research Unit: University of Cape Town: Pretoria*.

Tharme, R. E. (2003). A global perspective on environmental flow assessment: emerging trends in the development and application of environmental flow methodologies for rivers. *River research and applications*, *19*(5-6), 397-441.

The Nature Conservancy. (2009). Indicators of Hydrologic Alteration Version 7.1. [User's Manual]. rPurview LLC - Ted Rybicki, Totten Software Design, Smythe Scientific Software.

Tian, X., Zhao, G., Mu, X., Zhang, P., Tian, P., Gao, P., & Sun, W. (2019). Hydrologic alteration and possible underlying causes in the Wuding River, China. *Science of the Total Environment, 693,* 133556. https://doi.org/10.1016/j.scitotenv.2019.07.362.

Tong, Y., Gao, X., Han, Z., Xu, Y., Xu, Y., & Giorgi, F. (2021). Bias correction of temperature and precipitation over China for RCM simulations using the QM and QDM methods. *Climate Dynamics, 57, 1425-1443.*

Tong, Y., Gao, X., Han, Z., Xu, Y., Xu, Y., & Giorgi, F. (2021). Bias correction of temperature and precipitation over China for RCM simulations using the QM and QDM methods. *Climate Dynamics, 57, 1425-1443.*

Trang, N. T. T., Shrestha, S., Shrestha, M., Datta, A., & Kawasaki, A. (2017). Evaluating the impacts of climate and land-use change on the hydrology and nutrient yield in a transboundary river basin: A case study in the 3S River Basin (Sekong, Sesan, and Srepok). *Science of the Total Environment*, *576*, 586-598.

Trihey, E. W., & Stalnaker, C. B. (1985). Evolution and application of instream flow methodologies to small hydropower developments: an overview of the issues. In *Small Hydro/Fisheries Symposium*.

Try, S., Tanaka, S., Tanaka, K., Sayama, T., Khujanazarov, T., & Oeurng, C. (2022). Comparison of CMIP5 and CMIP6 GCM performance for flood projections in the Mekong River Basin. *Journal of Hydrology: Regional Studies*, *40*, 101035. https://doi.org/10.1016/j.ejrh.2022.101035

Trzaska, S., & Schnarr, E. (2014). A review of downscaling methods for climate change projections. United States Agency for International Development by Tetra Tech ARD, (September), 1-42.

Varis, O., Kajander, T., & Lemmelä, R. (2004). Climate and water: from climate models to water resources management and vice versa. *Climatic Change, 66*(3), 321-344.

Wang, W., Lu, H., Ruby Leung, L., Li, H. Y., Zhao, J., Tian, F., ... & Sothea, K. (2017). Dam construction in Lancang-Mekong River Basin could mitigate future flood risk from warming-induced intensified rainfall. *Geophysical Research Letters, 44(20), 10-378.* https://doi.org/10.1002/2017GL075037

Waseem, M., Kachholz, F., Klehr, W., & Traenckner, J. (2020). Suitability of a coupled hydrologic and hydraulic model to simulate surface water and groundwater hydrology in a typical North-Eastern Germany lowland catchment. *Applied Sciences, 10(4), 1281*.

Wild, T.B., Loucks, D.P., 2014. Managing flow, sediment, and hydropower regimes in the Sre Pok, Se San, and Se Kong Rivers of the Mekong basin. *Water Resource. Res. 50, 5141-5157.* https://doi.org/10.1002/2014WR015457

Winemiller, K. O., McIntyre, P. B., Castello, L., Fluet-Chouinard, E., Giarrizzo, T., Nam, S., ... & Saenz, L. (2016). Balancing hydropower and biodiversity in the Amazon, Congo, and Mekong. *Science*, *351*(6269), 128-129.

Woolridge, D. D., & Niemann, J. (2018). *Mountain basin hydrologic study* (Doctoral dissertation, Colorado State University. Libraries).

Woolridge, D. D., Niemann, J. D., Perry, M. A., Bauer, K. E., & McCormick III, W. T. (2020). Identifying runoff production mechanisms for dam safety applications in the Colorado front range. *Journal of Hydrologic Engineering, 25(8), 05020016.*

Wyatt, A. B., & Baird, I. G. (2007). Transboundary impact assessment in the Sesan River Basin: the case of the Yali Falls Dam. *Water Resources Development*, *23*(3), 427-442.

Xue, L., Zhang, H., Yang, C., Zhang, L., & Sun, C. (2017). Quantitative assessment of hydrological alteration caused by irrigation projects in the Tarim River basin, China. *Scientific Reports, 7(1), 4291.*

Xue, L., Zhang, H., Yang, C., Zhang, L., & Sun, C. (2017). Quantitative assessment of hydrological alteration caused by irrigation projects in the Tarim River basin, China. *Scientific Reports, 7(1), 4291.*

Yusuf, A. A., & Francisco, H. A. (2009). Climate Change Vulnerability Mapping for Southeast Asia. Economy and Environment Program for Southeast Asia (EEPSEA). Retrieved from http://www.eepsea.org

Zarfl, C., Lumsdon, A. E., Berlekamp, J., Tydecks, L., & Tockner, K. (2015). A global boom in hydropower dam construction. *Aquatic Sciences*, *77*, 161-170.

Zhang, L., Dawes, W. R., & Walker, G. R. (2001). Response of mean annual evapotranspiration to vegetation changes at catchment scale. *Water Resources Research*, *37*(3), 701-708. https://doi.org/10.1029/2000WR900325

Zhao, T., Bennett, J. C., Wang, Q. J., Schepen, A., Wood, A. W., Robertson, D. E., & Ramos, M. H. (2017). How suitable is quantile mapping for postprocessing GCM precipitation forecasts?. *Journal of Climate, 30(9), 3185-3196.*

Zinke, P. J. (1967). Forest interception studies in the United States. *Forest hydrology*, 137-161.

Ziv, G., Baran, E., Nam, S., Rodríguez-Iturbe, I., & Levin, S. A. (2012). Trading-off fish biodiversity, food security, and hydropower in the Mekong River Basin. *Proceedings of the National Academy of Sciences*, *109*(15), 5609-5614.

Zorita, E., & Von Storch, H. (1999). The analog method as a simple statistical downscaling technique: Comparison with more complicated methods. *Journal of climate*, *12*(8), 2474-2489.

Zuo, Q., & Liang, S. (2015). Effects of dams on river flow regime based on IHA/RVA. *Proceedings of the International Association of Hydrological Sciences, 368, 275-280.*